The Bio-Thing
- A Biodegradable Microphone for Monitoring Biodiversity



ET4300 - Master Thesis

TU Delft Delft University of Technology

EKL Else Kooi Laboratory

ECTM

The Bio-Thing - A Biodegradable Microphone for Monitoring Biodiversity

ET4300 - Master Thesis

Samhitha Duvvuri

Student Number - 5272734

Thesis Committee:

dr. Clémentine Boutry (Supervisor)

prof. dr. P.M. Sarro

dr. Y. Aslan

May 22, 2024

Electronic Components, Technology and Materials (ECTM)
Department of Microelectronics (EE-ME)
Faculty of Electrical Engineering, Mathematics and Computer Science (EWI)
Delft University of Technology

TU Delft Delft University of Technology

EKL Else Kooi Laboratory

ECTM

Acknowledgements

First and foremost, I would like to sincerely thank my supervisor, dr. Clémentine Boutry for her continued support, guidance and inspiration through my entire project, both academically and personally.

I am grateful to ECTM for broadening my skill set and giving me a chance to try and learn a wide spectrum of things I would never have had a chance to. I found my love for stereolithography here. For that, I will always be grateful.

I want to thank my friends Viswesh, Sandeep and Yash for being my permanent sounding boards and Casa 101: Tom, Öykü and Rocco for your unwavering love and support! I wouldn't have gotten through if not for all of you.

I would like to dedicate my thesis to all my grandparents and sincerely thank them from the bottom of my heart for being my constant source of encouragement and believing in me even when I didn't believe in myself.

Since it wouldn't be MY thesis without one,

What happens when one swallows a surveillance microphone?
You have a stomach bug!

P.S - The Pursuit of Happyness, Timestamp - 1:50:08

Abstract

Conventional techniques for audio monitoring, including Passive Audio Monitoring (PAM), often call for the use of environmentally unsustainable and challenging equipment. This among other limitations can disrupt the very environment that is meant to be studied and may also limit the ability to observe an ecosystem in its natural state.

This thesis explores the possibility of a passive wireless biodegradable microphone for the purpose of audio monitoring in fragile environments. This project introduces the "The BioThing - A biodegradable microphone for monitoring biodiversity". The BioThing uses a biodegradable material, to address the current challenges of state-of-art monitoring techniques. The design utilises a resonant cavity to function as a listening device through the implementation of the backscatter wave modulation technique and with a primary working resonant frequency of around 1.7 GHz.

This report presents a detailed analysis of the device's design and function to optimize its geometry for various frequencies, operational ranges, and functionalities by investigating the effect of critical parameters such as the variable capacitances namely the distance between the diaphragm and the tuning post, and the distance between the tuning post and the antenna. Additionally, it also analyses the effect of device geometry on resonance properties by investigating the impact of parameters such as tuning post height, membrane thickness, and cavity height. The report also investigates the possibilities for device enlargement for long-distance operation and device miniaturisation to facilitate faster degradation. This optimization process aims to achieve improved performance, ultimately leading to a more effective listening device. A prototype was fabricated using commercially available Zinc and plant-based resin.

This research works towards a new generation of ecologically sustainable audio monitoring equipment that will allow a deeper insight into the soundscapes of fragile environments without disturbing the ecosystems.
.

Contents

Acknowledgements V

Abstract VI

List of Figures XII

List of Tables XIV

1 Introduction 1
- 1-1 Need for Audio Monitoring in Ecosystems and Fragile Environments . . . 1
  - 1-1-1 Fragile Ecosystems . . . 3
  - 1-1-2 Current Methods for Audio Monitoring in Fragile Environments . . . 3
- 1-2 Limitations with Current Technology . . . 5
- 1-3 Motivation and Research Objective of the Project . . . 5
- 1-4 List of Requirements for the Project . . . 6
- 1-5 Organisation of the Thesis . . . 6

2 Design Selection for a Passive Wireless Biodegradable Microphone 8
- 2-1 Microphones . . . 8
  - 2-1-1 History . . . 8
  - 2-1-2 Types of Microphones . . . 10
- 2-2 Design Selection . . . 14
  - 2-2-1 Microwave Cavities for Audio Monitoring . . . 15
  - 2-2-2 The Thing (Great Seal Bug) . . . 15
- 2-3 Material Selection . . . 19
  - 2-3-1 Degradation mechanism . . . 19
  - 2-3-2 Biodegradable Metals . . . 21
  - 2-3-3 Selection of Biodegradable Material for the Microphone . . . 23

3 Theoretical Background **25**
3-1 Resonance and Resonators . . . 25
3-1-1 Resonance . . . 25
3-1-2 Resonators . . . 25
3-1-3 Q-factor . . . 26
3-2 Microwave Cavities . . . 28
3-2-1 Types of Cavity Resonators . . . 29
3-3 Antennas . . . 38
3-3-1 Antenna Parameters . . . 40
3-3-2 Types of Antennas classified by Shape . . . 41
3-4 Amplitude Modulation . . . 43
3-5 Backscatter wave technique . . . 45
3-5-1 Comparison between traditional and backscatter encoding . . . 46
3-5-2 Resonant cavities and backscatter modulation . . . 46

4 Simulations **47**
4-1 Background - Simulations for the Biodegradable Microphone based on the Great Seal Bug . . . 47
4-2 Software, Solvers and Primary Simulation parameters . . . 48
4-2-1 Choice of Software and Solvers . . . 48
4-2-2 Primary Simulation Parameters . . . 49
4-2-3 Dimensions of the Original Resonant Cavity (Great Seal Bug) . . . 50
4-3 Simulation of Original Great Seal Bug Microwave Resonator . . . 52
4-3-1 Electric boundary . . . 52
4-3-2 Open boundary . . . 52
4-4 Simulation of the microwave resonator with biodegradable metals . . . 54
4-4-1 Magnesium . . . 54
4-4-2 Zinc . . . 55
4-4-3 Iron . . . 56
4-4-4 Comparison of results across materials . . . 57
4-5 Device miniaturization and effect on resonance properties . . . 59
4-5-1 Parameter adjustments for different scaled-down variants . . . 59
4-5-2 Results . . . 60
4-6 Influence of device geometry variations on resonance properties . . . 62
4-6-1 Impact of distance between tuning post and membrane . . . 62
4-6-2 Impact of Distance between Tuning Post and Antenna . . . 63
4-6-3 Impact of Membrane thickness . . . 65
4-6-4 Impact of Tuning Post height . . . 66
4-6-5 Impact of Cavity Height . . . 67
4-6-6 Alternate Cavity Design . . . 68
4-7 Design Modification towards Longer-Distance Operation . . . 70
4-7-1 Parameter adjustments for different scaled-up variants . . . 70
4-7-2 Results . . . 71

5 Biodegradable Microphone Fabrication **74**
5-1 Microwave Resonator Fabrication . . . 74
5-1-1 Resonant Cavity . . . 74
5-1-2 Insulator . . . 75
5-1-3 Membrane . . . 76
5-2 Fabricated Device, Results and Challenges . . . 76
5-3 Anticipated performances of fabricated device vs original design . . . 79
5-4 Characterization Plan . . . 81
5-4-1 Proof of Concept . . . 81
5-4-2 Proposed Readout Setup . . . 82

6 Conclusion **84**
6-1 Concluding Remarks . . . 84
6-2 Outlook . . . 84

Bibliography **85**

A Appendix - The Thing: History and Background **92**

B Material File Configuration of Plant-Based Resin **95**

List of Figures

1-1 The global Living Planet Index from 1970 to 2018 1
1-2 Active monitoring Methods 2
1-3 Passive monitoring Methods 3
1-4 Workflow of a typical study utilising Passive Audio Monitoring System 4
1-5 SAFE Project - Example of a passive acoustic monitoring system 5

2-1 Early Examples of Mechanical Recording Devices 9
2-2 Alexander Graham Bell's First Patented Microphone 9
2-3 Schematic of a condenser microphone 10
2-4 Schematic of a dynamic microphone 11
2-5 Schematic of a ribbon microphone 12
2-6 Schematic of a carbon granule microphone 13
2-7 Wooden Housing of The Great Seal Bug 15
2-8 Technical Drawing from FBI Report 16
2-9 Reverse-Engineered Model of Great Seal Bug 17
2-10 Cross-Section of Great Seal Bug 17
2-11 Equivalent circuit diagram of Great Seal Bug 18
2-12 Working principle of Great Seal Bug 18

3-1 Q-factor of resonator 26
3-2 Illustration of the proposed resonator cavity design 29
3-3 Rectangular Cavity Resonator 30

3-4 TE_{101} mode for a rectangular cavity 30
3-5 Cylindrical Cavity Resonator 31
3-6 Electric and magnetic field of cylindrical cavity resonator 32
3-7 A Typical Reentrant Cavity Diagram 34
3-8 Types of reentrant cavities 36
3-9 Coaxial cavity structure 37
3-10 E-Field transition from a perfect-cylindrical to a perfect-coaxial resonator 37
3-11 Illustration of working of antenna in proposed design 38
3-12 Working of an Antenna 39
3-13 Horn Antenna Schematic 42
3-14 Schematic illustrating the Great Seal Bug's response to a modulated carrier signal 43
3-15 Amplitude Modulation 44

4-1 Dimensions of control device adapted from Great Seal Bug 50
4-2 E-Field of original device's dominant eigenmode 53
4-3 E-Field of Magnesium variant device's dominant eigenmode 55
4-4 E-Field of Zinc variant device's dominant eigenmode 56
4-5 E-Field of Iron variant device's dominant eigenmode 57
4-6 Impact of material used on different on Frequency and Total Q 58
4-7 Visualisation of parameter adjustment for device miniaturisation 59
4-8 Impact of miniaturisation on Frequency, Skin Depth and Total Q 61
4-9 Visualisation of parameter adjustment for membrane-tuning post (MP_h) distance 62
4-10 Impact of Distance between Tuning Post and Membrane on Frequency, Skin Depth and Total Q 63
4-11 Visualisation of parameter adjustment for TA_L distance 64
4-12 Impact of distance between tuning post and antenna on Total Q 64
4-13 Visualisation of parameter adjustment for Membrane thickness 65
4-14 Impact of Membrane thickness on Total Q 66
4-15 Visualisation of parameter adjustment for Tuning Post height ($B2_h$) 66
4-16 Impact of Tuning Post height on Frequency and Total Q 67
4-17 Visualisation of parameter adjustment for Cavity height (C_h) 67
4-18 Impact of Cavity height on Total Q 68
4-19 Visualisation of parameter adjustment an alternate design 69
4-20 3D CAD model of flattened cavity model variant 69

4-21 3D CAD model of flattened cavity model variant 69
4-22 Scale-Up Illustration 70
4-23 Impact of scaling up device on Frequency, Skin Depth and Total Q 72

5-1 CAD Model of resonant cavity 74
5-2 CAD Model of tuning post and thread 75
5-3 CAD Model of resonant cavity caps 75
5-4 CAD Model of insulator 75
5-5 CAD Model of membrane (diaphragm) 76
5-6 Resin Characterization Tests 76
5-7 Images of device fabricated at IWM 78
5-8 Images of 3D printed insulator with commercially available plant-based resin . . . 79
5-9 Full view of fabricated device 79
5-10 Comparison of cross-sections of devices 80
5-11 3D Model of Fabricated Device 80
5-12 E-Field of fabricated device's dominant eigenmode 81
5-13 Proposed Proof of Concept Setup Illustration 82
5-14 Proposed Proof of Concept Lab Setup 82
5-15 Schematic illustrating a readout setup designed to characterize a device's response to a modulated carrier signal 83
5-16 Characterization setup for the BioThing 83

A-1 Structure of Theremin's Great Seal Bug 93
A-2 The Great Seal Bug Housing 93

List of Tables

2-1 A comparison of material properties among biodegradable materials 21

4-1 Dimensions of control device adapted from Great Seal Bug 51
4-2 A comparative analysis of simulation results with findings from Brooker-Gomez Paper 52
4-3 Eigenmode solver results of original copper device with open boundary 53
4-4 Eigenmode solver results of magnesium device with open boundary 55
4-5 Eigenmode solver results of zinc device with open boundary 56
4-6 Eigenmode solver results of iron device with open boundary 57
4-7 Comparison of parameters of different biodegradable metals 58
4-8 Dimensions of control and scaled-down variant models 59
4-9 Comparison of results for Control MP_h Distance - 0.07mm 60
4-10 Comparison of results for Control MP_h Distance - 0.23mm 60
4-11 Results for variations of the distance between Tuning Post and Membrane (MP_h) 63
4-12 Results for variations of distance between Tuning Post and Antenna (TA_L) . . . 64
4-13 Results for variations of Membrane thickness 65
4-14 Results for variations of Tuning Post height ($B2_h$) 67
4-15 Results for variations of Cavity height (C_h) 68
4-16 Simulation Results Compared to Control Device for MP_h distance of 0.23mm . . 70
4-17 Dimensions of scaled-up variant models 71
4-18 Comparison of results for Control MP_h Distance - 0.07mm 71
4-19 Comparison of results for Control MP_h Distance - 0.23mm 72

5-1 Dimensions of original device and fabricated device 77
5-2 Simulation Results Compared to Control Device 80

Introduction

1-1 Need for Audio Monitoring in Ecosystems and Fragile Environments

The World Wildlife Fund for Nature's 2022 Living Planet Report [1] presents a concerning account of biodiversity depletion, displaying a steady decline in global wildlife populations. Since 1970, populations of tracked vertebrates, including mammals, birds, amphibians, reptiles, and fish, have seen a significant decline of 69% on average as in Figure 1-1. This translates to a near-catastrophic loss of nearly two-thirds of wildlife in less than five decades. This study among others provides a clear indication of the significant impact that human activities have on ecosystems globally, emphasising the urgent need for conservation initiatives to counteract this concerning trend The rapid rate at which species are becoming extinct is staggering prompting several experts to dub as the sixth mass extinction event [2]–[4].

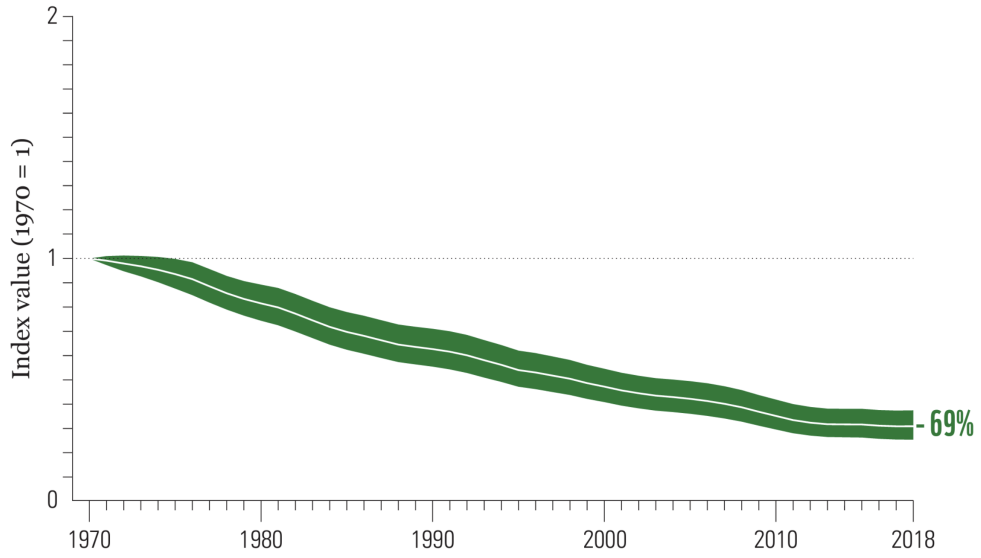


Figure 1-1: The global Living Planet Index from 1970 to 2018 [1]

Animals extensively depend on sound for many aspects of their life, such as communication, echolocation, mating, defending territory, and even unintentional sounds from movement and eating [5]. Historically, the discipline of bioacoustics largely concentrated on the study of

animal communication and sensory ecology [6]. Over the last ten years, owing to the growth in technology, there has been a significant increase in the use of acoustics for wildlife monitoring, which is sometimes referred to as passive acoustic monitoring (PAM) [6]. In contrast to camera trapping, which mostly captures bigger animals and birds by using remote, motion-triggered cameras to capture images without disturbing their natural behaviour, PAM has the capacity to detect a broader variety of species, irrespective of their size [6]. However, this approach has a restriction in that it can only be used to monitor living things that generate noises that can be heard. Additionally, in order to effectively monitor certain animals, it is necessary to be able to identify the calls according to a relevant category, such as species or genus [6].

Various studies have successfully utilised Passive Acoustic Monitoring (PAM) to monitor a wide range of animal species. These include birds [7]–[10], bats [11], [12], marine mammals [13], elephants [14], amphibians [15] and so on. The increase in the use of Passive Acoustic Monitoring (PAM) applications aligns with the progress made in both hardware and software, which has facilitated the collection and analysis of large acoustic datasets obtained from field environments [6]. Like camera traps, these advanced acoustic sensors can be used for long periods of time to facilitate wildlife monitoring for several purposes, including estimating species occupancy, abundance, population density, studying animal behaviour, and surveying and monitoring ecological communities [6].

The critical need for audio monitoring in ecosystems and fragile environments stems from the inherent challenge of understanding and protecting them. For many years, ecological monitoring has been a fundamental aspect of study. When not pursuing conventional active monitoring techniques, such as transect sampling (laying down a straight line in an area and collecting data at intervals along that line to understand how organisms or features are distributed), manual surveys, and active acoustic monitoring, are useful for gathering data. Conventional approaches also include passive monitoring technologies such as satellite or aerial surveys [6]. Although these approaches are valuable, they result in a substantial deficiency in order to comprehend the entire ecological fabric.



(a) Transect Sampling Method [16]



(b) Manual Survey Method [17]

Figure 1-2: Active monitoring Methods

Field data collection, while vital to ecological monitoring, has both advantages and disadvantages. Although conventional methods are crucial for scientific discovery and informed land management, they might inadvertently disturb the ecosystems they seek to comprehend. Satellite-based sensors provide valuable but limited information about the structure

and productivity of ecosystems worldwide, but they do not offer the amount of detail that can be obtained by on-site surveys [18].



(a) Satellite Monitoring [19]

(b) Aerial Monitoring Method [20]

Figure 1-3: Passive monitoring Methods

Field surveys, on the other hand, may need invasive techniques that could disrupt the fragile equilibrium of the specific ecosystem being studied. For example, while studying animal behaviour, it is often necessary to use traps or monitoring stations, which can add artificial elements to the habitat. The possibility of causing disturbance emphasises the requirement for inventive techniques of gathering data that reduce ecological harm while still offering the required level of precision.

These approaches face difficulties in accurately capturing the complex and detailed interactions occurring within an ecosystem, especially the diverse and informative soundscapes. Passive Acoustic Monitoring (PAM) is a highly effective method in this context. The Passive Acoustic Monitoring (PAM) technique is becoming increasingly popular globally as a non-invasive and eco-friendly way of sampling and monitoring ecosystems while offering a powerful solution to bridge the gap in our ecological understanding [21].

1-1-1 Fragile Ecosystems

Many environments worldwide are deemed fragile because of their intricate and delicately harmonised ecosystems. These ecosystems and environments, which include coral reefs in the deep sea and deep forests on land, are extremely susceptible to even small disturbances. Aforementioned conventional active monitoring techniques, such as transect sampling, manual surveys, and active acoustic monitoring, are useful for gathering data. However, they involve direct contact with the environment or other passive monitoring methods like drones flying over or submarines flowing through underwater generate noise that can affect animal behaviour and disturb the delicate equilibrium between living (biotic) and non-living (abiotic) elements.

1-1-2 Current Methods for Audio Monitoring in Fragile Environments

A typical PAM workflow is shown in Figure 1-4. Firstly, the sensors play a key role in this endeavour. The selection of the sensor depends on the delicate nature of the surroundings.

Factors such as the vocal range of the target species and the prevailing climatic circumstances will have an impact on this selection process. Following that is the survey design. This sets the methodology and timing for the placement of the sensor. This takes into account variables such as the specific region of interest, the required level of data detail, and any possible sources of interference or disturbance. These sights could include stationary sites, drifting buoys, or remote jungles depending on the design of the survey. Following this is the process of gathering information. Once the sensors are installed, they gather both audio data and information. Metadata may contain timestamps, geographical coordinates, and further particulars. The length of the recording varies depending on the survey's design. The subsequent stage involves audio processing. All of the gathered is then analysed and processed. Noise reduction is then performed. Researchers then identify and isolate certain characteristics for further examination. At last, the data is examined and studied. This leads to generating soundscapes to depict the auditory surroundings or undertaking analysis to discern patterns in species presence or activity [22].

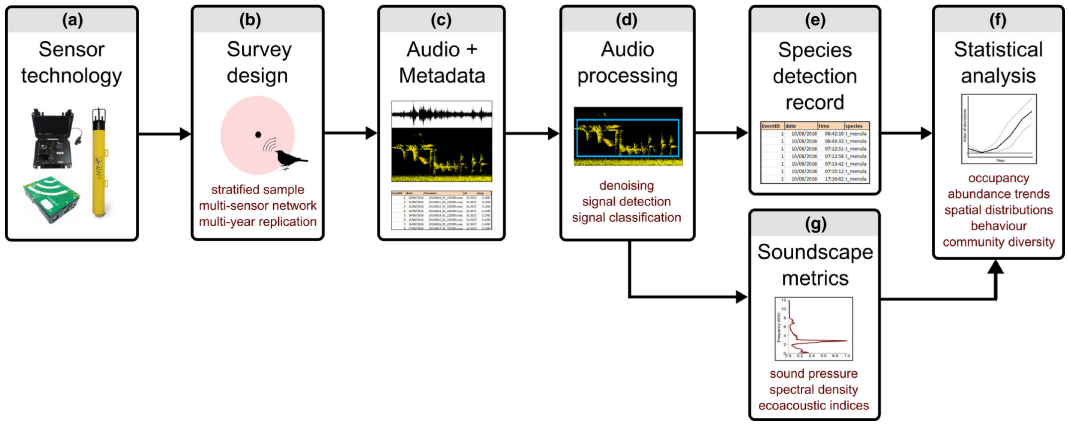


Figure 1-4: Workflow of a typical Passive Audio Monitoring System [22]

The Stability of Altered Forest Ecosystem (SAFE) Project centered on the rainforests of Malaysian Borneo, is a collaboration between the South East Asia Rainforest Research Partnership (SEARRP), researchers at Imperial College London and Cambridge University, and various community partners. Among its various initiatives is SAFE Acoustics , which combines eco-acoustics, engineering, and machine learning tools to automate biodiversity monitoring in the tropical forests [23].

The upcoming phase of the SAFE Project website aims to integrate biodegradable sensors [18], as part of Dr. Lorenzo Picinali (Audio Experience Design at the Dyson School of Design Engineering), and Dr. Sarab Sethi's (Ecosystem Sensing, Imperial College) research at Imperial College London. This integration is intended to address the challenges outlined in the forthcoming section. This thesis project is being conducted in collaboration with that objective.

An illustration of the SAFE Project's Passive Audio Monitoring system may be seen in Figure 1-5. A survey was conducted in Borneo that used eleven sensors with devices integrated with Raspberry Pi [24]. An extensive database was developed and published on the Internet. One of the primary challenges the researchers encountered was the deployment and retrieval of the sensors. This is explained in the subsequent section along with other constraints associated

with existing technology.

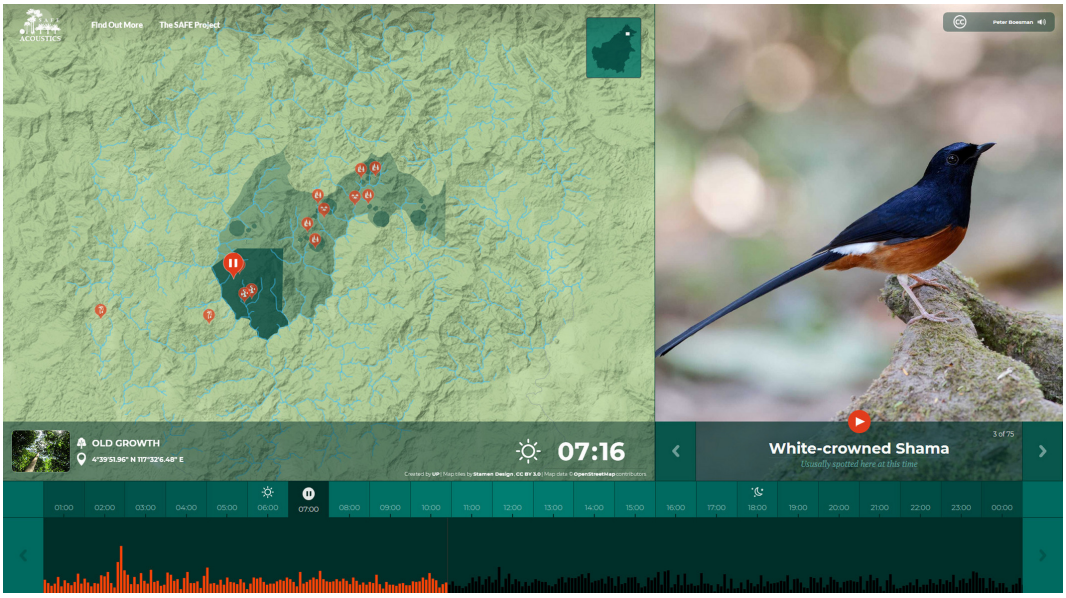


Figure 1-5: SAFE Project - Example of a Passive Audio Monitoring System [24]

1-2 Limitations with Current Technology

Conventional ecological monitoring techniques that involve the use of audio recording equipment have certain limitations. These methods need manual deployment and retrieval, which restricts the widespread adoption of this technique and may disrupt the ecosystems being studied. In addition, these devices have the potential to introduce hazardous substances during their use and eventually contribute to electronic trash, hence exacerbating environmental pollution. To this end, biodegradable sensors represent a promising solution [18]. Constructed only from materials that undergo safe decomposition upon usage, these sensors will possess the capability to exceed existing constraints by facilitating extensive, enduring data collection while minimising their ecological impact [18].

1-3 Motivation and Research Objective of the Project

This research establishes the groundwork for the development of a fully biodegradable, wireless passive microphone for monitoring biodiversity. This study is driven by the need for audio devices that can decompose naturally and the constraints of existing technology, presenting the research question,

Can Passive Acoustic Monitoring be achieved with a fully biodegradable batteryless audio recording device, while enabling wireless powering and data retrieval?

While the ultimate goal is a fully functional biodegradable device that is capable of passive acoustic monitoring with wireless powering and data retrieval, this project will focus on establishing the essential building blocks.

The objective of this project is to establish the core functionalities of the microphone. This includes conducting extensive simulations to comprehend the design principles, optimization the microphone's performance for passive acoustic monitoring and fabricating a first prototype using biodegradable material and preparation for testing.

1-4 List of Requirements for the Project

Based on the motivation and research objective of the project the following list of requirements was formulated,

- **PR-01**: **Design** - Identify a microphone design allowing for passive battery-less wireless operation
- **PR-02**: **Materials** - Identify the biodegradable materials compatible with the selected design, to fabricate a biodegradable microphone
- **PR-03**: **Simulations** - Identify the key parameters influencing the microphone properties to provide input and guidance for future steps
- **PR-04**: **Fabrication** - Fabricate a functional biodegradable prototype ready for testing
- **PR-05**: **Readout setup** - Propose a wireless setup to characterize the microphone

1-5 Organisation of the Thesis

Building on the motivations and research objectives outlined in Chapter 1, Chapter 2 lays the groundwork for the audio monitoring device. This chapter begins with a comprehensive review of various microphone types, providing a foundation for understanding the available options. Following this review, the chapter delves into the design considerations for the device and examines the Great Seal Bug, the inspiration for the proposed design. Through an thorough examination of the Bug's working principles and design, the chapter lists details that will be incorporated into the new device.

Having explored the available microphone technologies and the Great Seal Bug's design, Chapter 2 concludes by outlining the material selection process for the material to be used in the fabrication of the device.

Chapter 3 then delves into the theoretical concepts of the chosen design. This chapter explores the concepts of resonance, resonators, cavities resonators, antennas, amplitude modulation (AM), and backscatter wave technique. Understanding these principles is crucial for understanding and optimizing the device's functionality.

Chapter 4 builds upon the theoretical framework established in Chapter 3. It presents an extensive series of simulations conducted to optimize essential parameters of the device. These simulations will provide valuable insights and a full understanding of the device's behaviour before fabrication and characterisation.

Chapter 5 translates the design and theoretical concepts into a tangible prototype. This chapter details the design and outcomes of the fabricated prototype, aptly named "The BioThing." Additionally, it outlines the plan for characterizing and setting up the device, ensuring its proper functionality.

Finally, Chapter 6 presents concluding remarks and an outlook for future steps of the project. It summarizes the key findings of the project and discusses potential areas for further investigation.

Appendices A and B provide additional information that supports the main body of the work.

Design Selection for a Passive Wireless Biodegradable Microphone

2-1 Microphones

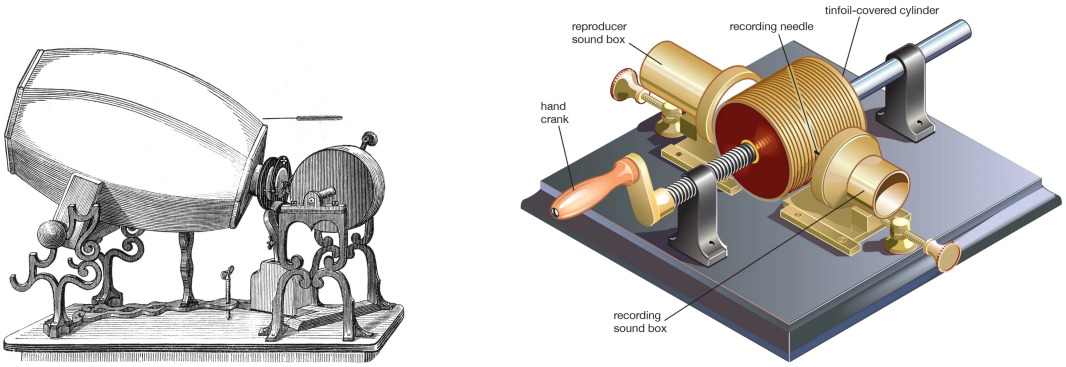
The following sections provide a brief background and insight into the history and various types of microphones.

2-1-1 History

The Industrial Revolution led to a transition in manufacturing techniques, with the majority of handcrafted items being replaced by machine-assisted methods of production. This era sparked significant advancements, prompting scientists and innovators to conceive some of the most remarkable inventions in history. This included endeavours to develop devices with the ability to emulate the functionality of human sensory organs, such as the camera, as well as technologies capable of capturing and reproducing sound.
The first documented device for capturing sound, The Phonoautograph [25] was officially patented in March 1857 by Édouard-Léon Scott de Martinville, a French inventor. Originally, this device was designed as a laboratory instrument for the study of acoustics. However, by 1860, the technology had advanced to the point where it could capture and document a person singing. The original recording of Au Clair de la Lune from 1860 was the first recorded sound presumably sung by Scott de Maatrinville [26] (Click the speaker icon to play when using Adobe Acrobat Reader).
This gave an enormous number of possibilities and motivated other innovators to try their hand towards improving it.

Exploring potential designs for microphones utilizing biodegradable technologies necessitates a return to fundamental principles. This is due to the employment of materials less sophisticated than silicon (Si), prompting consideration of earlier inventions in the field.

In 1878, Thomas Edison obtained a patent for the phonograph [28], a mechanical and analogue device designed for recording and playing back sound. The phonograph had a horn that was connected to a diaphragm. As sound propagated through the horn, it induced vibrations in the diaphragm. A stylus or needle was attached to the diaphragm. The device functioned by rotating a handle, causing the cylinder to spin. This rotation enabled the needle to etch a groove into a thin foil that was wrapped around the cylinder. This facilitated the capture of sound vibrations produced by speech to be etched onto the foil. The phonograph allowed

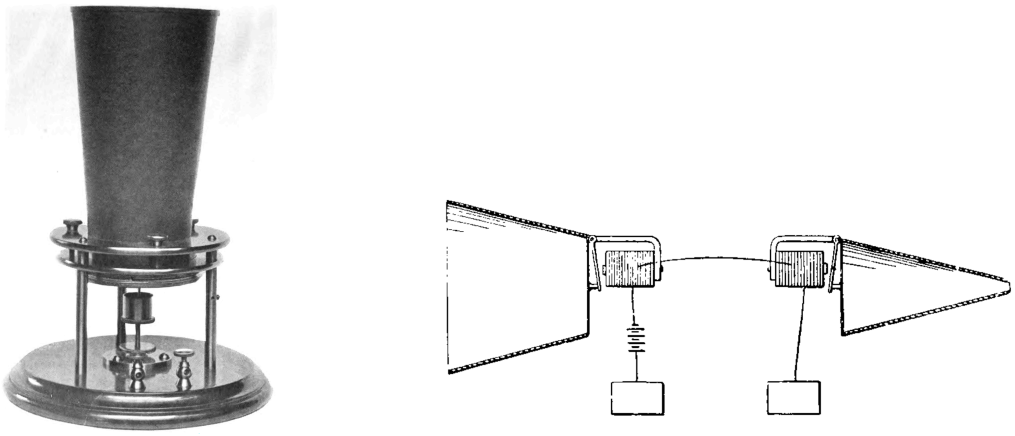


(a) The Early Phonautograph, 1859 [26] **(b)** Thomas Edison's Phonograph of 1877 [27]

Figure 2-1: Early Examples of Mechanical Recording Devices

the playback of the recorded sound. Subsequent improvements were made to this device, which later came to be known as the Gramophone. These two devices were among the initial examples of pure mechanical recording devices. They recorded a specific range of frequencies in the sound spectrum, from around 250 Hz to 2500 Hz.

Alexander Graham Bell received a patent in 1876 for the design seen in Figure 2-2b. In this case [29], the mechanical string was essentially substituted with a wire that carried an electrical current. Audio signals were generated and received using a moving armature transmitter and its corresponding receiver. Similar to the mechanical counterpart, the system supported transmission that could occur either way. The patent also demonstrates the acoustic benefit of using a horn to amplify the driving pressure at the transmitting end and a corresponding inverted horn to enhance the output pressure at the receiving end. Bell's further experiments with the transmitting equipment led to the development of the liquid transmitter, as seen in Figures 2-2a.



(a) Original liquid transmitter microphone [30] **(b)** Bell's original patent [29]

Figure 2-2: Alexander Graham Bell's First Patented Microphone

The subsequent Section 2-2 offers a more in-depth examination of microphone design relevant

to this project.

2-1-2 Types of Microphones

Microphones can be classified based on various criteria. For the purposes of this study, the microphones were categorised based on their functionality.

2-1-2-1 Active Microphones

Active microphones are microphones that necessitate an external power source known as "phantom power", for operation. Phantom power is a conventional method of supplying DC power to active devices via a balanced cable. These microphones typically record sound by a change in capacitance due to the air pressure. Usually, a voltage of 48 volts is applied to both signal wires of the balanced cable. This cable helps to inherently reduce electrical noise [31]. The most notable varieties include [29],

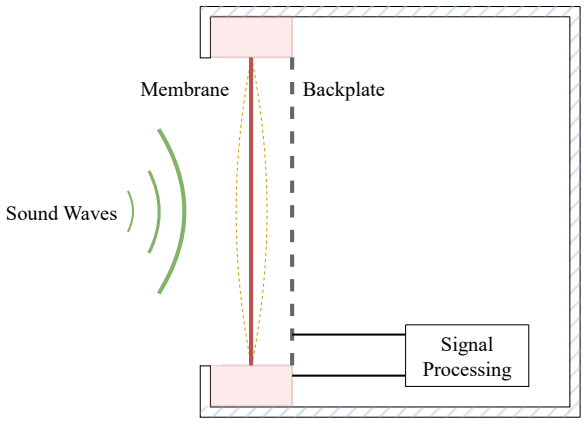


Figure 2-3: Schematic of a condenser microphone [32]

- **DC-biased Condenser Microphones** operate based on the principle of capacitance. This concept entails the presence of a voltage difference between two charged plates that are positioned at a short distance from each other. DC-biased condenser microphones establish their initial charge state by use of an externally provided DC voltage. The use of this bias voltage greatly increases the microphone's sensitivity, enabling it to accurately transform even the smallest changes in sound pressure into electrical signals. The specific value of the applied DC voltage is vital for attaining optimal efficiency and can be adjusted to suit particular purposes [29] [32].
- **RF Condenser Microphones** employ a high-frequency radio broadcast that delivers power directly to the microphone capsule. This eliminates the necessity of a cable connection between the microphone and the power source [29] [31].
- **Electret Condenser Microphones** contain a backplate built from a material that undergoes a unique manufacturing process, which modifies its molecular structure and imparts a constant electrical charge. This inherent charge eliminates the need for an external DC bias voltage [33].

- **Vacuum Tube Condenser Microphones** utilise a vacuum tube to enhance the weak signal generated by a condenser microphone capsule. It is also known as a valve microphone [34].

2-1-2-2 Passive Microphones

As implied by the name, passive microphones operate without the need for an external power source. The functionality is obtained by a variety of innovative technologies that directly convert sound waves into electrical signals. These microphones often possess uncomplicated design, durable build and are capable of withstanding high levels of sound pressure. Listed below are the commonly used passive microphone designs:

- **Dynamic Microphones** employ a moving coil and magnet to produce an electrical signal through the process of electromagnetic induction. Attached to the diaphragm is a tiny, movable induction coil that is present in the magnetic field of a permanent magnet as seen in 2-4. The sound waves cause the diaphragm to vibrate, resulting in the movement of the coil and the generation of a fluctuating voltage across it. Multiple membranes can be employed at various frequencies depending on their intended application. This results in a more intricate design, which eventually leads to higher costs [35] [29].

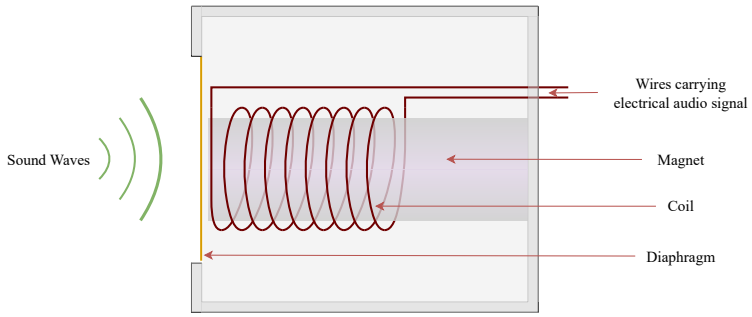


Figure 2-4: Schematic of a dynamic microphone [36]

- **Piezoelectric Microphones** Piezoelectric microphones utilise the inherent property of piezoelectric materials to produce an electric voltage in response to physical strain caused by sound waves. Sound waves induce variations in pressure on the piezoelectric material, resulting in the generation of a voltage that is proportional to the incoming sound pressure. They are often used as contact microphones [37].
- **Ribbon Microphones** utilise a slender piece of corrugated metal ribbon that is suspended within a magnetic field as seen in Figure 2-5. The ribbon vibrates when sound waves strike it within the magnetic field. The ribbon is connected to the output, and the vibration of the ribbon generates a small electric current that is directly proportional to the incoming sound [29].

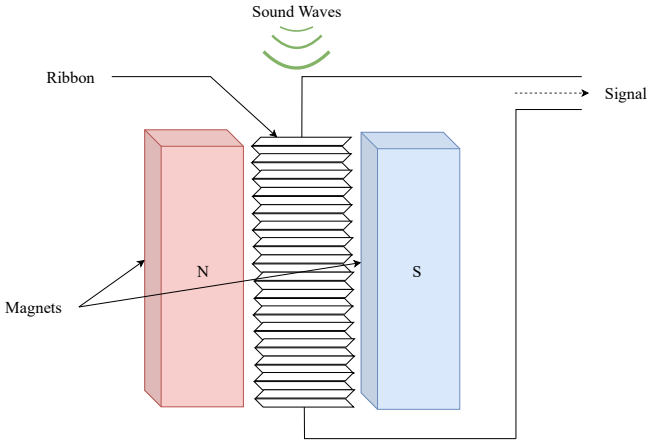


Figure 2-5: Schematic of a ribbon microphone [38]

- **Resonator Cavity Microphones** Certain configurations of resonator cavity microphones can be classified as passive when they depend exclusively on sound waves (and frequency) to generate an electric current within the cavity. These microphones depend on a carefully designed acoustic cavity to trap and vibrate at specific sound frequencies. Subsequently, the confined sound waves have the ability to generate a small electric current inside the enclosed space, transforming the sound pressure into an electrical signal. The microphone's frequency is determined by the design and tuning of its cavity. The working of these types of microphones will be explored in more detail in Section 2-2-1 [39] [40].

2-1-2-3 Unconventional Technologies

- **Carbon Microphones** use an older technology to convert sound waves into electrical signals. Their operation is reliant on the resistivity of carbon granules, which varies with pressure. These microphones typically include a capsule that contains carbon granules that are loosely packed and positioned between two metallic plates as seen in Figure 2-6. One of these plates serves as a diaphragm, which is directly exposed to the incoming sound waves. Sound waves cause vibrations in the diaphragm, which subsequently put varying pressure on the carbon granules. The variance in pressure has a direct influence on the electrical resistance between the plates. Greater sound pressure results in an increased contact area between the carbon granules, causing a decrease in resistance [29]. Conversely, when the sound pressure is reduced, there is a decreased contact area and therefore an increase in resistance. A constant direct current is applied across the plates, resulting in the flow of electric current through the carbon bed. The variations in resistance caused by pressure changes alter the flow of current, resulting in an electrical signal that reflects the characteristics of the original sound wave. However, carbon microphones have restrictions in their capacity to respond to different frequencies and are susceptible to more electrical noise. Their sound reproduction quality is known to be very poor [29].

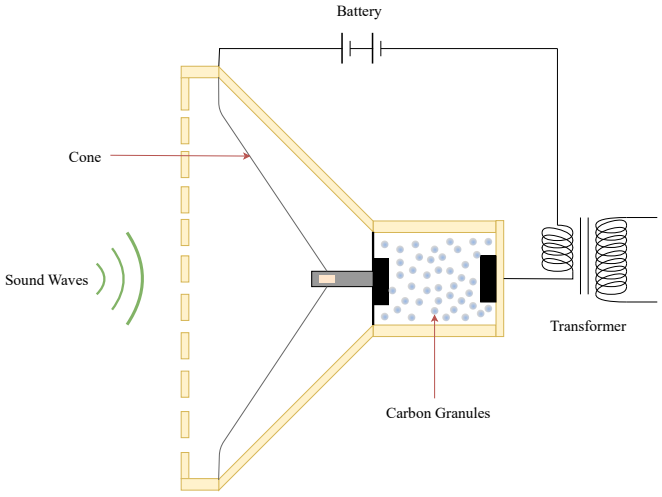


Figure 2-6: Schematic of a carbon granule microphone [41]

- **Fiber-optic Microphones** utilises variations in light, induced by sound waves to transform acoustic waves into an electrical signal. Typically, a beam of light emitted by a laser passes through an optical fibre in order to illuminate the surface of a reflecting diaphragm. The diaphragm's sound vibrations adjust the light's intensity by reflecting off the diaphragm. The modulated light is transmitted through a second optical fibre to a photodetector, which converts the modulated light into audio signals for transmission [42].
- **Laser Microphones** utilise lasers to detect and measure vibrations caused by sound on a remote target. The laser beam is reflected off the target, and any motion induced by sound waves modifies the parameters of the reflected beam. The sound information can be reconstructed by analysing these variations using the microphone. Laser microphones are highly effective at catching sound over extended distances or in dangerous conditions. Various laser microphones are currently being explored, including a device that utilises a laser beam along with smoke and vapour to detect sound vibrations in the free air. Sound pressure waves induce perturbations in the smoke, resulting in fluctuations in the amount of laser light detected by the photodetector [43].
- **Liquid Microphones** employ variations in sound wave pressure to generate vibrations within a chamber filled with liquid [29]. Subsequently, these vibrations can be transformed into an electric signal using different techniques, such as piezoelectric elements or changes in optical characteristics. Liquid microphones possess distinctive characteristics for capturing underwater sound or for applications that demand exceptional sensitivity. An early instance of this can be seen in Alexander Graham Bell's aforementioned microphone design shown in Figure 2-2a.
- **MEMS Microphones** utilise the technique of miniaturised mechanical components. A MEMS microphone commonly integrates a micro/nano pressure-sensitive diaphragm that is etched on to a silicon chip. The vibration of the diaphragm, caused by sound waves, is transformed into an electrical signal by the utilisation of several techniques, often based on capacitive principles. MEMS microphones are extremely compact, energy-efficient, and may be seamlessly incorporated into a wide range of devices [44].

- **Plasma Microphones** employ a plasma arc of ionised gas to capture sound. The sound waves induce pressure variations within the plasma, which can then be recognised through changes in electrical characteristics or the emission of light. Plasma microphones are currently still being developed, but they have the potential to provide benefits in challenging conditions or for collecting sounds with extremely high frequencies [45].

Several microphone designs were studied to determine which style would be most suitable for modification into a biodegradable variant. After considering various design styles, it became apparent that resonator cavity-style microphones are ideal for being adapted into a design that utilises biodegradable materials. The following section provides a more comprehensive analysis of this particular style of design.

2-2 Design Selection

The development of microphones utilizing biodegradable materials presents a unique challenge. Compared to established microphone technologies often based on mature integrated circuits (ICs), biodegradable materials currently offer less advanced functionalities. Consequently, focusing on simpler design principles employed in earlier microphone inventions becomes a strategic approach. This aligns well with the project's goals of facilitating the fabrication process using biodegradable materials and achieving a passive wireless design.

A review of potential design options revealed the following key limitations.

- **Power Requirements**: Dynamic, ribbon, piezoelectric, MEMS and plasma microphones all require additional power and do not align well with the battery-less goal of the project.
- **Design Complexity**: Laser and fibre-optic microphones are still in development and may require additional components to achieve efficiency. These may not be suited for biodegradable materials.
- **Environmental Considerations**: Liquid microphones can be bulky and may not be suited for portability. Additionally, the liquids used in the design might introduce further environmental concerns in the fragile environment.

Following a comprehensive evaluation of various design options, a resonator cavity emerged as the most suitable choice based on its compatibility with the high-level system requirements outlined below.

System Requirements

SR-01: The system should be biodegradable
SR-02: The system should be able to degrade in nature
SR-03: The system should have an operating distance of 100m
SR-04: The system should operate despite scattering elements in the ecosystem
SR-05: The system should facilitate an option to be miniaturized in later versions
SR-06: The system should facilitate an option to explore long-distance operation

2-2-1 Microwave Cavities for Audio Monitoring

Microwave cavities, also known as RF cavities, are metallic enclosures that are specifically built to contain electromagnetic fields at particular resonance frequencies. These cavities have a similar function to that of organ pipes in terms of transmitting sound waves. Electromagnetic wave resonance can occur in any confined environment that has conductive walls. The cavity exhibits distinct resonance frequencies when activated by external electromagnetic fields. In this volume, there is a periodic interchange of electric and magnetic energy, which establishes a resonant condition. The method entails the modulation of a microwave carrier signal using sound waves. Subsequently, the microwave cavity, which is tuned to the carrier frequency, can detect this modulated signal [46] [47].

The following Section 2-2-2 presents the design and functionality of such a resonator cavity microphone.

2-2-2 The Thing (Great Seal Bug)

The Great Seal Bug, also known as "The Thing", was the brainchild of Léon Theremin, also the creator of the Theremin (an electronic musical instrument controlled without physical contact by the performer using a proximity sensor) [48]. The mechanism used is the modulation of backscattering electromagnetic waves, which is similar to that of a passive microphone as it reflects the incoming wave. The Great Seal Bug is a passive communication device which does not consist of a battery, constant power supply or any active components. It was housed in a wooden model of the Great Seal of the United States as seen in Figure 2-7, giving it the name.

A more detailed insight into the background and history of the bug is given in Appendix A



Figure 2-7: Wooden Housing of The Great Seal Bug [49]

2-2-2-1 Physical Description

The bug comprises a resonant cavity, combined with a condenser microphone. Figure 2-9 shows a reverse-engineered model of the Great Seal Bug constructed from various data from publications and the original FBI report [50] technical drawing is shown in Figure 2-8.

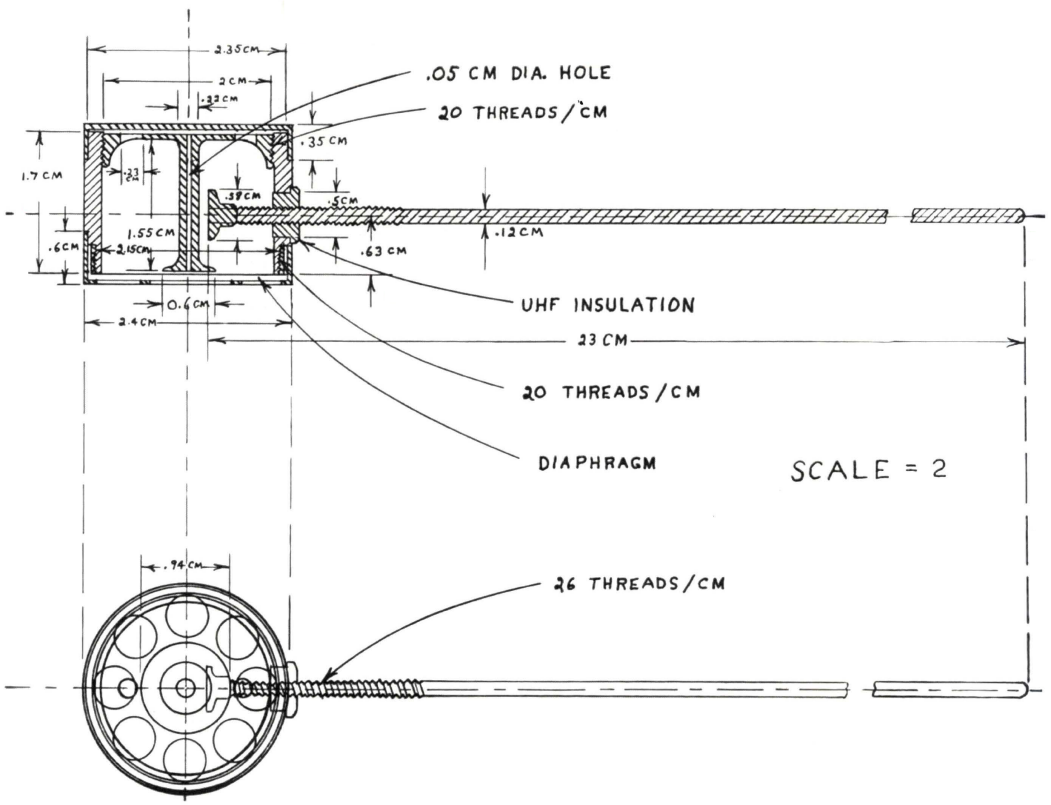


Figure 2-8: Technical Drawing from FBI Report [50]

- The device is machined from a copper cylinder and polished silver plated interior. It weighs 31.4 grams. The device itself has a diameter of 24mm and is 19mm long.
- Due to the polished silver the microwave re-entrant resonant cavity exhibits a High-Q, and has an inner diameter of 19.7mm and a height of 17mm.
- Within the cavity, there is a Tuning Post, with an adjustable mushroom-shaped disc with a diameter of 6mm with a flat but grooved surface on one end, which serves as one plate of the capacitor. This is about 15mm long and fits into a wide threaded rim base. This threaded rim fits into the internal threaded section at the closed end of the cavity.
- The other plate is the membrane which is approximately $6.35\mu m$ according to the report [50], which covers the open end of the bug. This acts as the Diaphragm.
- The distance between the diaphragm and the tuning post has exhibited various measurements in different studies. Nevertheless, the CIA's report on the lab results report [51] states that the gap measured around 230μm.
- A rod with a diameter of 1.2mm and 230mm length is inserted through a hole in the side of the cavity, the centre of which is 6.3mm from the open end of the cavity. This acts as the Antenna. The antenna is capacitively coupled to the circuit.
- There is an insulator which is threaded along with the rod that fits into this hole in the cavity.
- The device is covered with a slip-fit brass grill on the side of the affixed membrane and sealed off on the threaded side of the cavity.
- The above description corresponds to the Figures 2-9 and 2-10.

According to the report [52], this device has an estimated theoretical operational range of around 25 km in an ideal free space without any obstacles. Nevertheless, after accounting for variables such as the presence of walls and other barriers, a distance of 20 metres was used in the testing of the device while conducting the experiments.

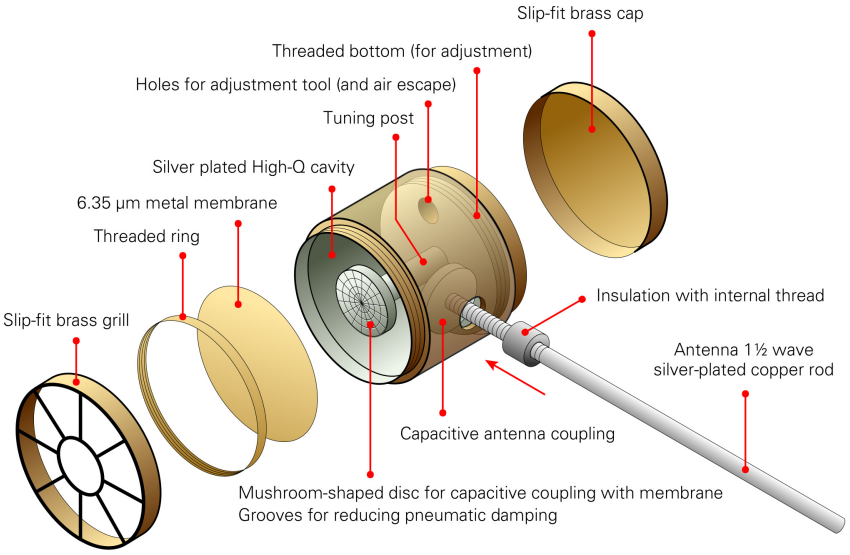


Figure 2-9: Reverse-Engineered Model of Great Seal Bug [40]

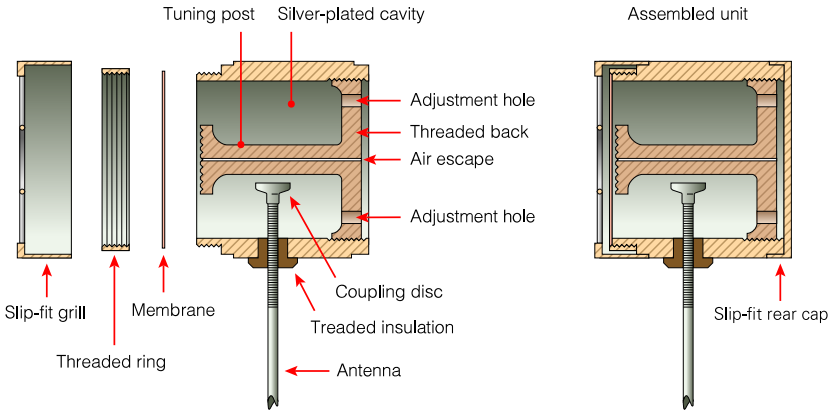


Figure 2-10: Cross-Section of Great Seal Bug [40]

2-2-2-2 Working

The Great Seal Bug is essentially a resonant circuit made from distributed elements. The circuit diagram and working as seen in Figures 2-11 and 2-12 show that the device is a distributed element resonant circuit. This kind of circuit will have minimal losses and a higher Q factor. The losses that do exist are due to ohmic losses and the skin depth (as seen later in the thesis). This was made even lower by using a lot of surface area and low resistive loss material such as silver was used to polish the inside of the cavity.

Figure 2-11 illustrates the theoretical representation of the resonant cavity microphone, which

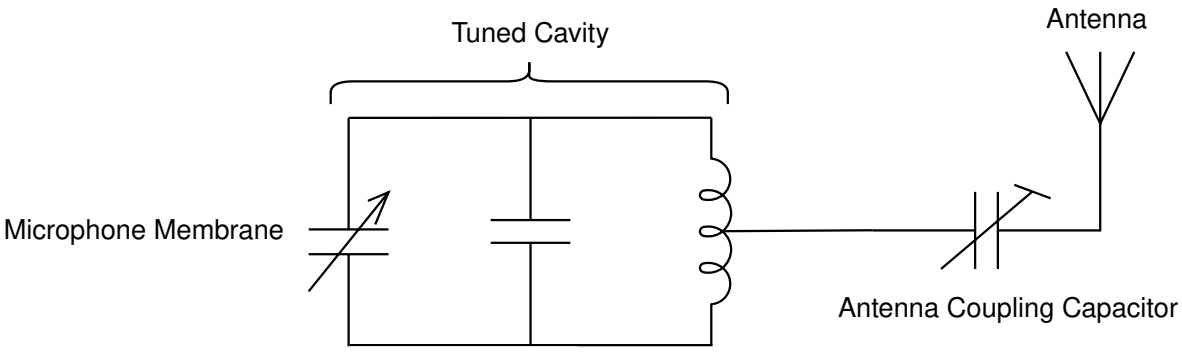


Figure 2-11: Equivalent circuit diagram of Great Seal Bug

is essentially a tuned circuit comprising an inductance and a capacitance. A portion of the capacitance is adjustable since it functions as a microphone. The antenna is connected to the tuned circuit using a capacitive coupling. This capacitance is also variable. In the given case as observed in Figure 2-12, the antenna captures a carrier wave that is emitted by a radio transmitter. The carrier wave has a frequency that is very close to the resonance frequency of the tuned circuit it is connected to. The antenna re-radiates a portion of the intercepted energy. The magnitude of the re-radiated energy is directly correlated with the impedance of the tuned circuit. Significantly, the impedance of the tuned circuit experiences a dynamic variation as the operating frequency gets closer to and passes through the resonant point.

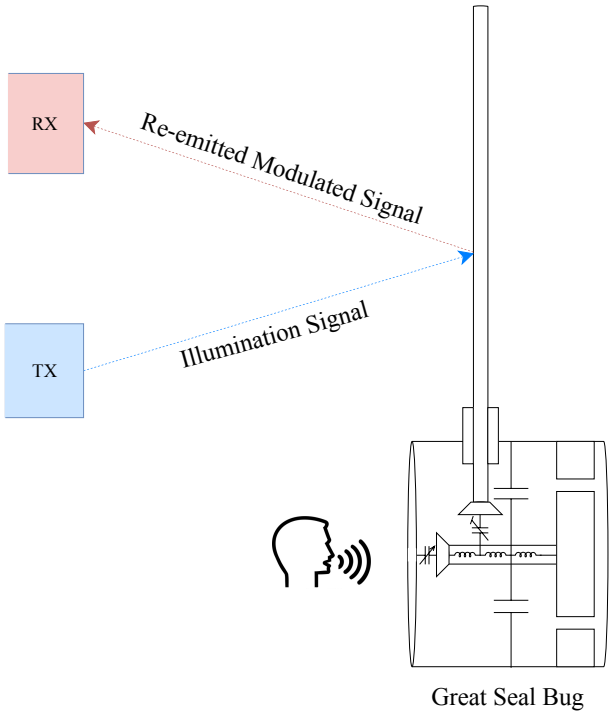


Figure 2-12: Working principle of Great Seal Bug

Essentially, when a directional signal with a high frequency is aimed at the antenna of the device, it is illuminated. The sound waves induce vibrations in the thin membrane, resulting in the low-frequency signal overlapping and re-emitting a portion of the wave. Modifications to this impedance result in changes to the magnitude of the re-emitted radio wave. The outcome can be observed as the amplitude modulation (AM) of the re-radiated radio wave [40].

2-3 Material Selection

This section explores the selection process for the microphone's biodegradable material. Biodegradable materials degrade in a controlled manner within a reasonable timeframe, ultimately minimizing environmental impact. Three commonly used biodegradable metals, iron (Fe), magnesium (Mg), and zinc (Zn), were investigated for their suitability based on the following key requirements:

Material Requirements

MR-01: The material must be biodegradable
MR-02: The material must have high conductivity
MR-03: The material must facilitate efficient manufacturing.

Given that most research on biodegradable technologies prioritizes medical applications, especially those implanted within the body (in-vivo), this section explores potential connections to this project by drawing from relevant information in sources focused on this area. These sources include [53]–[59].

2-3-1 Degradation mechanism

The biodegradability of these metals is due to their high susceptibility to dissolution in water-based environments like soil moisture or pore water that can be found in forests. This process can be controlled to occur at a desired rate.

Another factor to consider when selecting a biodegradable metal for a forest environment is its standard electrode potential (SEP). SEP indicates a metal's tendency to lose electrons during an electrochemical reaction, with lower SEP values corresponding to faster degradation in water-based environments as they lose electrons more easily accelerating the electrochemical reactions. Measured against the standard hydrogen electrode (0V), lower SEP values indicate a greater tendency to oxidize. Magnesium has a negative SEP (-2.37V) compared to Zinc (-0.763V) and Iron (-0.440V). As we see Mg is the easiest to oxidize followed by Zn and then Fe [53].

The rate of biodegradation can be modulated by the pH of the surrounding environment. pH is a measure of the concentration of hydrogen ions (H^+) in a solution. A lower pH indicates a more acidic environment (higher H^+ concentration), while a higher pH indicates a more basic environment (lower H^+ concentration) [60]. Acidic environments (with lower pH) can accelerate the degradation process by increasing the rate of metal oxidation because increased H^+ concentration can enhance the dissolution of metal cations from the surface.

Basic environments (higher pH) can slow down the degradation process because as the pH increases, the formation of a metal hydroxide layer on the surface becomes more favourable. This layer can passivate the metal surface hindering further oxidation and degradation [60].

Corrosion, an electrochemical process involving metal oxidation, also plays a role in the breakdown of biodegradable metals in forests. Similar to the body, these metals undergo oxidation, generating positively charged ions and releasing electrons (as represented in Equation 2-1). These freed electrons can then participate in reduction reactions, influencing the entire degradation process.

The specific reactions in the body can be categorized as either water reduction or oxygen reduction depending on the material. For instance, magnesium-based materials primarily undergo water reduction (Equation 2-2), while iron-based materials favor oxygen reduction (Equation 2-3). These reactions generate hydroxide ions (OH^-), which can react with metal cations to form a metal hydroxide layer on the surface (Equation 2-4).

This is represented in a series of equations [54],

Immediately after contacting the body fluid, the biodegradable metal is oxidized into metal cations,

$$M \rightarrow M^{n+} + ne^- \quad (anodic\ reaction) \tag{2-1}$$

The generated electrons are consumed by a cathodic reaction corresponding to the water reduction for Magnesium-based materials,

$$2H_2O + 2e^- \rightarrow H_2 + 2OH^- \quad (cathodic\ reaction) \tag{2-2}$$

and the dissolved oxygen reduction for Iron-based materials

$$2H_2O + O_2 + 4e^- \rightarrow 4OH^- \quad (cathodic\ reaction) \tag{2-3}$$

The galvanic coupling reactions initiated by the potential difference between the metal matrix and intermetallic phases, or grain boundaries, are not localized but rather occur ubiquitously across the entire coupled surface.

$$M^{n+} + nOH^- \rightarrow M(OH)_n \quad (product\ formation) \tag{2-4}$$

For example, let us consider the element zinc (Zn). Upon being implanted, zinc easily undergoes oxidation, as shown in Equation 2-1. The initial anodic reaction entails the liberation of electrons (e^-) from the metal, resulting in the conversion of the metal into positively charged zinc cations (Zn^{2+}). Subsequently, these freed electrons actively engage in cathodic reactions, influencing the entire degradation process. Contrary to magnesium-based biodegradable metals that mainly undergo water reduction, zinc has a more intricate cathodic behaviour. Although water reduction (Equation 2-2) is possible, the existence of dissolved oxygen can result in an alternate cathodic pathway that involves oxygen reduction (similar to Equation 2-3 for iron). The dominant reaction is contingent upon multiple elements within the physiological environment.

By following both potential cathodic pathways, hydroxide ions (OH^-) are produced. Subsequently, the hydroxide ions undergo a reaction with the zinc cations, as depicted in Equation

2-4, resulting in the formation of a zinc hydroxide layer on the metal's surface. The interconnected reactions highlight the crucial importance of electrochemistry in facilitating the breakdown of zinc and other metals that can be broken down by biological processes in the body or potentially liquids that can simulate body fluid.

While the explanation discusses the mechanism in the body, and in a broader sense be compared to water-based environments, the metal in forests can experience slower degradation owing to lower and less consistent temperatures. Other factors like oxygen availability and so on can influence the dominant cathodic reaction (water vs. oxygen reduction). Furthermore, the presence of specific ions in forest environments can lead to the formation of metal-ion complexes, impacting the degradation process.

2-3-2 Biodegradable Metals

This research investigated Iron, Magnesium, and Zinc, which are among the most commonly utilised biodegradable metals, especially in the biomedical sector. The following sections provide basic concise information about each metal.

Material	**Basic Properties**	**Electrical Conductivity (S/m)**
Iron (Fe)	- Density: 7.87 g/cm^3 - Melting Point: 1538°C - Boiling Point: 2861°C - Malleable and ductile at high temperatures - Ferromagnetic	10.0 x 10^6
Magnesium (Mg)	- Density: 1.74 g/cm^3 - Melting Point: 650°C - Boiling Point: 1107°C - Lightweight and strong - Hexagonal close-packed crystal structure	2.1 x 10^7
Zinc (Zn)	- Density: 7.14 g/cm^3 - Melting Point: 419.5°C - Boiling Point: 907°C - Brittle at room temperature	1.7 x 10^7

Table 2-1: A comparison of material properties among biodegradable materials

2-3-2-1 Zinc (Zn)

Zinc shows great potential as a material in the field of biodegradable metals. It is classified as biodegradable due to its inherent ability to undergo corrosion or decomposition over a period of time. This is a key factor contributing to its extensive adoption in the biomedical industry. The residual byproducts of zinc degradation are naturally eliminated. Zinc exhibits a high

degree of bio-compatibility, as it is easily tolerated in regulated quantities. Zinc in its pure form has inherent limits as a material. It benefits from the mechanical strength and stiffness, despite the challenges they provide in the biomedical field. Combining zinc with components such as magnesium allows for the creation of a biodegradable alloy.

The degradation of Zn will lead to products of this degradation to react with the soil and could potentially influence the ecosystem. As Zn degradesm it dissolves and releases Zn ions (Zn^{2+}) into the soil's pH. At a lower pH, Zn^{2+} can move freely in the soil because the soil particles are positively charged at a lower pH repelling the Zn^{2+} facilitating movement which affects its bioavailability. However, components in the soil like clay minerals and organic matter can bind the Zn^{2+} ions depending on the soil chemistry, beneficially reducing the mobility and preventing the Zn^{2+} from reaching plants or microbes at toxic levels. While zinc is an essential micronutrient, exceeding a threshold can hinder plant growth [61].

The corrosion formula for zinc is as follows:

$$Zn(s) + 2H^{+}(aq) + 2Cl(aq) \rightarrow ZnCl_2(aq) + H_2(g)$$
$$Zn \rightarrow Zn^{2+} + 2e^{-}$$

The rate of corrosion of zinc in an immersion test is 0.08 mm/year and 0.02mm/year in vivo [53].

2-3-2-2 Magnesium (Mg)

Magnesium degrades at a faster and more controllable in the body rate compared to other materials, making it suitable for use in cases like medical implants. However, its lower mechanical strength, particularly its softness, compared to other materials makes it difficult to work with during the fabrication process. While magnesium alone might not be ideal, it shows promise when combined with other elements like iron. Further research is needed to overcome these limitations and ensure biocompatibility. This could be a potential option for future developments.

This controllable degradation property also makes magnesium interesting for environmental applications. Similar to zinc, the degradation of magnesium (Mg) in a forest environment leads to the formation of byproducts that interact with the soil and potentially influence the ecosystem. As Mg degrades, it dissolves and releases Mg^{2+} ions into the soil. The mobility of these ions depends on soil properties, especially pH. At lower pH, Mg^{2+} is more mobile, potentially increasing its bioavailability for plants.

Similar to Zn, soil components like clay minerals and organic matter can adhere to Mg^{2+} or cause them to precipitate depending on the soil chemistry. This can limit Mg^{2+} mobility and reduce the impact on the surrounding environment. Mg is a crucial macronutrient essential for plant growth. However, high concentrations of Mg^{2+} in the soil might disrupt the uptake of other essential cations like Ca^{2+} (calcium) by plant roots, potentially altering the nutrient balance. Mg^{2+} is generally beneficial for most soil microbes as it is a vital element for their growth and metabolic processes.

The corrosion formula for magnesium is as follows:

$$Mg(s) + 2H_2O(I) + O_2(g) \rightarrow Mg(OH)_2(s)$$
$$Mg \rightarrow Mg^{2+} + 2e^-$$

The rate of corrosion of Mg in an immersion test is 0.10 ± 0.07 mm/year [53].

2-3-2-3 Iron (Fe)

Iron, although its breakdown rates vary across environments, plays a role in the development of biodegradable technologies due to its potential for controlled degradation and lower environmental impact compared to some traditional materials. Fe offers good mechanical strength and is readily available, making it a common construction material. However, it rusts easily when exposed to moisture and oxygen, requiring protective coatings or being used in controlled environments.

While SEP offers a theoretical ranking, it is not the sole determinant of degradation rate. Other factors include surface properties and the specific environment play a significant role. Fe exhibits complex degradation behaviour due to its ability to exist in multiple states (Fe^0, Fe^{2+}, Fe^{3+}). Here as well, the environment plays an important role.

In a forest, Fe degrades slower compared to Zn and Mg. This is partly due to its higher SEP value (less tendency to oxidize), than Zn and Mg. The specific oxidation state can significantly impact its degradation rate. Fe^0 (metallic iron) is more susceptible to oxidation and degradation than Fe^{2+} and Fe^{3+} ions. Factors like soil pH, oxygen availability and the presence of specific ions (like chloride) can significantly influence Fe's degradation rate in a forest environment. Acidic environments can accelerate iron degradation.

An important factor to consider is that Fe readily forms rust in the presence of oxygen and moisture. While rust itself is relatively stable, factors such as soil pH, and microbial activity influence can break it down further. This breakdown releases byproducts like Fe^{2+}, which is a vital micronutrient for plants in small quantities.

The corrosion formula for Iron is as follows,

$$Fe(s) + 2H_2O(I) + O_2(g) \rightarrow Fe(OH)_2(s)(Rust)$$
$$Fe \rightarrow Fe^{2+} + 2e^-$$

The rate of corrosion of Fe in an immersion test is 0.012 mm/year [53].

2-3-3 Selection of Biodegradable Material for the Microphone

All three metals, zinc (Zn), magnesium (Mg), and iron (Fe), are good options for biodegradable technologies due to their ability to degrade over time. They offer advantages over other biodegradable materials as they are metals and are good conductors as seen in Table 2-1. All three metals are naturally occurring elements, making them suited for the objective of this project. Additionally, their degradation products can contribute essential nutrients for plant growth in controlled amounts.

A key difference lies in their degradation rates within a forest environment. Magnesium seemingly degrades the fastest, with its breakdown byproducts readily contributing to plant uptake and has the best conductivity among the three. However, the fabrication process for the proposed design may prove difficult as Mg is soft and difficult to work with. Iron degrades slower than Zn and Mg and exhibits complex behaviour influenced by factors like soil pH and its oxidation state. In forests, Fe generally degrades slower than zinc and magnesium. While this slower degradation can be beneficial for longer-lasting applications, it does not align with the objectives of this project. Zinc finds a middle ground, offering a controllable degradation rate and good conductivity and the metal itself is easy to work with during the fabrication process.

Zinc was selected as the material for the proposed design based on the fulfilment of the material requirements mentioned at the beginning of the section, as it is biodegradable, has high conductivity, is easy to work with and is readily available.

Theoretical Background

3-1 Resonance and Resonators

3-1-1 Resonance

Resonance is the occurrence of an object vibrating or oscillating in response to oscillations at a frequency that corresponds to or closely matches its resonant frequency [39]. It occurs when a system exhibits its highest interaction with electromagnetic radiation at a specific frequency. The resonant frequency, in the context of resonators, refers to the specific frequency at which a resonator exhibits a high absorption or emission of electromagnetic radiation. Some key characteristics include that,

- They exhibit a propensity to oscillate at a certain frequency and its higher harmonic frequencies, which are multiples of the fundamental frequency.
- They exhibit spatial standing waves

The objects and systems inherently vibrate at a definitive frequency known as the resonant frequency or natural frequency. The resonant frequency is dictated by various physical features of the resonator, including its dimensions, shape and material [62].

3-1-2 Resonators

Resonators are essential elements used for selecting, amplifying, or filtering specific frequencies of electromagnetic (EM) waves. They utilise the concept of resonance, in which a system exhibits a significantly greater amplitude of vibration at its resonant frequency in comparison to other frequencies.

The applications of EM Resonators include,

- **Filters:** Resonators are employed in communication systems and radio circuits to selectively transmit desired frequencies while blocking unwanted frequencies. This capability is crucial to isolate particular channels and minimise signal interference.
- **Oscillators:** Resonators can play a vital role in oscillator circuits which generate electromagnetic waves with a specific frequency. This component is utilised in radio transmitters, clock circuits, and various other applications that require a consistent and accurate frequency.
- **Antennas:** Resonators function as effective receivers of electromagnetic waves because they inherently filter unwanted frequency bands.

The efficacy of a resonator depends on a critical parameter known as the quality factor, or Q-factor. A greater Q-factor indicates a resonator that is more selective, meaning it effectively resonates with a narrow range of frequencies. This will be explored in the upcoming section.

3-1-3 Q-factor

The Q-factor is a significant measure of performance for a resonant circuit. The Q-factor quantifies the ability of a resonant circuit to store electromagnetic energy while also accounting for the waste of energy as heat. The bandwidth of a resonator is inversely proportional to its Q-factor as seen in Figure 3-1.

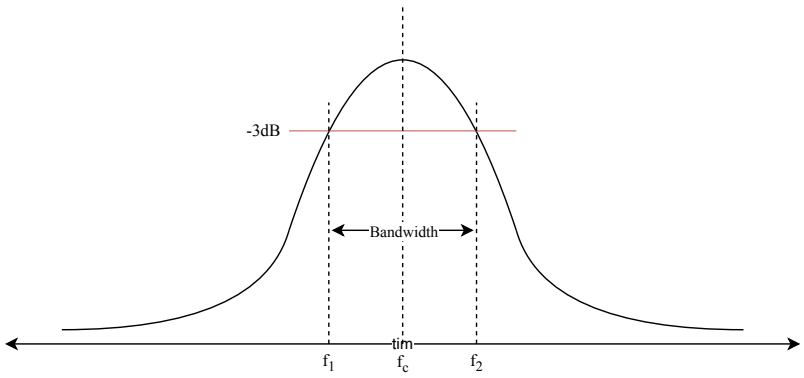


Figure 3-1: Q-factor of resonator [47]

Resonators with an optimal volume-to-surface area ratio are ideal for attaining a high Q-factor [63]. The reason for this is that energy is primarily stored within the volume of the resonator, while energy dissipation occurs at the walls. Hence, resonators such as spheres, cylinders, and prisms could potentially have a bigger Q-factor as compared to resonators with reentrant sections [47].

The Q-factor of a cavity resonator is defined as the ratio of the energy stored in the resonator's fields and the energy lost per cycle, as expressed by the following equation [47],

$$Q = 2\pi \frac{Energy\ Stored}{Energy\ Lost\ per\ cycle} \tag{3-1}$$

As it holds the same level of significance as a lumped resonant circuit, it may be defined as [47],

$$\Delta f = f_2 - f_1 \tag{3-2}$$

$$Q = \frac{f_c}{\Delta f} \tag{3-3}$$

Within the context of resonant cavities, the Loaded Q, Unloaded Q, and External Q all play a role in determining the Total Q-factor of the cavity. These parameters directly affect the cavity's ability to store energy and the sharpness of its resonance.

3-1-3-1 Unloaded Q

The unloaded Q refers to the inherent quality factor of the isolated cavity, disregarding any external factors or connections. It takes into consideration the energy losses occurring within the cavity as a result of factors such as ohmic losses and dielectric losses [64]. The unloaded Q represents the inherent efficiency of energy storage in the cavity. Measuring this directly in practice can be challenging and is typically estimated using simulations or calculations based on other measurable quantities.

The resonant frequency is given by [64]

$$f_0 = \frac{1}{2\pi\sqrt{LC}} \tag{3-4}$$

The unloaded Q-factor is denoted by [64],

$$Q_0 = \frac{2\pi f_0 C}{G_0} \tag{3-5}$$

The finite conductance (G_0) of the resonator causes dissipation of energy.

3-1-3-2 External Q

The External Q represents the quality factor of the external system or load itself, independent of the cavity. This reflects the power losses specific to the external system, such as losses in the antenna [64]. External Q reflects the energy storage efficiency of the external system on its own. It can be calculated from the properties of the external system but is usually not measured directly.

Based on the Equation: 3-5, External Q can be given as [64],

$$Q_{ex} = \frac{2\pi f_0 C}{G_{ex}} \tag{3-6}$$

where,
f_{ex} is almost equal to f_0 as the frequency shift is so small, it is of little consequence [64],
Q_{ex} represents the external Q-factor,
G_{ex} represents the conductance of the load.

3-1-3-3 Loaded Q

The loaded Q-factor is a measure of the overall quality factor of the cavity when it is connected to a load, such as an antenna or circuit. This includes all the losses considered in Unloaded Q, as well as additional losses resulting from external connections such as coupling losses and radiation losses. Loaded Q is the comprehensive energy storage efficiency of the complete system, encompassing the losses caused by the external connections [39], [64]. Measurement of loaded Q is simpler as compared to unloaded Q as it can be obtained by analysing resonant properties using a network analyzer. The addition of load results in a slightly changed resonance frequency of the resonator. Secondly, when an external conductance (G_{ex}) is connected

in parallel with the intrinsic conductance (G_o) of the resonator, the total conductance of the system increases. This rise in total conductance leads to a decrease in the overall quality factor (Q) of the resonator. The resulting Q-factor in this loaded condition is denoted as Q_L. It can expressed as [64],

$$\frac{1}{Q_L} = \frac{1}{Q_0} + \frac{1}{Q_{ex}} \tag{3-7}$$

As observed from the Equation: 3-7, the Loaded Q (Q_L) is always lower than or equal to both Unloaded Q (Q_0) and External Q (Q). The lower the external Q or unloaded Q, the lower the overall loaded Q of the system.

The relationship between unloaded Q and Loaded Q can be written as [64],

$$Q_0 = Q_L(1 + \kappa) \tag{3-8}$$

where κ is the coupling coefficient, which is the ratio of power dissipated in the external circuit to the power dissipated in the resonator [64].

3-2 Microwave Cavities

Microwave Cavities are essentially metallic enclosures that are designed to confine the electric and magnetic forms of energy. The resonators serve as a means to store and dissipate energy. When analyzing the overall performance of microwave cavity resonators, the energy storage arises from confined electromagnetic fields, while dissipation occurs primarily due to ohmic losses in the cavity walls.

Resonance of electromagnetic waves can occur inside any closed surface with conducting walls. When exposed to electromagnetic fields, this type of surface resonates at specific frequencies. The conducting walls surround an area where electric and magnetic energy is stored [46].
A microwave cavity has multiple resonant modes, each with a different frequency. Each mode has a specific pattern for the electric and magnetic fields inside the cavity. The amplitude of the electromagnetic field reaches its maximum at the resonant frequency for a particular mode.

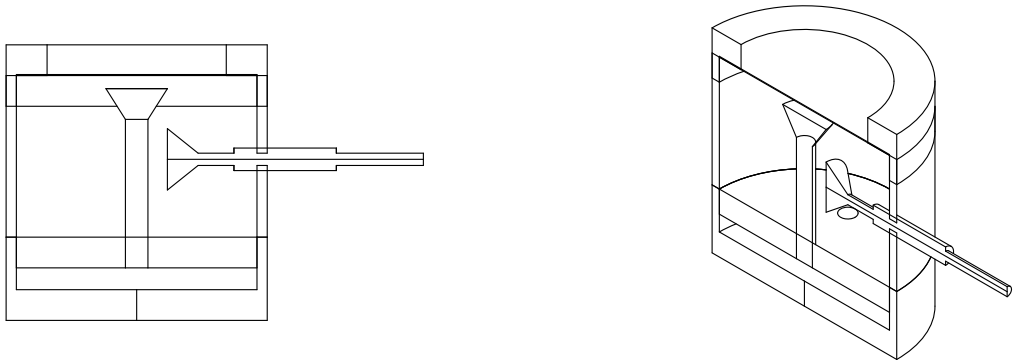
Cavity resonators provide various benefits for high-frequency applications, including simplicity, compact physical size, high Q-factor, lower power dissipation and high shunt impedance compared to other types of resonators (like lumped element resonators) [39].
The Q-factor is a key parameter that influences the storage and dissipation of energy in a cavity resonator. The energy lost can be estimated by calculating the shunt resistance of the cavity. At resonance, the reactive components of the impedance cancel out and only the real part remains which consumes some amount of current and dissipates energy. For a cavity, the shunt impedance is defined in terms of the voltage produced in the cavity for a given power dissipation,

The upcoming section covers the topics of the types of resonators, the Q-factor and its measurement.

3-2-1 Types of Cavity Resonators

The design and dimensions of the cavity resonator have a direct relation to the proposed design's capability to convert acoustic energy into electromagnetic signals. This section contains an analysis of the operational principles, signal transmission efficiency, and effectiveness of the proposed design by investigating the types of cavity resonators.

Delving into the various types of cavity resonators offers valuable insights into how they manipulate sound waves. This knowledge is particularly relevant for understanding the proposed design, as illustrated in Figure 3-2



(a) Front view **(b)** 3D cross-section

Figure 3-2: Illustration of the proposed resonator cavity design

Microwave resonators can be designed using enclosed sections of a waveguide. Due to the fact that the radiation loss from an open-ended waveguide is substantial, waveguide resonators are often short-circuited at both ends to form a cavity resonator. The shape of this cross-section corresponds to the type of cavity resonator. The most popular kinds are listed below [39].

3-2-1-1 Rectangular Resonator Cavity

A rectangular waveguide is a metallic tube with a hollow interior and a cross-section that is rectangular. By enclosing the open sides of a rectangular waveguide with a short-circuiting plate, we can construct a rectangular cavity resonator [39].

It is assumed that a wave is propagating along the z-axis as seen in Figure 3-3. Within the hollow cavity, the excitation can occur in either TE mode or TM mode, depending on the wave equations that exhibit harmonic variations along the z-axis and adhere to the specified boundary conditions.
The electromagnetic field in the cavity resonator must adhere to Maxwell's equations. As per the boundary condition, the electric field's tangential component and the magnetic field's normal component would both be zero [39], [65], [66].

The dominant mode of a rectangular resonator where a > b < d is the transverse electric mode $TE_{mnp} = TE_{101}$. The resonant frequency for any given mode can be calculated as [39],

$$f_r = \frac{1}{2\sqrt{\mu\epsilon}}\sqrt{(\frac{m}{a})^2 + (\frac{n}{b})^2 + (\frac{p}{d})^2} \tag{3-9}$$

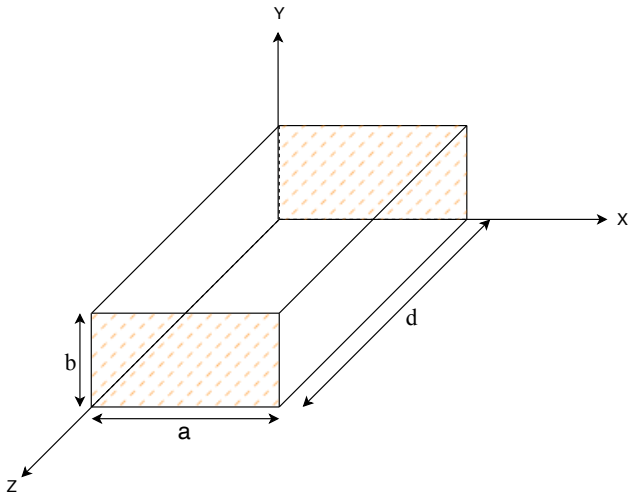


Figure 3-3: Rectangular Cavity Resonator

where,
m=0,1,2,3... Represents the number of half-wave cycles in the x-direction
n=0,1,2,3... Represents the number of half-wave cycles in the y-direction
p=1,2,3,4... Represents the number of half-wave cycles in the z-direction

The dominant mode in a resonator refers to the specific mode of electromagnetic wave propagation that has the lowest cut-off frequency. This indicates that the resonator is most capable of supporting this mode at a specific frequency. This is represented in Figure 3-4 Due to their ability to be generated and transmitted with less loss, lower frequencies are typically the preferred and most commonly used mode in resonators. Therefore, in the case of a rectangular cavity resonator, the TE_{101} mode is the most significant [39].

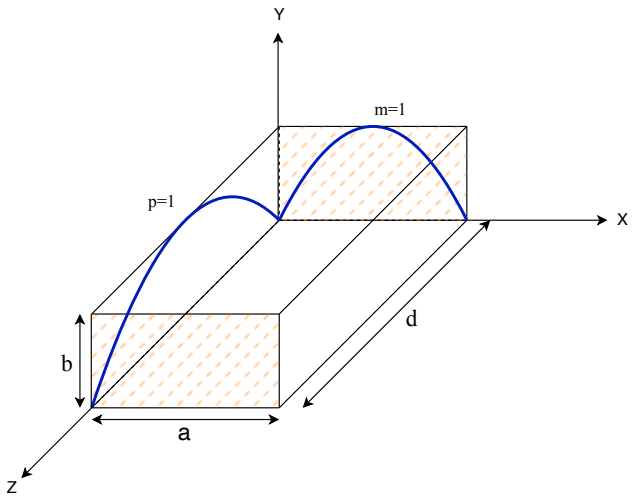


Figure 3-4: TE_{101} mode for a rectangular cavity

3-2-1-2 Cylindrical Resonator Cavity

Similar to the rectangular cavity resonator, a cylindrical cavity resonator can be constructed by shorting both ends of a circular waveguide leveraging the inherent properties of wave propagation for efficient electromagnetic field confinement. TE_{11} mode is the dominant mode for a circular waveguide [39] and offers advantages for signal transmission, including a well-defined field pattern and ease of excitation. However, in a cylindrical cavity resonator, the functionality shifts from efficient signal transmission to effective energy storage. To achieve this, there is a change in the dominant mode. TE_{111} is the dominant mode for a cylindrical cavity resonator [39], and is similar to the TE_{11} mode with an additional variation in the circumferential direction. This variation is represented by the third "1" in the designation, which corresponds to an extra cycle of the EM field around the circumference of the cylinder. This improves the mode's ability to confine EM energy and store it within the cavity.

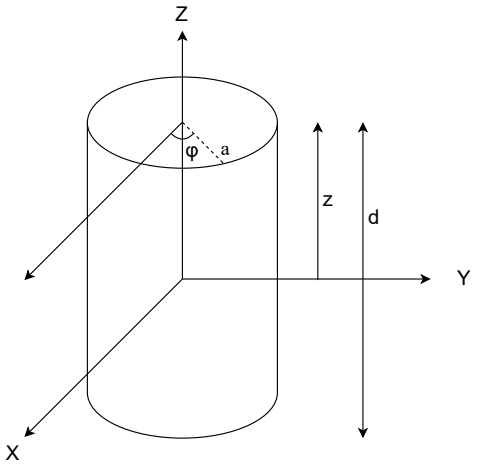


Figure 3-5: Cylindrical Cavity Resonator

The cavity is designed with a top wall that can be moved to adjust the resonance frequency mechanically [39]. Additionally, the cavity is loosely coupled to a waveguide via a small opening. During operation, the cavity will consume power as it shifts to the system's operating frequency. There is often a mechanical tuning ring which can be used to calibrate the frequency. The electrical and magnetic fields inside a circular cavity resonator must adhere to Maxwell's equations When the walls of a waveguide or cavity are constructed from a material with perfect conductivity, such as a PEC, and the surrounding medium is air functioning as a dielectric [39],

$E_t = 0$
$H_n = 0$

- The tangential component of the electric field (E_t) is zero [39], [65]. This is a boundary condition that arises due to the properties of ideal conductors. An ideal conductor possesses infinite conductivity, which implies that any tangentially applied electric field on its surface will generate currents that entirely neutralise the initial field within the

conductor. This results in no net electric field within the conductor. As there is no tangential E-field to drive current flow along the surface of the conductor, there is no loss of energy due to ohmic heating (resistance) within the conductor at the boundary.

- The normal component of the magnetic field (H_n) is zero [39], [65]. This represents an important boundary condition. It indicates that H_n which is perpendicular to the surface of the conductor is considered continuous across the boundary. Although, at high frequency a very thin layer of displacement current can form due to the changing electric field. This can cause a slight discontinuity in the normal component of the H_n field.

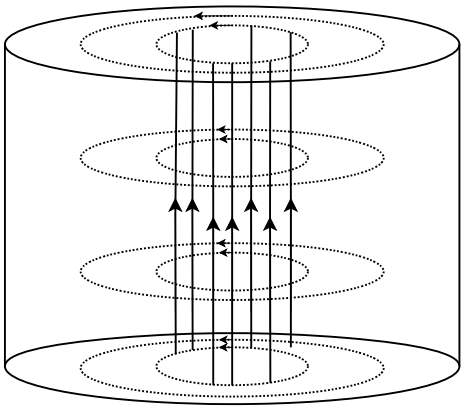


Figure 3-6: Electric and magnetic field of cylindrical cavity resonator [67]

Figure 3-6 illustrates the electric and magnetic fields inside a cylindrical cavity resonator, where the dotted lines represent the magnetic field and the solid lines represent the electric field.

The following equation can be used to determine the equation for resonant frequency corresponding to TE mode and TM mode [66].

$$k^2 = \omega^2 \mu \epsilon \tag{3-10}$$

For TE_{npg},

$$f_r = \frac{1}{2\pi\sqrt{\mu\epsilon}} \sqrt{(\frac{X'_{np}}{a})^2 + (\frac{q\pi}{d})^2} \tag{3-11}$$

For TM_{npg}

$$f_r = \frac{1}{2\pi\sqrt{\mu\epsilon}} \sqrt{(\frac{X_{np}}{a})^2 + (\frac{q\pi}{d})^2} \tag{3-12}$$

where,
n=0,1,2,3... No. of periodicity in ϕ direction
p=1,2,3,4... No. of zeros of field in radial direction

q=1,2,3,4... No. of half waves in z-direction

X_{np} gives the point at which the bessel's function tends to 0 and X'_{np} gives the point where the slope of the function where the function tends to 0. Hence, X_{np} is the p^{th} root of n^{th} order bessel function and X'_{np} is the derivative of X_{np}.

As seen previously, the unloaded Q (Q_0) is the quality factor of the cavity resonator that is not connected to any external load. Q_0 depends on both the conductivity of the cavity material itself and the conductivity of any materials filling the cavity interior. The equation is as follows [67],

$$Q_0 = (\frac{1}{Q_c} + \frac{1}{Q_d})^{-1} \tag{3-13}$$

where,
Q_c is the Q-factor of the metal conducting wall,
Q_d is the Q-factor of the filled material

$$Q_0 = Q_c = \frac{2V}{S\sqrt{\frac{2}{\omega\mu\sigma}}} \tag{3-14}$$

where,
V is the volume of the cavity resonator,
S is the surface area of the cavity resonator,
σ is the conductivity of the metal wall

As seen previously in Equation: 3-7, when the cavity resonator is connected to an external circuit which itself has the Q-factor of Q_{ex}, the external circuit will lower the overall Q-factor of the system. This can be seen below, in continuation with Equation: 3-7,

$$Q_0 = \frac{R}{\omega_0 L} \tag{3-15}$$

$$Q_{ex} = \frac{R_L}{\omega_0 L_L} \tag{3-16}$$

3-2-1-3 Reentrant Resonator Cavity

The information in this section is combined from multiple sources [39], [47], [68]–[70].

Reentrant cavities have similarities with conventional waveguide resonators in that they also function as resonators and are composed of waveguides. However, a reentrant cavity resonator differs from rectangular and circular cavity resonators in that it has a non-uniform cross-section area.
In theory, a resonator has an infinite number of resonating modes, with each mode corresponding to a definite resonance frequency. When the frequency of an input signal matches

the resonant frequency, a standing wave with maximum amplitude is generated and the peak energy stored in the electric and magnetic fields is equal.
A reentrant cavity is characterised by metallic borders that extend into the interior of the cavity. By incorporating protrusions and bulges into a cylindrical cavity, it is possible to create a cylindrical reentrant cavity. To achieve resonance at a desired operating frequency in a reentrant cavity resonator, the electrical properties such as the inductance and capacitance of the cavity can be modified. However, the overall goal is to manipulate the reactance (opposition to current flow) such that it cancels out at the target frequency. Minimizing the reactance at this frequency allows the remaining resistance to determine the cavity's Q-factor. A reentrant cavity design enables a broader spectrum of resonance frequencies in comparison to rectangular or cylindrical cavity resonators.
Nevertheless, the extent of this range is limited and influenced by the physical characteristics of the cavity. The cavity has a finite capacity to accommodate a specific number of distinct resonant modes.

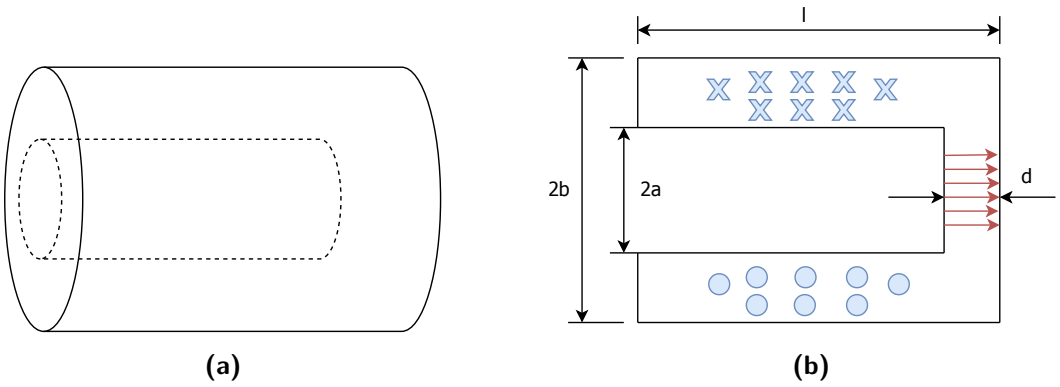


Figure 3-7: A Typical Reentrant Cavity Diagram [68]

Applying the transmission line theory,

$$Z_0 = \frac{1}{2\pi}\sqrt{\frac{\mu}{\epsilon}} l_n(\frac{b}{a}) \tag{3-17}$$

a and b are defined in Figure 3-7b

The input impedance of the shorted line can be given by

$$Z_{in} = j\ Z_0\ tan(\beta l) \tag{3-18}$$

where,
l indicates the length of the reentrant cavity
Substituting the value of Z_0,

$$Z_{in} = j\ \frac{1}{2\pi}\ \sqrt{\frac{\mu}{\epsilon}}\ l_n(\frac{b}{a})\ tan(\beta l) \tag{3-19}$$

The inductance of this cavity is given by,

$$L = \frac{2Z_{in}}{\omega} = \frac{1}{\pi\omega}\ l_n(\frac{b}{a})\ tan(\beta l) \tag{3-20}$$

The capacitance of the gap is given by,

$$C_g = \epsilon \frac{\pi a^2}{d} \tag{3-21}$$

where,
d is the thickness of the gap

At resonance,

$$\omega L = \frac{1}{\omega C_g} \tag{3-22}$$

that is, the inductive reactance is equal to the capacitive reactance

$$\frac{1}{\pi} \sqrt{\frac{\mu}{\epsilon}}\ l_n(\frac{b}{a})\ tan(\beta l) = \frac{d}{\omega \epsilon \pi a^2} \tag{3-23}$$

$$tan(\beta l) = \frac{d}{\omega a^2} \sqrt{\frac{1}{\mu \epsilon}}\ \frac{1}{l_n(\frac{b}{a})} \tag{3-24}$$

$$\omega = \frac{d}{a^2 tan(\beta l)} \sqrt{\frac{1}{\mu \epsilon}} \frac{1}{l_n(\frac{b}{a})} \tag{3-25}$$

$$f_r = \frac{d}{2\pi a^2 tan(\beta l)} \sqrt{\frac{1}{\mu \epsilon}} \frac{1}{l_n(\frac{b}{a})} \tag{3-26}$$

In accordance with Equation: 3-26, increasing the radius of the cavity leads to a lower resonant frequency. This can be interpreted as the increased space available for the magnetic field within the larger cavity, effectively raises the inductance which can also be seen from Equation: 3-20 and consequently lowers the resonant frequency according to the established relationship in Equation: 3-4.

Due to the infinite number of solutions of the tangent function as seen in Equation: 3-24, it can be deduced that there will be an infinite number of frequencies or modes that result in the resonant frequency of a coaxial cavity.

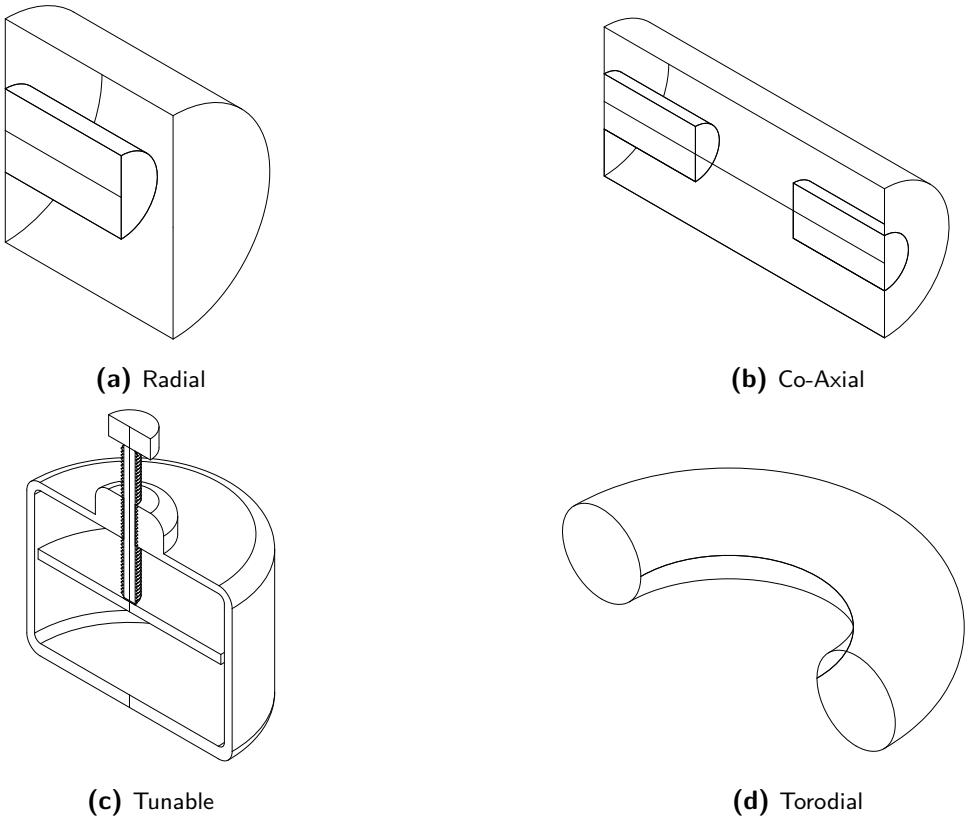
Resulting design considerations

A larger a (as depicted in Figure 3-7b) size results in an increase in capacitance, thereby causing a decrease in frequency. If the distance d (as depicted in Figure 3-7b) is increased, the capacitance will drop and the frequency will increase.

The resonant frequency of a reentrant cavity resonator may be altered by modifying the dimensions, introducing elements that affect its overall reactance, or using a conductive paddle. The resonant frequency of reentrant resonators is highly responsive to the size of the gap between the reentrant parts, particularly when the distance d is small. The resonant frequency

of the system can be influenced by coupling loops, which introduce reactance into the resonator. For example, by positioning a copper paddle inside the resonator to intersect certain field lines 3-10, the resonant frequency may be optimized. Altering the paddle's location as seen in will result in a different outcome. This can be used to modify the resonance frequency [47], [71].

The reentrant cavity can have several shapes as depicted in Figure 3-8:



(a) Radial **(b)** Co-Axial

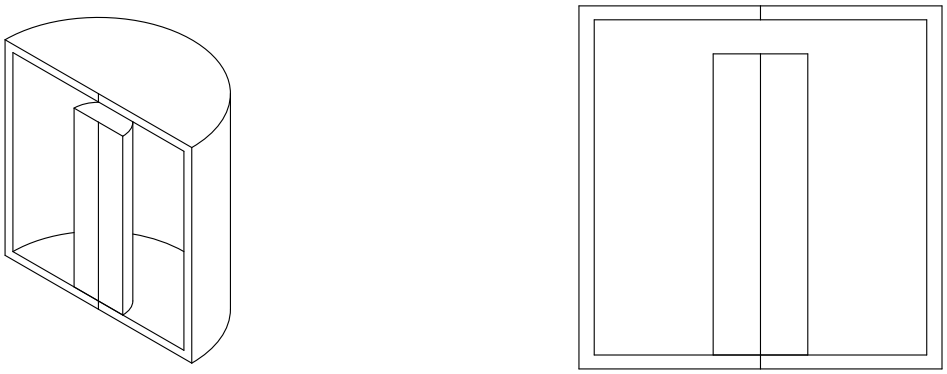
(c) Tunable **(d)** Torodial

Figure 3-8: Types of reentrant cavities

Co-axial cavity resonator

A co-axial cavity resonator is a cylindrical cavity that resembles a finite-length coaxial transmission line. It consists of a central conductor and outer conductor, and the central conductor is is closed at both ends and one end is shorted to the outer conductor, as shown in Figure 3-9. The space between the inner and outer conductor forms a capacitance similar to that of a parallel plate capacitor. Various factors influence the performance of a coaxial cavity resonator. In order to minimise the losses of the electromagnetic wave inside the cavity, it is necessary to ensure that the inner surface is as smooth as feasible. Ensuring a strong short-circuit connection between the inner and outer conductors is crucial [47].

Introducing reentrant structures and altering the cavity's shape will affect the resonance frequency. These cavities are called Evanescent mode cavities. By evanescently loading a cavity,



(a) Co-axial 3D cross-section **(b)** Co-axial Front View

Figure 3-9: Coaxial cavity structure

the frequency may be reduced by an order of magnitude, while maintaining a reasonably high Q-factor [72].

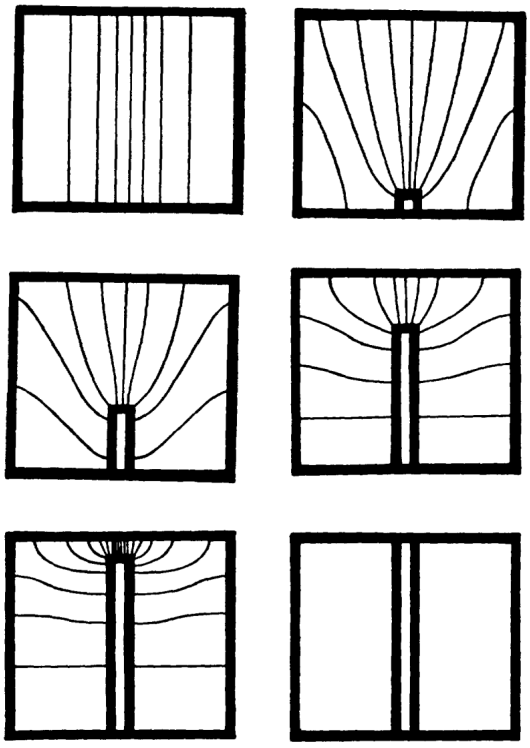


Figure 3-10: E-Field transition from a perfect-cylindrical to a perfect-coaxial resonator [73]

As the reentrant section, the centre conductor, is gradually placed into the cylindrical cavity as seen in 3-10, the resonant frequency first declines slowly and then rapidly until it approaches zero frequency asymptotically when the centre conductor is fully inserted and shorted to the end plate. Therefore, by reducing the gap size, it is possible to achieve low frequencies [74].

The Q-factor of this device can be approximated using the following equation [47]

$$\frac{1}{Q_0} = \frac{R_S}{2\pi\mu f_0}\left(\frac{\frac{1}{a}+\frac{1}{b}}{ln\frac{b}{a}} + \frac{2}{h}\right) \tag{3-27}$$

where R_S is the sheet resistance. It can also be written as [47],

$$R_S = \frac{\rho}{t} = \frac{1}{\sigma\delta} \tag{3-28}$$

where δ is the Skin Depth. It is a property of a conductor that describes the depth at which the amplitude of an electromagnetic wave is attenuated to 1/e (approximately 37%) of its original value. In simpler terms, it represents how far an electromagnetic wave can travel into a conductor before its strength is significantly reduced.

It is given by, [47]

$$\delta = \frac{1}{\sqrt{\pi\mu f_0\sigma}} \tag{3-29}$$

The next crucial component of the proposed design is the antenna. The upcoming section provides a better understanding of the fundamentals of antenna theory as it is essential to understand the concepts to comprehend the full workings of the proposed design.

3-3 Antennas

The information in this section is compiled from multiple sources [39], [62], [65], [66], [75].

Conventional communication systems use dedicated transmitters and receivers. This section on antennas provides a fundamental basis for understanding the transmission and receiving components of the proposed design.

Figure 3-11 illustrates the antenna coupled to the cavity and the two antennas used for sending a carrier wave and receiving the modulated signal in the proposed design.

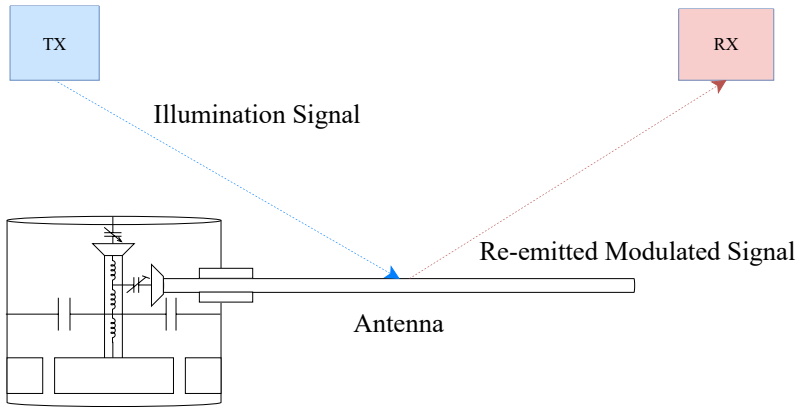
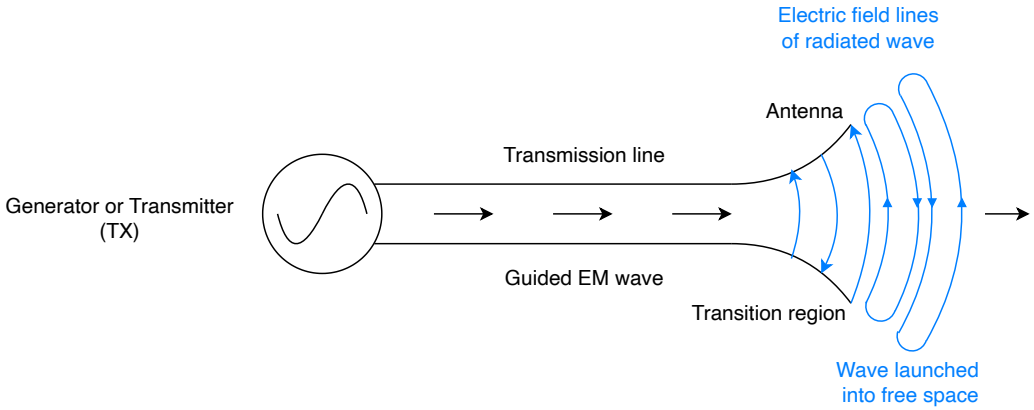
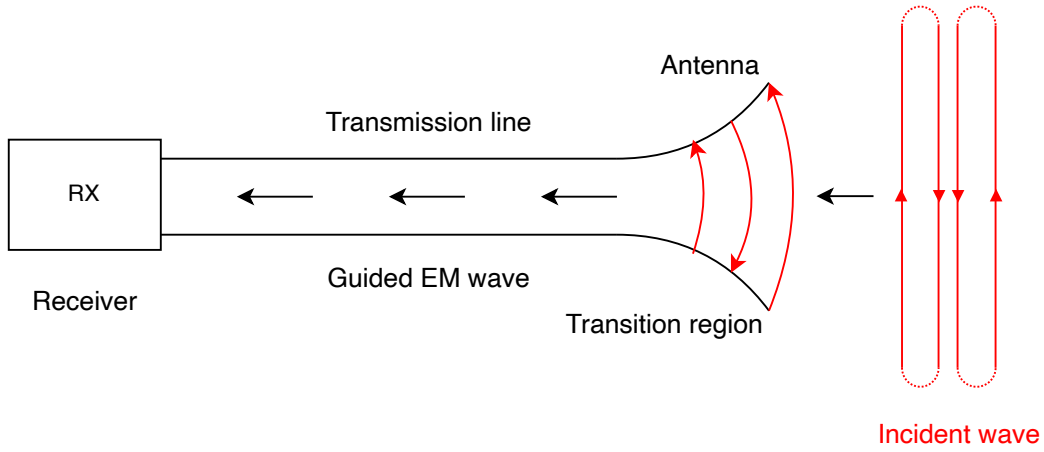


Figure 3-11: Illustration of working of antenna in proposed design

Antennas are critical components that transform electrical signals into electromagnetic waves, and vice versa. The proposed design uses an external radio wave as the carrier signal. The design of the device incorporates a resonant cavity that modulates the carrier wave with the sound it has detected.



(a) Transmission Mode



(b) Reception Mode

Figure 3-12: Working of an Antenna [75]

An antenna is a transducer that converts a guided wave propagating on a transmission line into an electromagnetic wave propagating in an unbounded medium (usually free space), or vice versa [62].
Figure 3-12a depicts the generator, also known as a transmitter (Tx), generating a signal in the form of voltage and currents at the required frequency.

There is a transmission medium that carries the signal from the transmitter to the antenna. This medium is referred to as a transmission line. Transmission lines include various kinds, including waveguides, coaxial cables, optical fibres, and more. In a similar manner, the antenna receives a signal, as seen in Figure 3-12b. The received signal is then sent over the transmission line back to the receiver (Rx). The antenna's dimensions should be comparable to the wavelength of the operating wave. A high operational frequency corresponds to a small

wavelength and requires a small antenna. Conversely, a low operational frequency requires a larger antenna.

Similarly, several parameters can influence the transmission and reception of signals. These parameters have been discussed below.

3-3-1 Antenna Parameters

It is essential to understand the properties of antennas, such as radiation patterns and directivity, in this particular context. The design of the Great Seal Bug's antenna, although not explicitly identified as a conventional antenna, impacts its ability to receive external radio waves and likely influences the transmission of modulated waves carrying sound information. As exploring the basics of antenna theory provides an improved understanding of the underlying principles that may have been used in the design of the Great Seal Bug, this is useful when the exact functioning of the bug and the significance of its antenna are explored. This section provides the basic information regarding antenna parameters needed to analyse the functioning of the Great Seal Bug and understand the passive listening approach it employs.

The parameters may be categorized into three main types, namely [65],

1. Circuit Quantities
    - **Antenna Impedance (Z_A)**, This represents the opposition an antenna presents to current flow when an EM wave is applied. It's similar to resistance in a DC circuit but can be complex, involving both resistive and reactive components.
    - **Radiation Resistance,** R_r This is a part of the antenna impedance that represents the power efficiently radiated as an EM wave. It's an ideal concept; real antennas have additional losses.
    - **Antenna Temperature,** T_A This is a theoretical temperature assigned to an antenna based on the noise power it generates due to its resistance. It's not a physical temperature but helps quantify the noise performance.
2. Physical Quantities
    - **Size** The physical dimensions (length, width, height) of the antenna.
    - **Weight** The mass of the antenna.
3. Space Quantities
    - **Radiation Patterns** ($E_\theta(\theta,\phi)$, $E_\phi(\theta,\phi)$, $E_\delta(\theta,\phi)$), These describe the spatial distribution of the electric field strength of the EM wave radiated by the antenna. They are typically represented mathematically as functions of theta (θ) and phi (ϕ), which denote angles in spherical coordinates.
    - **Polarization** (LP,CP,EP), This refers to the orientation of the electric field vector in the radiated EM wave. Common types include linear polarization (LP), circular polarization (CP), and elliptical polarization (EP).
    - **Power Patterns** $P_n(\theta,\phi)$, These describe the spatial distribution of the power radiated by the antenna as a function of direction (theta and phi). It's related to the radiation patterns but expressed in terms of power density.
    - **Beam Area** Ω_A, This is the solid angle encompassing the main lobe of the radiation pattern, where most of the power is radiated.
    - **Directivity**, (D) This is a measure of how well the antenna concentrates its radiated power in a particular direction compared to an isotropic source (radiating

equally in all directions).

- **Gain** (G) This is a measure of the power an antenna radiates in a specific direction compared to a reference antenna (usually an isotropic source). It takes into account both directivity and the antenna's efficiency.
- **Effective Aperture** (A_e), This is a hypothetical area that relates the power density of the radiated wave to the received power at a distant point. It reflects the antenna's ability to collect incoming EM waves.
- **Radar cross-section** (σ), This is a measure of how much radar energy an object reflects back towards the radar source. A high radar cross-section makes an object more easily detectable by radar.

3-3-2 Types of Antennas classified by Shape

Antennas may be classified in two forms, on the basis of the dimensions and the other based on the mode of operation [62], [75]. The types relevant to this work are listed below.

3-3-2-1 Wire Antennas

Wire antennas are often used in television broadcasting, satellite communications, radio transmissions, and aircraft systems. They are composed of metallic wires of varying thicknesses that may be shaped into different forms for diverse applications. For example, the Helical Antenna, is used in satellite communications, telemetry, and other related applications, the Folded-Dipole antenna is utilised in radio receivers and TV receiver antennas and the Loop antenna is typically used in search missions.

3-3-2-2 Aperture Antennas

Aperture, as its name implies, indicates an opening. Examples of this include the Horn Antenna. A waveguide is usually present, with a horn structure at the output. The electromagnetic waves inside the waveguide are emitted as radiation via the horn. Its most prominent use is in its utilisation as a feed for the large parabolic reflector transmitter antennas employed in satellite communications.

Horn Antennas The information in this sub-section is compiled from multiple sources ([39], [62], [65], [76]).

In order to improve the radiation efficiency and directivity of the beam, it is necessary to give the waveguide a broadened aperture that will effectively emit all of the energy in the desired forward direction. This phenomenon is often referred to as flaring.

Horn Antennas are constructed by flaring of the waveguide. They improve impedance. The frequency of the horn antenna can range from around 300MHz to up to 30GHz. They can be utilized for long-distance applications. The energy of the beam is transformed into radiation. Losses are reduced and the focusing of the beam improves. The directivity is improved while the diffraction is reduced.

The flare angle, ϕ of the horn antenna is an important factor. If this value is too small, then the resulting wave will be spherical instead of plane and the radiated beam will not be directive. The flare angle has an optimal value related to waveguide geometry. In order to have a higher antenna gain, there must be a larger antenna aperture. The gain of a horn antenna is typically around 20dB.

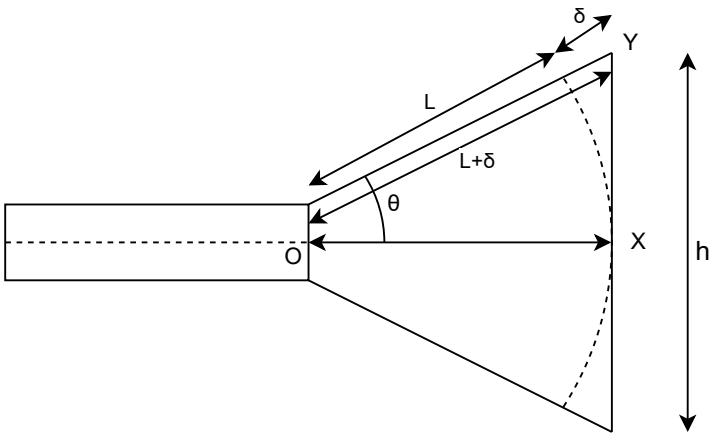


Figure 3-13: Horn Antenna Schematic [76]

From the geometry of the figure, we obtain the design equations of the Horn Antenna,
$cos\theta = \frac{L}{L+\delta}$ and $tan\theta = \frac{h}{2L}$
Therefore [76],

$$\theta = tan^{-1}\ (\frac{h}{2L}) = cos^{-1}\ (\frac{L}{L+\delta}) \tag{3-30}$$

Considering the triangle OYX, applying Pythagoras theorem,

$$(L+\delta)^2 = L^2 + (\frac{h}{2})^2$$

$$L^2 + 2L\delta + \delta^2 = L^2 + \frac{h^2}{2}$$

Since $\delta \ll L$, δ^2 can be neglected. Hence,

$$2L\delta = \frac{h^2}{4}$$

$$L = \frac{h^2}{8\delta} \tag{3-31}$$

The advantages include the absence of a resonance element in the structure allowing for the operation over a wide bandwidth, providing good impedance matching, and providing high directivity.
The limitations include the dependence on the flare angle and due to the large flare, the antenna is sometimes bulky.

3-4 Amplitude Modulation

This section delves into the technique of Amplitude Modulation (AM), which involves modifying a carrier wave to transmit information. While the previous section discussed traditional antennas mostly used for transmission or receiving, the proposed design uses a distinct approach. This passive listening device utilises a resonant cavity to modulate an external radio wave with sound information. In essence, the incoming radio wave serves as a medium for transmitting the sound captured by the proposed design. This section provides a comprehensive explanation of the theory of amplitude modulation (AM), utilising the operational concepts of the Great Seal Bug as the foundation as seen in Figure 3-14. This demonstrates how amplitude modulation can be applied to non-conventional transmitters.

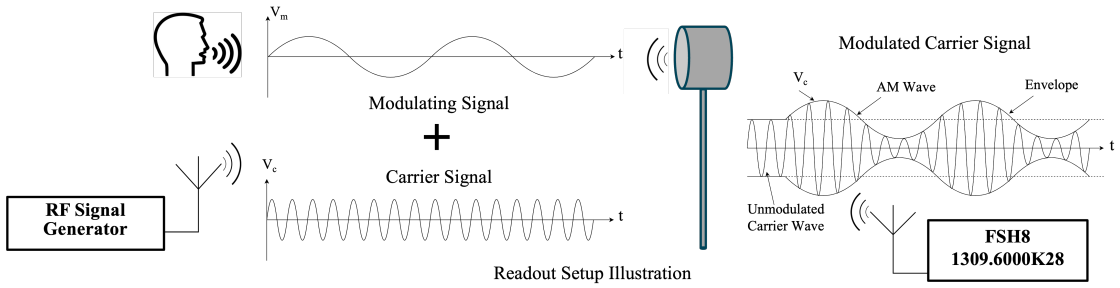


Figure 3-14: Schematic illustrating the Great Seal Bug's response to a modulated carrier signal: A radio frequency (RF) signal generator produces a carrier signal, which is subsequently modulated by an external signal. The modulated carrier signal generated is used to illuminate the device (The BioThing). functionality

In amplitude modulation (AM), the modulating signal as seen in Figure 3-15a, which contains the information to be transmitted, is superimposed with a high-frequency carrier wave as seen in Figure 3-15b. This operation modifies the amplitude of the carrier signal according to the changes in the information signal, as seen in Figure 3-15c. The resulting modulated wave conveys the encoded information, which may be subsequently retrieved at the receiver to extract the original message.

The next part provides a more in-depth understanding of the mathematical representation of Amplitude Modulation (AM). The equation for an amplitude-modulated wave is derived. This equation serves as a fundamental basis for understanding the process of embedding information into a carrier wave using amplitude modulation (AM) and then retrieving it at the receiving end.

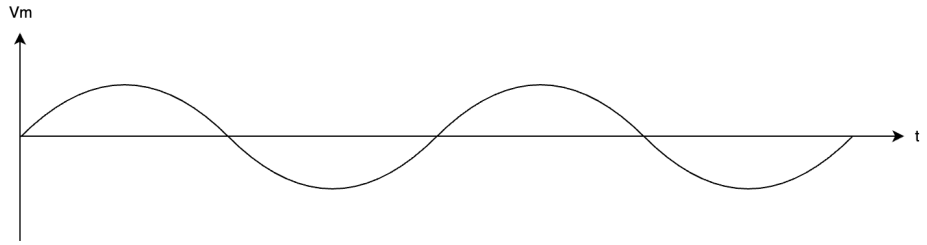
Carrier Signal can be written as $Acos(\omega t + \theta)$ or $Asin(\omega t + \theta)$

If the amplitude of the carrier wave is changing, the frequency and phase should be kept constant.

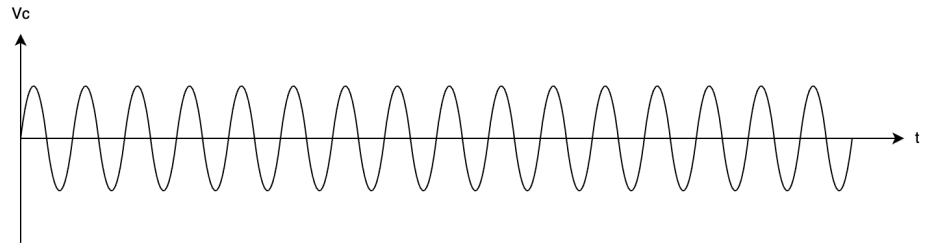
Using the notation,

$$C(t) = Asin(\omega t + \theta) \tag{3-32}$$

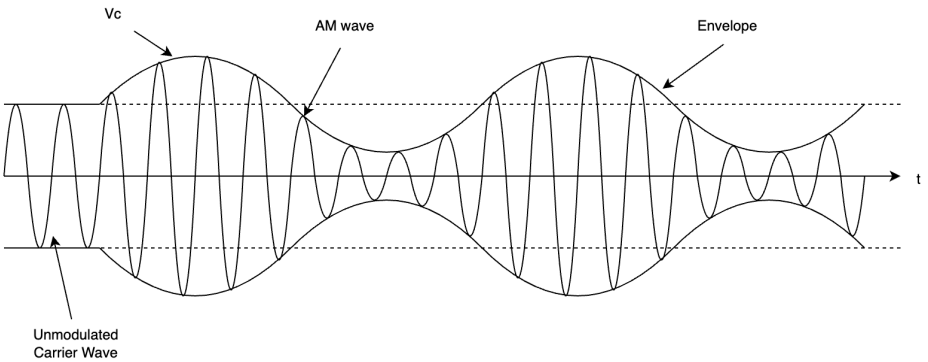
where,
C is the carrier signal
C(t) is the carrier wave signal which is changing w.r.t time
A is the amplitude of the carrier signal
θ represents the phase



(a) Modulating Signal



(b) Carrier Signal



(c) Modulated Carrier Wave

Figure 3-15: Amplitude Modulation [47]

As in this case, the amplitude is shifting and ω and θ are kept constant, this is referred to as amplitude modulating signal. This is represented in the Figure 3-15.

Figure 3-15a depicts a modulating signal of low frequency. Figure 3-15b represents the carrier signal of a high frequency. Figure 3-15c represents the modulating carrier signal. As observed, the amplitude of the carrier signal changes w.r.t the modulating signal.

The sine wave carrier can be expressed by [47], [77],

$$v_c = V_c sin\ 2\pi f_c t \tag{3-33}$$

where,
v_c is the instantaneous voltage of carrier signal,
V_c is the maximum amplitude of carrier signal,
f_c is the frequency of the carrier signal,
t is the time

A sine wave modulating signal can be written as,

$$v_1 = V_c + v_m = V_c + V_m cos\ 2\pi f_m t \tag{3-34}$$

where,
v_m is the amplitude of the modulating signal,
$v_1$is the total voltage at a point in time,
f_m is the frequency of the modulating signal

$$v_2 = v_1 sin\ 2\pi f_c t \tag{3-35}$$

where v_2 is the modulated signal

Substituting and expanding, we get,

$$v_2 = V_c\ sin 2\pi\ f_c t + \frac{V_m}{2} sin\ 2\pi(f_c + f_m)t + \frac{V_m}{2} sin\ 2\pi(f_c - f_m)t \tag{3-36}$$

The modulated signal, as represented above, comprises of three components: a carrier wave and two additional pure sine waves, known as sidebands. These sidebands have frequencies that deviate slightly above and below the carrier frequency f_c [77]. The value that it deviates by is dependent on f_m.

3-5 Backscatter wave technique

The information in this section was compiled from multiple sources [47], [78]–[81].

Backscatter specifically refers to the reflection of electromagnetic waves, when they come into contact with a medium. The properties of the reflecting medium, including its geometry and impedance, influence the backscattered wave [47]. This technique has been investigated as a possible means of encoding information for the proposed design.

3-5-1 Comparison between traditional and backscatter encoding

Traditionally, information is encoded onto the carrier radio frequency (RF) signal using modulation techniques such as amplitude modulation (AM), frequency modulation (FM), or phase modulation (PM). However, backscatter provides an alternative approach. The concept involves using changes in the backscattered wave itself, resulting from variations in impedance or other material properties, to encode information.

It is important to recognise that utilising impedance changes as a means of encoding in common wireless communication is not a widely adopted approach. Nevertheless, there are particular and specialised uses, especially in relation to resonant cavities.

3-5-2 Resonant cavities and backscatter modulation

A resonant cavity is a structure that confines electromagnetic waves at specific frequencies, similar to how a tuning fork resonates with specific sound waves. These cavities can be designed to incorporate controlled impedance variations within their structure. Here is how they can be utilised in conjunction with backscatter:

Frequency selective backscattering

A structure that backscatters certain frequencies within the incident RF signal can be developed by adjusting the cavity's shape and material properties. This process of selective backscatter electromagnetic waves can be utilised to encode information in a binary manner. For instance, the existence or nonexistence of a specific reflected frequency could indicate a binary value of 1 or 0 in a stream of data.

This project utilises frequency selective backscattering. The antenna selectively reflects a specific frequency. With a high quality factor, the device would exhibit the ability to selectively reflect a specific frequency while disregarding other frequencies. Essentially, the bandwidth is limited because even a minor shift in frequency prevents the device from reflecting the wave back. By reducing the Q-factor, the device becomes more tolerant of minor frequency variations. Even with a small amount, reflection occurs. This causes amplitude modulation. The movement of the membrane essentially results in a change in frequency that is proportional to the amplitude of the reflected wave. This results in amplitude modulation as seen in Figure 3-15

An optimal Q-factor must be determined based on the thickness of the membrane and the distance d (as in Figure 3-7b). If the membrane is thick and rigid, its mobility is limited. Due to the limited mobility of the membrane, a smaller distance d, is sufficient and a higher Q is required for the device to be sensitive to a smaller change in membrane gap d. While decreasing the gap can lead to higher fringe losses, it can also increase the capacitance between the post and the membrane.

A thinner membrane is more sensitive to sound, and the cavity can be designed with a larger gap to allow greater movement. This higher change in capacitance can compensate for a lower Q-factor. Another consideration is the strength of the membrane as excessively thin membranes risk tearing, so a balance must be struck between sensitivity and durability.

Simulations

4-1 Background - Simulations for the Biodegradable Microphone based on the Great Seal Bug

The objective of this project is to comprehend the functioning and fabrication of a biodegradable microphone. The Great Seal Bug was adapted to the design of this device. In order to gain a deeper understanding of different parameters, after looking into the theory, simulations were conducted. The simulations were conducted on the entire listening device, which was a 3D CST model adapted from the great seal bug.

This chapter makes use of simulations to analyse key questions in order to gain an in-depth understanding of the resonator.

- Firstly, the simulated performance characteristics, such as resonant frequency, will be compared to the observed values in the original device in order to determine accuracy of the model.
- Secondly, simulations will be conducted to determine how substituting the current material with biodegradable metals affects the resonator's performance, taking into account variations in conductivity, resistivity, and skin depth.
- Furthermore, the effects of device miniaturization on resonant frequency and Q-factor will be investigated, exploring how scaling down the device influences its resonance properties.
- In addition, simulations will assess the effects of adjusting the distances between the tuning post and both the membrane and antenna, which function as variable capacitors according to the schematic in Figure 2-12.
- The simulations will also examine the impacts of altering the thickness of the membrane and the height of the tuning post.
- A subsequent section will compare the efficiency of the existing cylindrical design in comparison to a larger, flatter alternative through the use of simulations.
- Ultimately, simulations will explore the results of increasing the size of the device for achieving longer-range operation, specifically in terms of its frequency and Q-factor.

By conducting a comprehensive investigation of these parameters, significant insights on enhancing the performance of the device and exploring possible design variants can be gained.

4-2 Software, Solvers and Primary Simulation parameters

4-2-1 Choice of Software and Solvers

CST Studio Suite is a software application primarily utilised for conducting electromagnetic (EM) simulations. The software enables the generation of 3D models of the device and simulates the interaction of electromagnetic fields with the device, with a focus on the resonator and antenna [82].

4-2-1-1 Solvers

The solvers that were of interest to this project are [82]:

- **Time Domain Solver** simulates the transient behaviour of electromagnetic fields. The primary technique employed is the Finite-Difference Time-Domain (FDTD) approach. It is applicable for examining the pulse propagation and/or the integrity of signals in circuits. Additionally, it is helpful for analysing devices that utilise non-linear materials or movable and/or variable components. The results include the plot of field variations as a function of time, providing a visual representation of how the fields propagate and change within the device. Additionally, it computes the current flow across the device at each time step. This facilitates the analysis of the induction and distribution of electrical currents resulting from the application of the signal. The voltage waveforms can be acquired at specific points to analyse signal integrity and detect any reflections or distortions.
- **Frequency Domain Solver** utilises the Finite Element Method (FEM) to solve Maxwell's equations and examine the characteristics of electromagnetic fields at specific frequencies or within a designated range. It is typically used for the analysis of S-parameters, which are essential for comprehending the transmission and reflection of signals in devices such as antennas. S-parameters quantify the scattering and transmission of electromagnetic signals at various frequencies. The results are plotted as a function of frequency. The S-parameters provide a way to determine the power that is reflected, transmitted, or absorbed by the device. The two primary S-parameters here are the,
  (a) **Reflection Co-efficient (S11)**, which quantifies the amount of the incoming signal reflected back from the device. A reflection coefficient nearing zero indicates good impedance matching, indicating minimum signal reflection.
  (b) **Transmission Coefficient (S21)**, quantifies the amount of the input signal that is transmitted through the device. A transmission coefficient approaching 1 signifies the effective transmission of signals.

  It is applicable for determining the resonance frequency and the radiation pattern. The collected data can be utilised in order to understand the magnitude of signal transmission or reflection at different frequencies, determine the resonant frequency, and display the current distribution of the device at specific frequencies.
- **Eigenmode Solver** The eigenmode solver is primarily concerned with identifying the resonant modes of a given device. Eigenmodes refer to distinct electromagnetic field patterns that occur at specific frequencies within an enclosed structure. The Advanced Krylov Subspace (AKS) approach is a specialist approach that is employed. The eigenmode solver can be used for analysing cavities in order to comprehend the eigenmodes,

which are vital to predicting the behaviour of these devices at specified frequencies. The results determine the eigenmodes and their accompanying electromagnetic field patterns of the device. This makes it easier to comprehend the manner in which the device will vibrate and subsequently radiate or absorb electromagnetic energy. The results for each mode include the

(a) **Resonant frequencies (f)**, which indicate the particular frequencies at which the device resonates. These frequencies correspond to the specific wavelengths at which EM waves can be confined and amplified within the given structure.

(b) **Total Q** represents the degree of loss of the corresponding resonance. A greater Q-factor signifies a more ideal resonance with lesser energy dissipation over time. In other words, it represents the efficiency at which the device can store the energy in that eigenmode.

(c) **Accuracy** value quantifies the level of precision of the estimated resonance frequency and other derived parameters.

(d) **Electric Field (E-Field)** Distributions provide a visual representation of the variations in the electric (and magnetic) field within the device for each eigenmode. It helps to understand the nature of the resonance and how the electric field is concentrated within the device.

4-2-1-2 Boundary Conditions

Boundary conditions are another crucial aspect. The boundary conditions establish the behaviour of electromagnetic waves at the outer limits of the simulation domain. They fundamentally dictate the behaviour of the waves upon reaching the boundaries of the model. This study investigates two boundary conditions [82]:

(a) **Electric Boundary** functions as a Perfect Electric Conductor (PEC). The tangential electric field is set to zero at the boundary. This confines the EM waves within the boundary and causes them to be reflected back, as the presence of an electric field parallel to the surface of the wall is not possible. This condition is frequently employed to simulate enclosed cavities or structures with metallic walls, as it effectively replicates the behaviour of a metal enclosure that limits the electromagnetic fields within the simulation domain.

(b) **Open Boundary** represents a free space boundary and allows for free movement. The boundary permits the outward propagation of electromagnetic waves with minimum reflection while entering waves can traverse it with minimal influence. This is frequently employed to simulate radiating structures, such as antennas or waveguides, in which the fields are designed to propagate outward.

In this project, the majority of the simulations were conducted with an open boundary and a waveguide port using the eigenmode solver.

4-2-2 Primary Simulation Parameters

The simulation parameters were selected to correspond precisely with the theoretical principles of the Great Seal Bug device. Open boundaries were utilised in combination with the eigenmode solver. This approach presents multiple advantages:

- **Open boundaries** represent the lack of physical constraints that enclose the device. This facilitates the unhindered transmission of electromagnetic (EM) waves, resulting in a more accurate representation of real-world circumstances as opposed to electric boundaries which mimic a PEC wall which reflects waves back.
- **Eigenmode Solver** is particularly suited for this kind of analysis as it computes the resonant modes (or eigenmodes) of the device. These modes correspond with particular frequencies at which the device exhibits optimal performance. In addition, the eigenmode solver calculates the Q-factor, a critical metric that measures the efficiency of energy storage in the resonator, as well as the distribution of the electric field within the device.

4-2-3 Dimensions of the Original Resonant Cavity (Great Seal Bug)

This section contains the dimensions for the Great Seal Bug model that will be the control device for all of the simulations. These dimensions were adapted from Figure 2-8 which was taken from the Official declassified FBI Report [50].

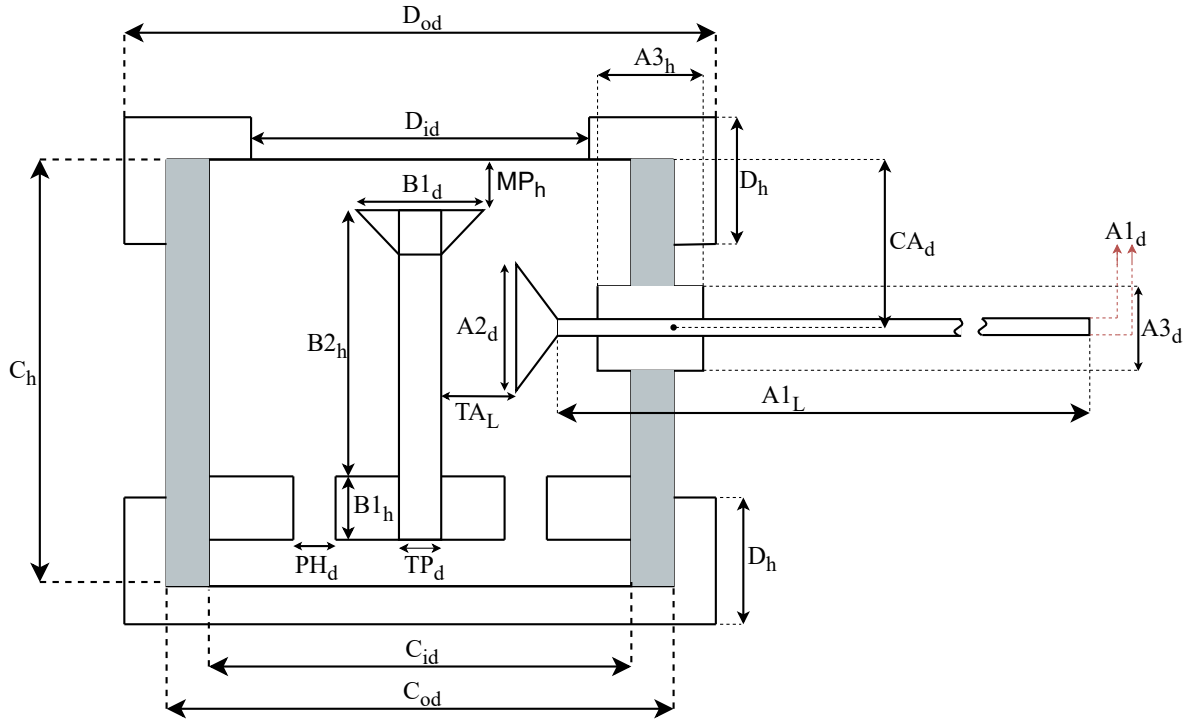


Figure 4-1: Dimensions of control device adapted from Great Seal Bug

Figure 4-1 serves as a detailed blueprint of the resonator's geometry employing specific variables to denote dimensions that are mentioned in Table 4-1. These variables include:

(a) Resonator Cavity Caps:
- D_{od} (outer diameter)
- D_{id} (diameter of membrane opening for the top cap)
- D_h (height)

Dimension Name	Value (mm)
D_{od}	25.5
D_{id}	17.5
D_h	5
C_{id}	23.5
C_{od}	25.5
C_h	17
CA_d	6.3
$A1_L$	230
$A3_d$	5
$A1_d$	1.2
$A2_d$	6
$A3_h$	5
$B1_d$	2
$B1_h$	3
PH_d	2.25
$B2_h$	12.5
TA_L	3
MP_h	0.23

Table 4-1: Dimensions of control device adapted from Great Seal Bug

(b) Resonator Cavity:
- C_{od} (outer diameter)
- C_{id} (inner diameter)
- C_h (height)

(c) Antenna:
- CA_d (insulator hole distance from cavity edge to the centre of insulator hole)
- $A1_L$ (length)
- $A1_d$ (diameter)
- $A2_d$ (antenna plate diameter)

(d) Insulator:
- $A3_d$ (insulator diameter)
- $A3_h$ (insulator length)

(e) Tuning post:
- TP_d (diameter)
- $B1_h$ (thread thickness)
- $B2_h$ (height)

(f) Gap Distances:
- MP_h (distance between tuning post and membrane)
- TA_L (distance between tuning post and antenna)

(g) Pneumatic holes:
- PH_d (diameter)

Defining and using consistent variables throughout this chapter ensures clear descriptions of the resonator's geometry. This also simplifies the analysis of how changes in dimensions affect performance as these variables are referenced.

4-3 Simulation of Original Great Seal Bug Microwave Resonator

Is it possible to obtain through simulations the same resonator performances as measured in the original device?

The original Great Seal Bug resonator employed copper with a silver polished interior to improve Q. The resonant frequency of the Great Seal Bug was measured at 1.8 GHz as per the FBI Report [50]. This was the starting point of the simulations. The selection of materials for further optimisation will be addressed at a later stage. A three-dimensional (3D) model of the device was created on CST, which included the dimensional specifications corresponding to the original device dimensions given in Table 4-1 and illustrated in Figure 4-1. The material was set as pure copper.

4-3-1 Electric boundary

The Brooker-Gomez paper [83] analyzed the Great Seal Bug using simulations in HFSS. However, the paper used modified dimensions and provided limited details. Only the eigenmode solver with six modes was mentioned. The results are presented in Table 4-2a.

This thesis work replicated these simulations with the original dimensions and electric boundary condition. The results are shown in Table 4-2b.

Mode	Frequency (GHz)	Total Q
1	1.81	1911
2	6.55	2225
3	15.77	5475
4	16.48	4888
5	16.98	5340
6	18.17	5670

(a) Eigenmode solver results of Brooker-Gomez paper [83]

Mode	Frequency (GHz)	Total Q
1	0.87	1617
2	1.48	2128
3	1.73	1919
4	2.11	2517
5	2.76	2637
6	3.41	2983

(b) Eigenmode solver results of original copper device with electric boundary in this work

Table 4-2: A comparative analysis of simulation results with findings from Brooker-Gomez Paper

Table 4-2 compares the simulation results. As the table shows, the eigenmodes with frequencies around 1.8 GHz in both works have similar Q-factors (1911 and 1919). However, using the electric boundary condition is not suited for this project. An electric boundary reflects the modulated signal as it confines the EM waves within the boundary, representing Q-factor values that are not relevant to the current investigation. Therefore, subsequent simulations were run using an open boundary condition.

4-3-2 Open boundary

This simulation was conducted using Eigenmode solver with open boundary condition. The primary objective of this initial simulation was to determine the resonator's operating frequency and Q-factor in its original design, which is made of copper.

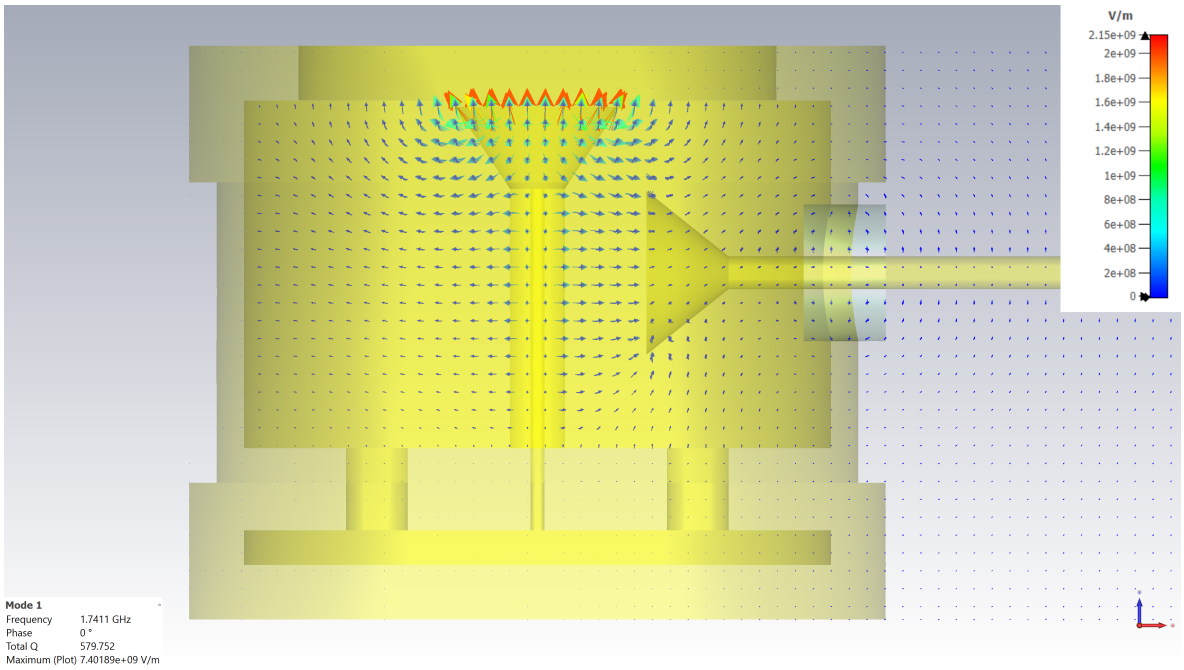


Figure 4-2: E-Field of original device's dominant eigenmode

The Eigenmode solver identified six different eigenmodes, as outlined in Table 4-3. Mode 1 showed the highest quality factor (Q-factor) among these modes, which is a critical characteristic that affects the functioning of the resonator. The resonant frequency of this mode was measured at 1.73 GHz. This value deviates by 0.07 GHz (3.9%) from the expected resonance frequency of the original device (1.8 GHz).

Mode	Frequency (GHz)	Total Q (-)
1	1.74	580
2	1.8	1.20
3	2.4	1.62
4	3.17	2.04
5	3.8	2.50
6	4.5	3.00

Table 4-3: Eigenmode solver results of original copper device with open boundary

Based on the data shown in Table 4-3 and Figure 4-2, it can be observed that the electric field between the tuning post and membrane is concentrated in Mode 1. This concentration of the electric field improves the capacitance. The device is capable of functioning at a frequency of 1.7 GHz, with a Total Q of 580, against a frequency of 1.8 GHz of the original device.

Simulations performed in CST software for the resonator geometry exhibit unrealistically high electric field values, in this case, reaching approximately 2 GV/m. These extreme values are primarily attributed to the meshing process and the presence of sharp edges within the model. The meshing process in CST software discretizes the geometric model into small elements for numerical calculations. Sharp edges or corners can cause the mesh to become highly refined

in those localized regions. This refinement can lead to an artificial inflation of the electric field intensity in those areas. These values are not a realistic representation of the actual electric field distribution within the resonator While the simulation results may show these high electric field values, it's crucial to recognize them as potential meshing anomalies. A more reliable indicator for analysis is the relative variation of the electric field within the cavity. In this case, Figure 4-2 highlights the significant difference observed, with the field being nearly 10 times stronger near the tuning post and antenna compared to other regions of the cavity.

This same trend is observed with all of the simulations in the Section 4-4.

4-4 Simulation of the microwave resonator with biodegradable metals

Is it possible to obtain through simulations the same resonator performances if the material is replaced with biodegradable metals?

After successfully simulating the original device model with a frequency that closely matched the original, the next step was to replace the material with a biodegradable material. Three biodegradable metals, Magnesium, Zinc and Iron were chosen. The results are in the sections that follow.

4-4-1 Magnesium

Leveraging the identical solver settings and boundary conditions employed in the previous copper simulation (Section 4-3-2), this section explores the behaviour of the device with magnesium as the material. The primary distinction lies in the material property of conductivity. Magnesium exhibits a conductivity of $2.3 \times 10^7 (S/m)$, representing a decrease of 61% compared to copper.

Like the simulation from Section 4-3-2, the Eigenmode solver identified six eigenmodes. Table 4-4 lists the results of the eigenmode solver. Similar to the original copper device, Mode 1 showed the highest quality factor (Q-factor). It was also the mode with the strongest coupling between the tuning post and the membrane as seen in Figure 4-3. The resonant frequency obtained in this mode was 1.7 GHz, which was the same as that of the copper variant.

Consistent with the copper simulation, the eigenmode solver identified six distinct eigenmodes. The results are summarized in Table 4-4. Similar to the copper variant, Mode 1 displays the highest Q-factor and exhibits the strongest coupling between the tuning post and the membrane as depicted in Figure 4-3. Notably, the resonant frequency obtained in this mode, 1.7 GHz remains the same as the copper variant.

A more detailed comparison of results across all materials is made in the upcoming Section 4-4-4.

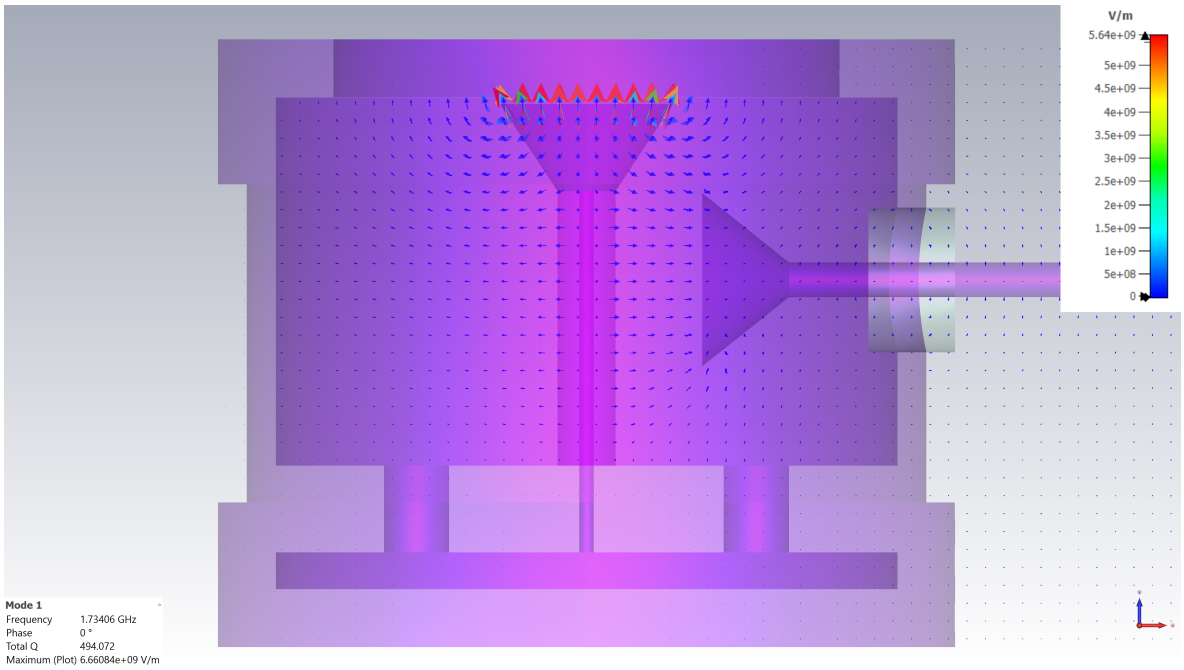


Figure 4-3: E-Field of Magnesium variant device's dominant eigenmode

Mode	Frequency (GHz)	Total Q (-)
1	1.73	494
2	1.8	1.20
3	2.4	1.62
4	3.17	2.05
5	3.8	2.50
6	4.5	3.00

Table 4-4: Eigenmode solver results of magnesium device with open boundary

4-4-2 Zinc

Building upon the prior simulations, this section investigates the behaviour of the device when the material is replaced with zinc. The simulation setup remains identical, employing an open boundary condition and the eigenmode solver. The primary distinction lies in the material properties, specifically the electrical conductivity. Zinc exhibits a significantly lower conductivity $1.7 \times 10^7((S/m))$ compared to copper, representing a reduction of 71%.

Consistent with the previous observations, Mode 1 displays the most concentrated electric field intensity near the membrane and tuning post. Additionally, the direction of the electric field aligns with the prior simulations. The frequency remains consistent at 1.7 GHz. A slight variation in total Q-factor exists between zinc and magnesium. A comprehensive comparison across all materials will be presented in Section 4-4-4.

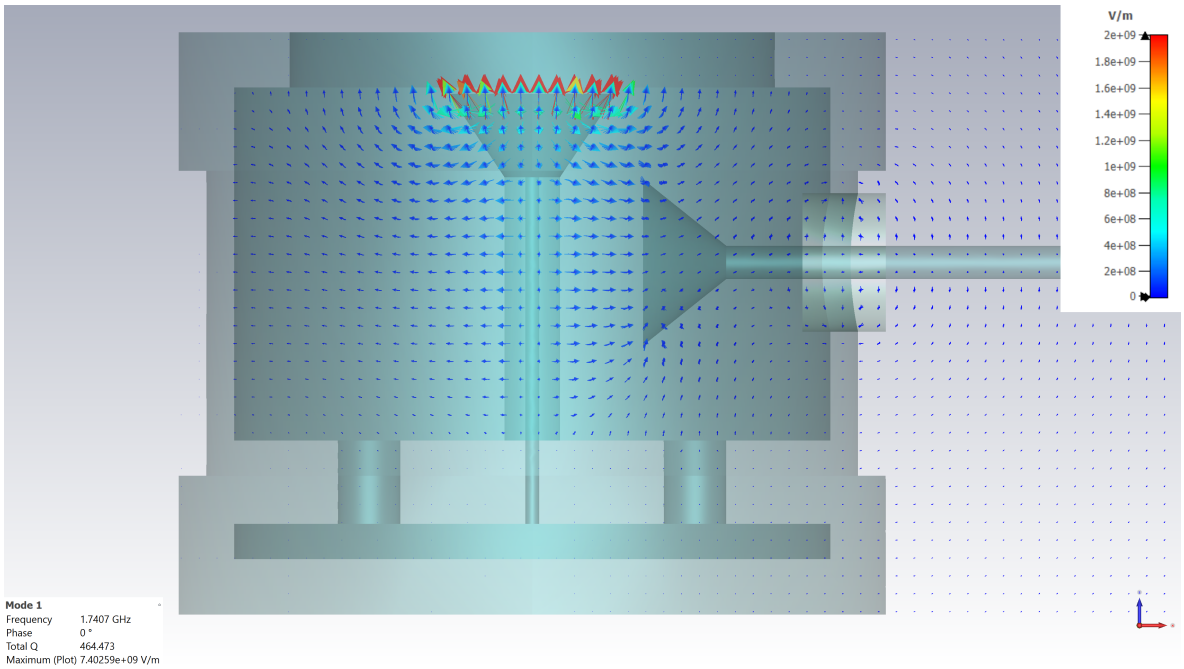


Figure 4-4: E-Field of Zinc variant device's dominant eigenmode

Mode	Frequency (GHz)	Total Q (-)
1	1.74	464
2	1.8	1.212
3	2.4	1.63
4	3.17	2.06
5	3.8	2.519
6	4.5	3.02

Table 4-5: Eigenmode solver results of zinc device with open boundary

4-4-3 Iron

Extending the investigation to iron, this section presents the results obtained with the same eigenmode solver configuration and open boundary condition as Section 4-3-2. The primary variable that was changed is the material itself, as iron possesses a much lower conductivity of $1 \times 10^7 (\sigma(S/m))$ compared to copper, representing an 83% reduction.

The eigenmode analysis, presented in Table 4-6, shows a consistent trend across all materials: Mode 1 remains the dominant mode, maintaining the strongest coupling between the tuning post and the membrane as seen in Figure 4-5.

The resonant frequency in this mode 1.7 GHz remains consistent with the previous simulations. The total Q-factor for iron is 412. A more in-depth examination of these findings will be provided in Section 4-4-4.

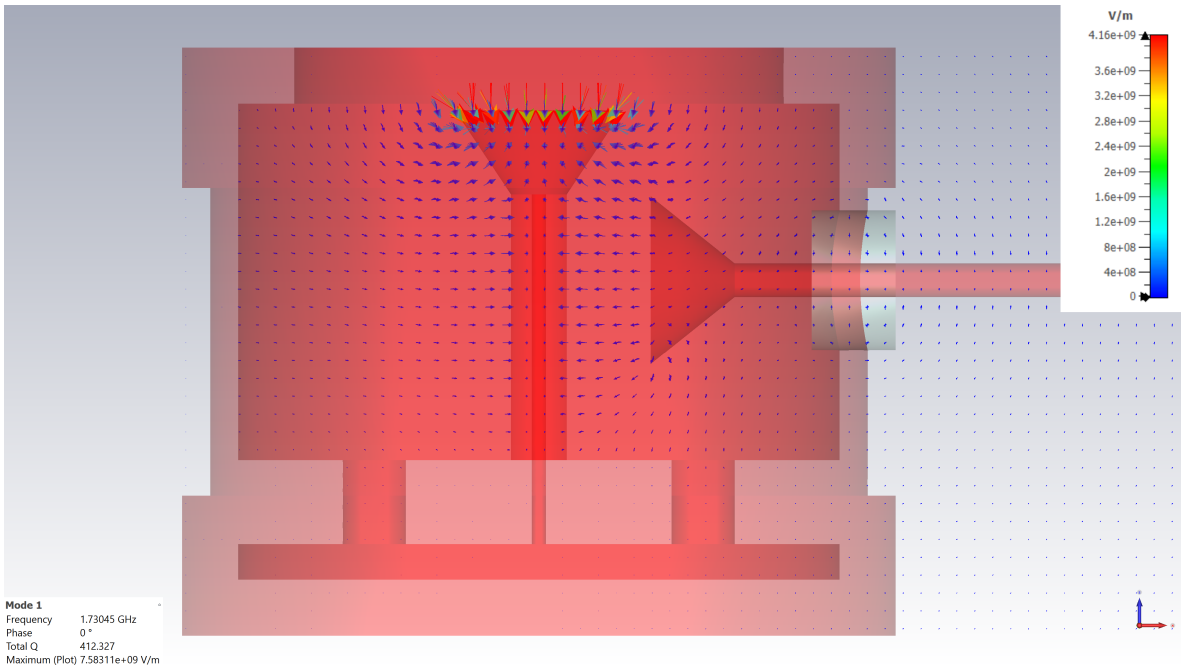


Figure 4-5: E-Field of Iron variant device's dominant eigenmode

Mode	Frequency (GHz)	Total Q
1	1.73	412
2	1.8	1.20
3	2.4	1.61
4	3.17	2.04
5	3.8	2.50
6	4.5	2.99

Table 4-6: Eigenmode solver results of iron device with open boundary

4-4-4 Comparison of results across materials

The relative permeability of all the materials used is almost the same as seen in Table 4-7. Using the above simulation results, we observe the resonant frequency remains around 1.7 GHz for all metals used.

From Equation: 3-29,

$$\delta \propto \frac{1}{\sqrt{\sigma}}$$

Hence a higher conductivity leads to a lower skin depth.

For the impact on sheet resistance, from Equation: 3-28,

$$R_S = \frac{\sqrt{\pi \mu \sigma f_0}}{\sigma}$$

for the same frequency and relative permeability,

$$R_S \propto \frac{1}{\sqrt{\sigma}}$$

So we can conclude R_s is proportional to δ given that the frequency and relative permeability remain constant for all the materials used in this set of simulations.

Since R_s is proportional to δ which is inversely proportional to $\sqrt{\sigma}$, we can conclude that for a given dimension, frequency and relative permeability, from Equation: 3-27,

$$Q \propto \sqrt{\sigma}$$

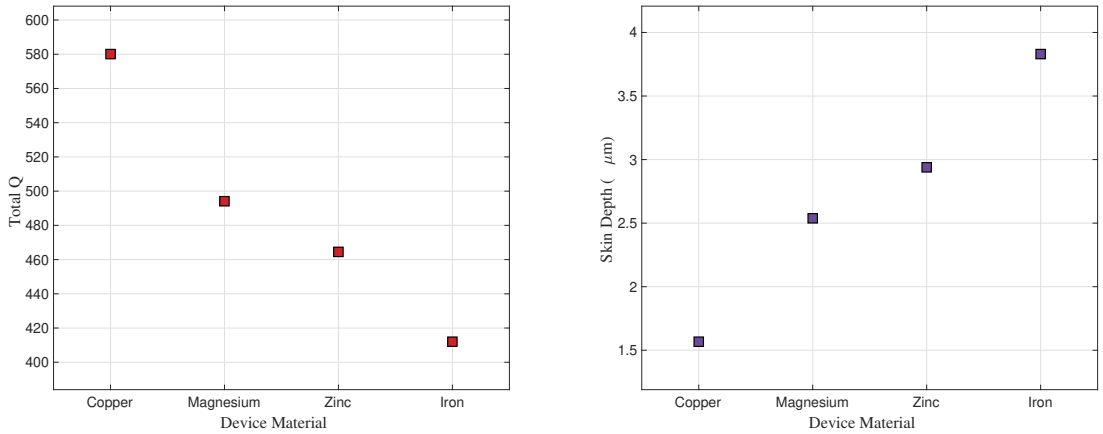
So it can be concluded that a higher conductivity leads to a better Q-factor.

Material	**Conductivity** ($\sigma(S/m)$)	**Resistivity** (ρ ($\Omega.m$))	**Relative Permeability** (μ_r)	**Frequency (GHz)**	**Total Q**	**Skin Depth** (μm)
Copper	5.96×10^{7}	1.7×10^{-8}	1	1.7	580	1.57
Magnesium	2.3×10^{7}	4.4×10^{-8}	1	1.7	494	2.54
Zinc	1.7×10^{7}	5.9×10^{-8}	1	1.7	464	2.94
Iron	1×10^{7}	9.7×10^{-8}	1	1.7	412	3.83

Table 4-7: Comparison of parameters of different biodegradable metals

Understanding the skin depth properties of various materials is crucial, as it directly affects the sheet resistance of the conductor, which is a key factor influencing the overall Q-factor of the device.

Given that both the physical dimensions and relative permeability remain constant across all material variations, the primary factor influencing skin depth becomes the conductivity of the chosen material. The skin depth for each material can be calculated by using Equation: 3-29. The necessary data for frequency, conductivity and relative permeability is listed in table 4-7.



(a) Impact on Total Q

(b) Impact on Skin Depth at 1.7 GHz

Figure 4-6: Impact of material used on different on Frequency and Total Q

4-5 Device miniaturization and effect on resonance properties

What impact would scaling down the device have on the Frequency and Q-factor?

This simulation investigates the effects of miniaturization on the performance of the device. The control device is the zinc variant with the dimensions as listed in the Table 4-8

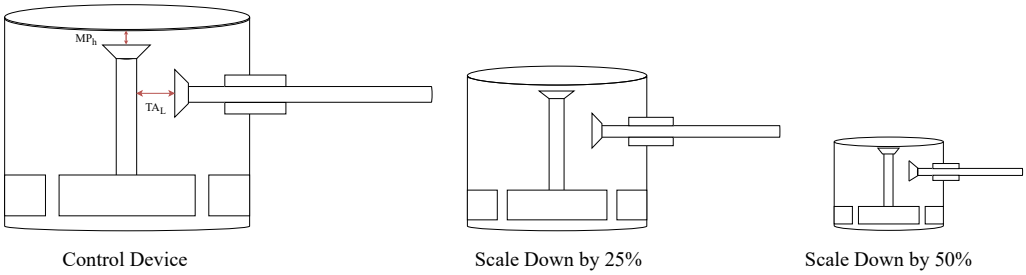


Figure 4-7: Visualisation of parameter adjustment for device miniaturisation

4-5-1 Parameter adjustments for different scaled-down variants

Parameters	Dimensions (mm)	Scale Decreased by				
		25%	**50%**	**75%**	**85%**	**95%**
C_h	17	12,75	8,5	4,25	2,55	0,85
C_{id}	21,5	16,12	10,75	5,37	3,22	1,07
C_{od}	23,5	17,62	11,75	5,87	3,52	1,17
CA_d	6,3	4,725	3,15	1,57	0,94	0,31
$B1_h$	3	2,25	1,5	0,75	0,45	0,15
TP_d	2	1,5	1	0,5	0,3	0,1
PH_d	2,25	1,68	1,12	0,56	0,33	0,11
$B2_h$	12,5	9,37	6,25	3,12	1,87	0,62
$B1_d$	6	4,5	3	1,5	0,9	0,3
$A1_d$	1,2	0,9	0,6	0,3	0,18	0,06
$A1_L$	230	172,5	115	57,5	34,5	11,5
$A2_d$	6	4,5	3	1,5	0,9	0,3
$A3_d$	5	3,75	2,5	1,25	0,75	0,25
$A3_h$	5	3,75	2,5	1,25	0,75	0,25
D_{od}	25,5	19,12	12,75	6,37	3,82	1,27
D_{id}	17,5	13,12	8,75	4,37	2,62	0,87
D_h	5	3,75	2,5	1,25	0,75	0,25
TA_L	3	2,25	1,5	0,75	0,45	0,15
MP_h	0,23	0,1725	0,115	0,0575	0,0345	0,0115
MP_h	0,07	0,0525	0,035	0,0175	0,0105	0,0035

Table 4-8: Dimensions of control and scaled-down variant models

The device is scaled down five different times in the manner as illustrated in Figure 4-7, and the dimensions for all variants are listed in Table 4-8. In addition to these parameters, it is

important to note that membrane thickness was kept constant at 6.35 μm as per the control dimensions. Scaled-down by 25% indicates that the device has been scaled down by 25% from the control dimensions.

4-5-2 Results

Two sets of simulations were run. These were classified based on the 2 different control MP_h distances (Gap between Tuning Post and Membrane), 0.07mm and 0.23mm.

The observed results suggest a trade-off between device size and performance. As the device is scaled down, an increase in frequency is observed. This trend accelerates as the device is scaled down further. Although the same scale-down percentage scales down both the radius and MP_h, the area is reduced in proportion to the $radius^2$. Consequently, the capacitance decreases as the scale-down percentage increases.

Scale When Decreased by	**Frequency**		**Total Q**		**Skin Depth (μm)**
	Device Frequency (GHz)	**Difference compared to Control Device**	**Device Total Q (-)**	**Difference compared to Control Device**	
Control Device	1.05		638		3.77
25%	1.38	27%	562	-13.5%	3.29
50%	2.10	66%	479	-33.2%	2.67
75%	4.12	4x	358	-78.2%	1.90
85%	6.97	6x	288	-1.2x	1.46
95%	20.89	20x	175	-2.6x	0.84

Table 4-9: Comparison of results for Control MP_h Distance - 0.07mm

Scale When Decreased by	**Frequency**		**Total Q**		**Skin Depth (μm)**
	Device Frequency (GHz)	**Difference compared to Control Device**	**Device Total Q (-)**	**Difference compared to Control Device**	
Control Device	1.73		464		2.94
25%	2.30	28%	415	-12%	2.55
50%	3.25	61%	398	-16.5%	2.14
75%	6.87	4x	313	-48.2%	1.47
85%	11.45	6x	268	-73%	1.14
95%	33.63	20x	181	-1.5x	0.66

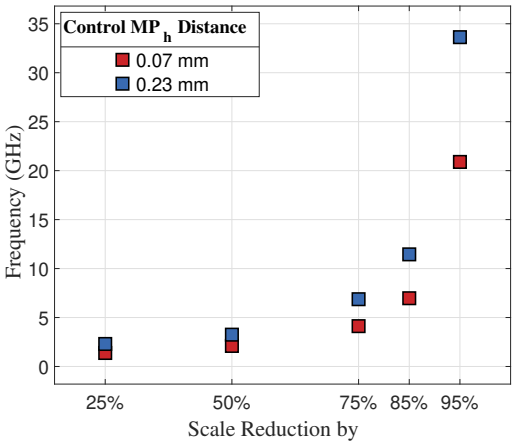
Table 4-10: Comparison of results for Control MP_h Distance - 0.23mm

The analysis shows that the frequency increases by the same factor for both sets of simulations as seen in Tables 4-9 and 4-10. This is because the frequency depends solely on the inductance and capacitance which is dependent on the dimensions of the device. However, the Q-factor is not only dependent on dimensions but also various other factors such as coupling effect,

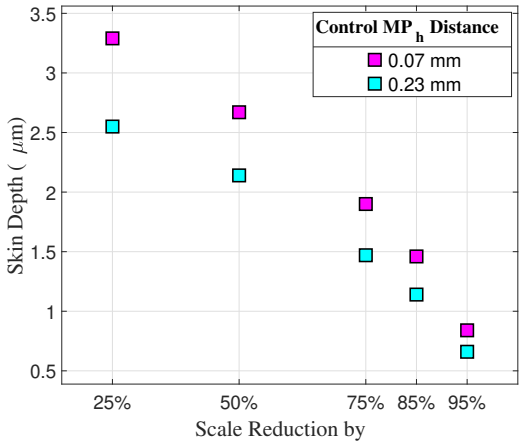
dielectric losses, fringing effect, ohmic losses and so on. These parameters are significantly impacted when the device is miniaturized. Compared to the control device, the energy loss observed after scaling down with an MP_h of 0.07mm is greater than that observed after scaling down with an MP_h of 0.23mm.

It is important to note that the optimal MP_h and TA_L will vary depending on specific device geometry. However, adjusting this parameter alongside other design considerations will make it possible to achieve a better Q-factor even with a miniaturised device.

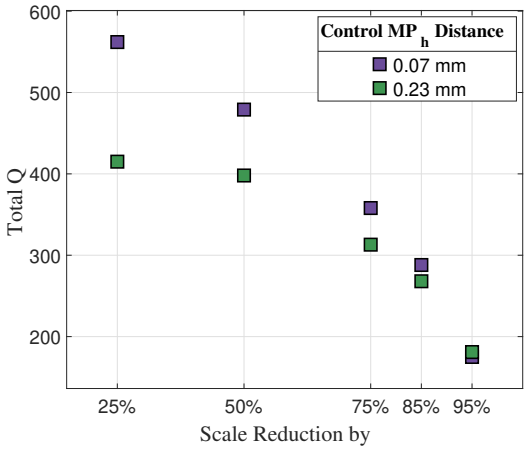
For the purposes of this simulation, all parameters besides the overall device scale were maintained constant relative to the control device, allowing for a focused analysis of the miniaturization effect.



(a) Impact on Frequency



(b) Impact on Skin Depth



(c) Impact on Total Q

Figure 4-8: Impact of miniaturisation on Frequency, Skin Depth and Total Q

In conclusion, although the Q-factor of the control device is greater with an MP_h distance of 0.07mm, scaling down the device with this MP_h, the Q-factor results as seen in Table 4-9 decrease rapidly when compared to the results of devices scaled down with an MP_h of 0.23mm as seen in Table 4-10. Based on the results, it is recommended to scale down the

device with a control MP_h distance of 0.23mm. However, because the current information pertains to the control version, separate simulations would be required to determine the best dimensions for the smaller device(s).

4-6 Influence of device geometry variations on resonance properties

A series of simulations are conducted to analyse the variations of resonance properties due to the influence of device geometry. The simulations are performed with the Zinc variant of the control device with dimensions as listed in Table 4-1.

4-6-1 Impact of distance between tuning post and membrane

What is the impact of the distance between the tuning post and membrane?

This section analyses the impact of the distance between the tuning post and the membrane (MP_h) as illustrated in Figure 4-9, on the performance of the device. This parameter has a substantial influence on crucial performance metrics such as frequency and Total Q as seen previously in Equation: 3-26 as d.

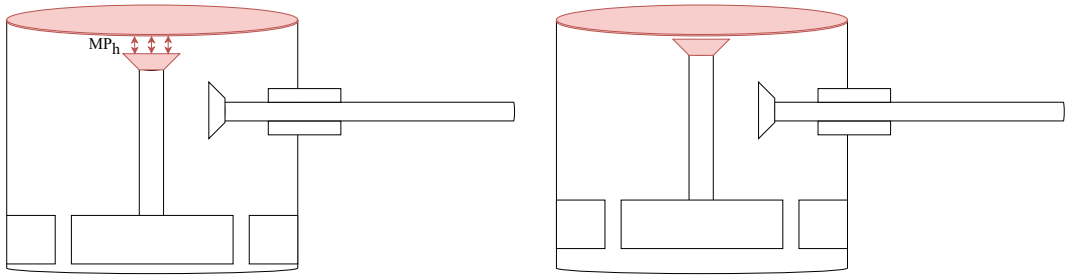


Figure 4-9: Visualisation of parameter adjustment for membrane-tuning post (MP_h) distance

As the MP_h increases, the electric field density decreases causing a decrease in capacitance between the tuning post and the membrane. This results in an increase in resonant frequency as given by the Equation: 3-4. This can be seen in Table 4-11.

A lower frequency can weaken the electromagnetic coupling between the resonant cavity and its surroundings, particularly for radiative losses. This minimization of radiation loss contributes to an increased Q-factor at the lower resonant frequencies.

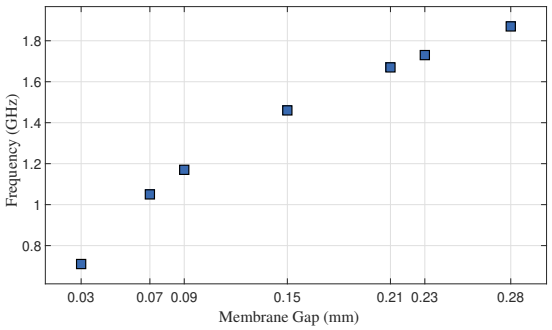
Extremely small gaps could have an effect on the overall Q-factor. Parasitic effects, such as dielectric losses and leakage currents, become more apparent as the gaps decrease in size. These effects contribute to overall energy loss, thereby lowering the Q-factor as seen for n MP_h of 0.03mm.

At higher frequencies, fringe field losses become more prominent, contributing to the observed decrease in Q-factor due to an increase in loss tangent [84].

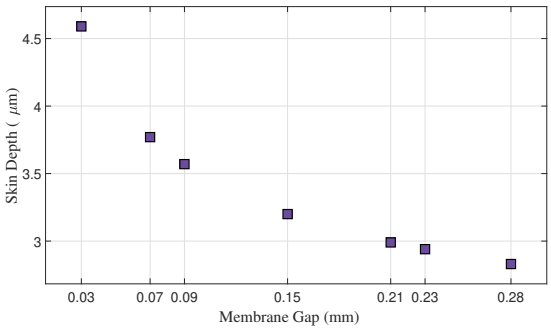
It is recommended to use a distance of 70 microns since this would operate at a lower frequency compared to the control, and also ensure a good Q-factor.

S.No	MP_h Distance (mm)	Frequency (GHz)	Total Q (-)	Skin Depth (μm)
1	0.03	0.71	634	4.59
2	0.07	1.05	638	3.77
3	0.09	1.17	631	3.57
4	0.15	1.46	536	3.20
5	0.21	1.67	485	2.99
6	0.23	1.73	464	2.94
7	0.28	1.87	415	2.83

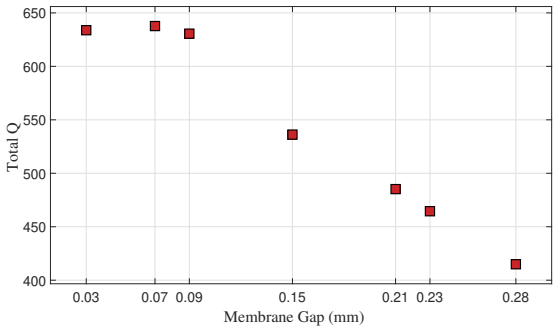
Table 4-11: Results for variations of the distance between Tuning Post and Membrane (MP_h)



(a) Impact on Frequency



(b) Impact on Skin Depth



(c) Impact on Total Q

Figure 4-10: Impact of Distance between Tuning Post and Membrane on Frequency, Skin Depth and Total Q

4-6-2 Impact of Distance between Tuning Post and Antenna

What is the impact of the distance between the tuning post and antenna?

As the antenna is moved closer to the tuning post, there is a greater transmission of energy due to the increased coupling between the two. This results in more current to flow which leads to an increase in ohmic losses in conductors with poor conductivity. As observed in the case of zinc, it is less conductive in comparison with better conductors like copper. Therefore, ohmic losses in the conductor increase. This contributes to a drop in the Q-factor. As the TA_L distance (illustrated in Figure 4-11) increases, the volume-to-surface area ratio increases contributing to improving the Q-factor as seen in Table 4-12.

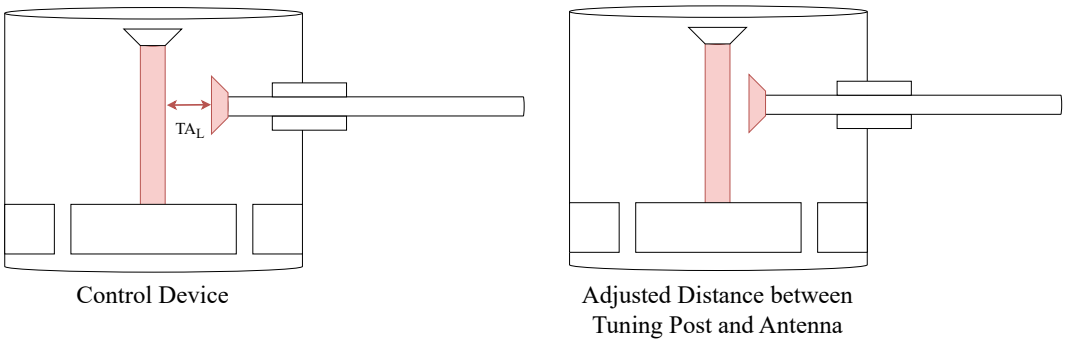


Figure 4-11: Visualisation of parameter adjustment for TA_L distance

S.No	TA_L Distance (mm)	Frequency (GHz)	Total Q (-)
1	2	1.73	291
2	2.5	1.73	373
3	3	1.73	465
4	3.5	1.73	558
5	4	1.73	650

Table 4-12: Results for variations of distance between Tuning Post and Antenna (TA_L)

The change in the TA_L does not affect the membrane capacitance and inductance due to which the frequency remains unchanged.

In conclusion, adjusting the TA_L distance is a way to improve the Q-factor while maintaining a constant frequency. This modification can be implemented to enhance the Total Q once the resonance frequency has been determined and is no longer adjustable.

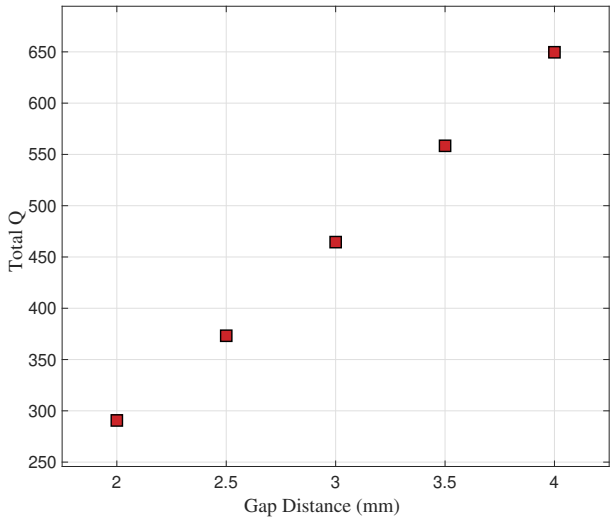


Figure 4-12: Impact of distance between tuning post and antenna on Total Q

4-6-3 Impact of Membrane thickness

What is the impact of changing the membrane thickness?

Adjusting the thickness of the membrane seemingly does not have an effect on the frequency or Q-factor. The resonant frequency mainly depends on the dimensions of the device. Hence, it remains unchanged despite the varying thickness of the membrane.

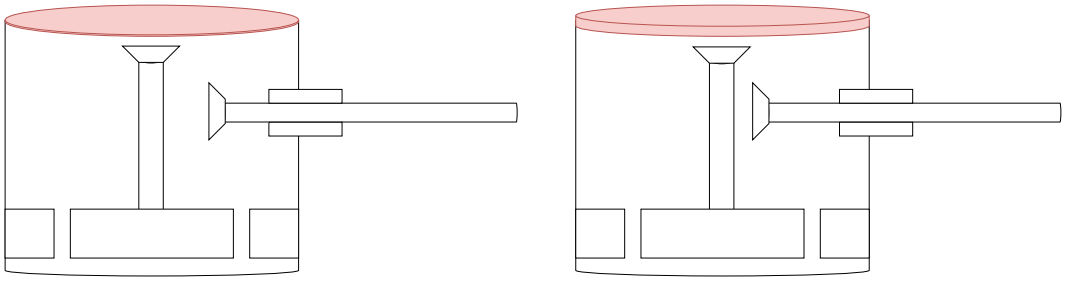


Figure 4-13: Visualisation of parameter adjustment for Membrane thickness

However, membrane thickness plays a crucial role in the device's ability to function properly as a microphone. A thicker membrane translates to increased rigidity in the diaphragm. A rigid diaphragm vibrates less efficiently in response to sound waves, hindering sound capture and signal encoding.

S.No	Membrane Thickness (mm)	Frequency (GHz)	Total Q (-)
1	0.0015	1.73	465
2	0.0030	1.73	464
3	0.0040	1.73	465
4	0.0063	1.73	464
5	0.009	1.73	465
6	0.0115	1.73	464
7	0.033	1.73	464
8	0.063	1.73	464
9	0.093	1.73	465
10	0.123	1.73	464
11	0.15	1.73	466

Table 4-13: Results for variations of Membrane thickness

In conclusion, while Table 4-13 does not show significant changes in frequency and Q-factor with varying thickness, maintaining a thin membrane is crucial for optimal microphone performance. A thin, flexible diaphragm ensures efficient vibration and accurate sound capture.

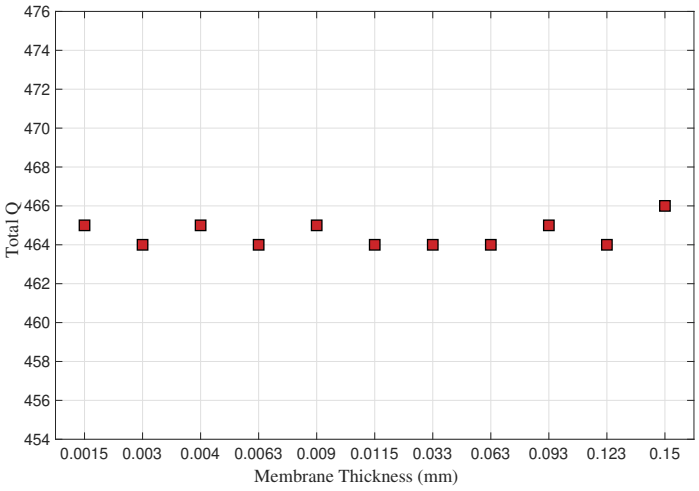


Figure 4-14: Impact of Membrane thickness on Total Q

4-6-4 Impact of Tuning Post height

What is the impact of changing the length of the tuning post?

This section investigates the effect of changing the tuning post height on the resonant frequency and Q-factor of the resonant cavity. The simulations were conducted while maintaining a constant distance between the membrane and the tuning post (MP_h).

When the distance between the membrane and the tuning post is kept constant, an increase in the height of the tuning post can allow more space for the magnetic field inside the cavity which results in an overall increase in inductance as seen previously in Equation: 3-20. The resulting increase in inductance leads to a decrease in frequency. The increase in height increases the overall resistance and leads to more ohmic losses.

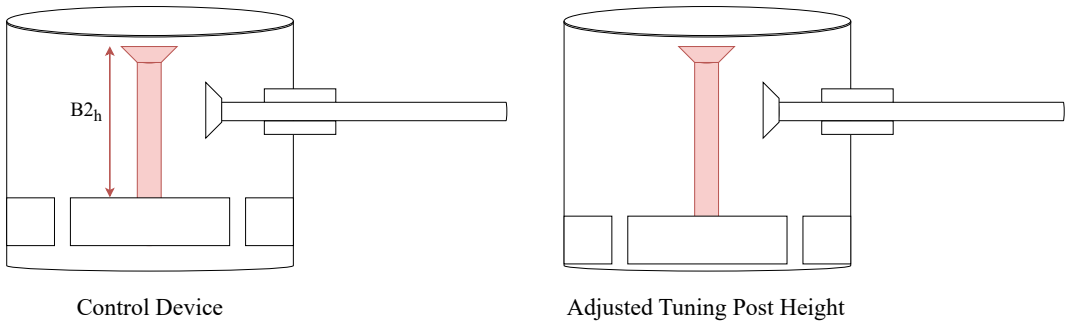
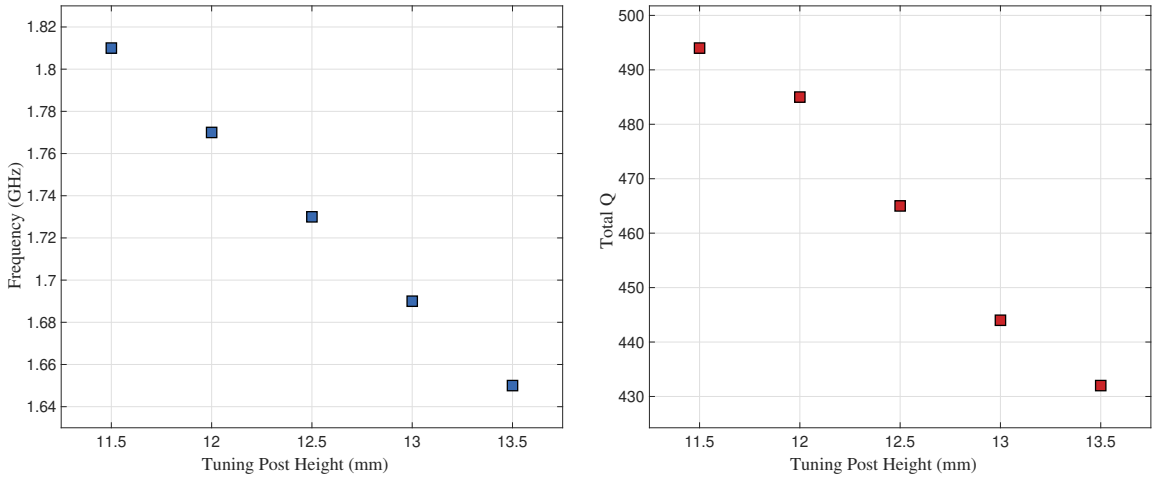


Figure 4-15: Visualisation of parameter adjustment for Tuning Post height ($B2_h$)

In conclusion, increasing the tuning post height decreases both Q-factor and resonance frequency. It is recommended to not have a height longer than 12.5mm which is the control dimension, as it reduces the Q-factor. Reducing the height to 11.5mm could help increase the Q-factor but it is important to note that this will also increase the frequency.

S.No	Tuning Post Height (mm)	Frequency (GHz)	Total Q (-)
1	11.5	1.81	494
2	12	1.77	485
3	12.5	1.73	464
4	13	1.69	444
5	13.5	1.65	432

Table 4-14: Results for variations of Tuning Post height ($B2_h$)



(a) Impact on Frequency **(b)** Impact on Total Q

Figure 4-16: Impact of Tuning Post height on Frequency and Total Q

4-6-5 Impact of Cavity Height

What is the impact of changing the height of the cavity?

In this simulation, the height of the cavity is varied systematically to see its effect on resonance properties. Figure 4-17 highlights the adjusted parameter for a better understanding.

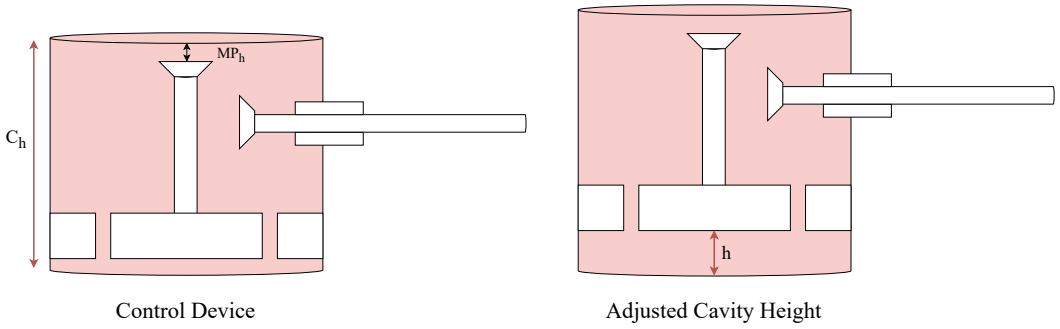


Figure 4-17: Visualisation of parameter adjustment for Cavity height (C_h)

The only parameter adjusted is the height of the cavity. The MP_h distance, which refers to the distance between the membrane and the tuning post, is maintained at a constant distance

of 0.23mm. Consequently, when the cavity height increases, the space under the tuning post and the cap, indicated by h in Figure 4-17 also increases, due to the unchanged tuning post and MP_h.

S.No	Cavity Height (mm)	Frequency (GHz)	Total Q (-)
1	16	1.72	462
2	17	1.73	464
3	18	1.73	464
4	19	1.73	465
5	20	1.73	464

Table 4-15: Results for variations of Cavity height (C_h)

Upon examining the findings shown in Table 4-15, it can be observed that the frequency stays consistent while the total Q shows slight variations. This is because the electromagnetic field stays unaltered owing to the constant tuning post height and MP_h gap, since by increasing the cavity height in these circumstances, only the space increases below the thread. As a result, the frequency and total Q are only marginally altered.

To conclude, the resonance and energy flow are localized only in the upper region of the cavity. The increase in cavity height (C_h) increases h as seen in Figure 4-17. There is minimal impact on frequency and Q-factor.

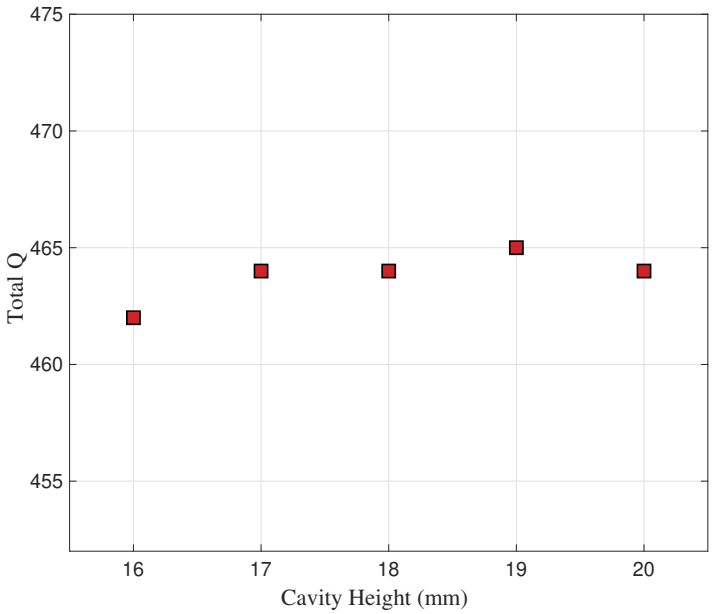


Figure 4-18: Impact of Cavity height on Total Q

4-6-6 Alternate Cavity Design

What is the impact of changing the cylinder to a larger flatter version?

In order to experiment with an alternative approach for the device, it underwent a change in design. The cavity height was reduced and flattened, with a height of 5mm as compared to 17mm. The diameter, on the other hand, almost doubled in size from 23.5mm to 40mm. Subsequently, the same simulation as Section 4-3 was executed and the outcomes were compared with those of the control devices.

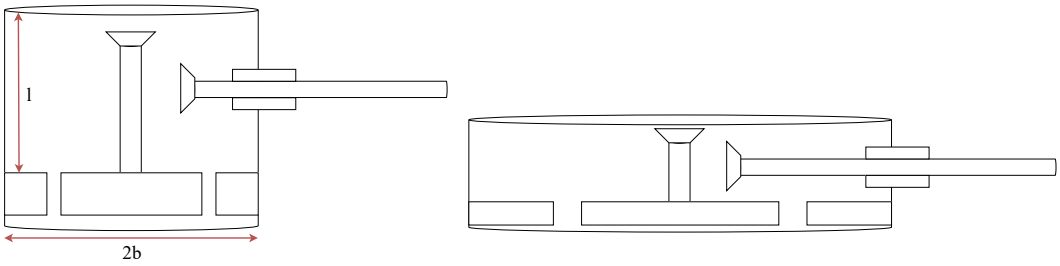


Figure 4-19: Visualisation of parameter adjustment an alternate design

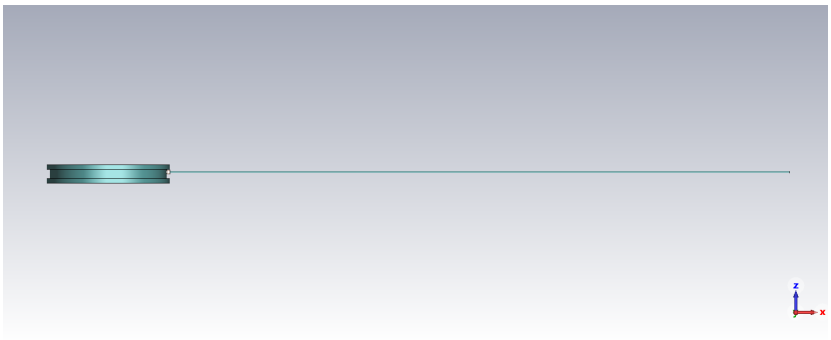
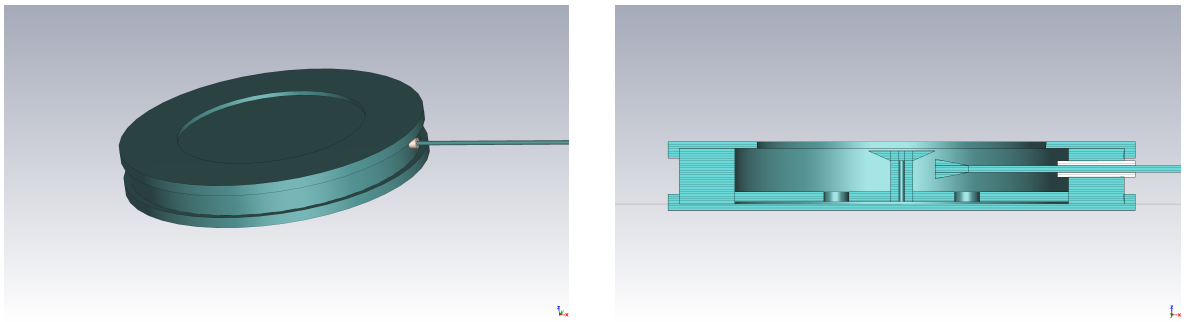


Figure 4-20: 3D CAD model of flattened cavity model variant



(a) View of flattened model variant **(b)** Cross-section of flattened model variant

Figure 4-21: 3D CAD model of flattened cavity model variant

As seen in the results in Table 4-16, the frequency and the Q-factor increase. This is because the reduction in height of the tuning post leads to a decrease in resistance, resulting in a reduction in ohmic losses. The Q-factor sees a significant improvement, increasing by a factor of 66.2% from control zinc.

Additionally, increasing the radius of the cavity results in a higher ratio of volume-to-surface

area. This contributes to an increase in the Q-factor. The reduction in post height reduces the space for the magnetic field, resulting in a decrease in inductance and an increase in resonant frequency.

It can also be seen in Equation: 3-26 that an increase in b, which is the radius of the cavity (as illustrated in Figure 4-19) tends to decrease the resonant frequency. However, the effect caused by the decrease of l (length from the base of the tuning post until the membrane) is more dominant, resulting in a higher frequency.

Model	Frequency (GHz)	Total Q (-)	Skin Depth (μm)
Control Copper	1.73	580	1.57
Control Zinc	1.73	494	2.94
Flattened Variant	2.98	821	2.24

Table 4-16: Simulation Results Compared to Control Device for MP_h distance of 0.23mm

4-7 Design Modification towards Longer-Distance Operation

What impact would scaling up the device have on the Frequency and Q-factor?

This simulation investigates the effects of scaling up the device on the resonance properties. The control device is the zinc variant with the dimensions as given in Table 4-17.

4-7-1 Parameter adjustments for different scaled-up variants

The device is scaled up three times as illustrated in Figure 4-22, and the dimensions for all variants are given in Table 4-17. Scaled-up 25% indicated that the device has been scaled up 25% from the control dimensions. Although the diameter of the membrane varied, the thickness of the membrane was kept constant at 6.35 μm in line with the control device.

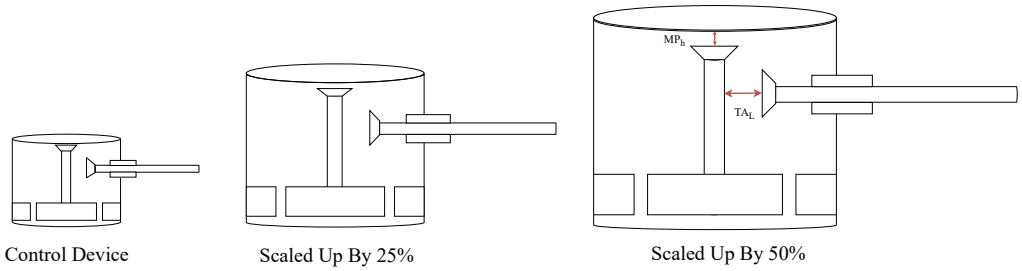


Figure 4-22: Scale-Up Illustration

Similar to Section 4-5, two sets of simulations were run. They were classified based on two different control MP_h, distances (Gap between Tuning Post and Membrane), 0.07mm and 0.23mm.

Table 4-17 shows the variations in the dimensions. The whole device was scaled three different times in the manner as illustrated in Figure 4-22. Scaled up by 25% means that the device was scaled up by 25% from the control dimensions, and so on.

Parameters	Dimensions (mm)	Scale Increased by		
		25%	**50%**	**75%**
C_h	17	21,25	25,5	29,75
C_{id}	21,5	26,87	32,25	37,62
C_{od}	23,5	29,37	35,25	41,12
CA_d	6,3	7,87	9,45	11,02
$B1_h$	3	3,75	4,5	5,25
TP_d	2	2,5	3	3,5
PH_d	2,25	2,81	3,375	3,93
$B2_h$	12,5	15,62	18,75	21,87
$B1_d$	6	7,5	9	10,5
$A1_d$	1,2	1,5	1,8	2,1
$A1_L$	230	287,5	345	402,5
$A2_d$	6	7,5	9	10,5
$A3_d$	5	6,25	7,5	8,75
$A3_h$	5	6,25	7,5	8,75
D_{od}	25,5	31,87	38,25	44,62
D_{id}	17,5	21,87	26,25	30,62
D_h	5	6,25	7,5	8,75
TA_L	3	3,75	4,5	5,25
MP_h	0,23	0,2875	0,345	0,4025
MP_h	0,07	0,0875	0,105	0,1225

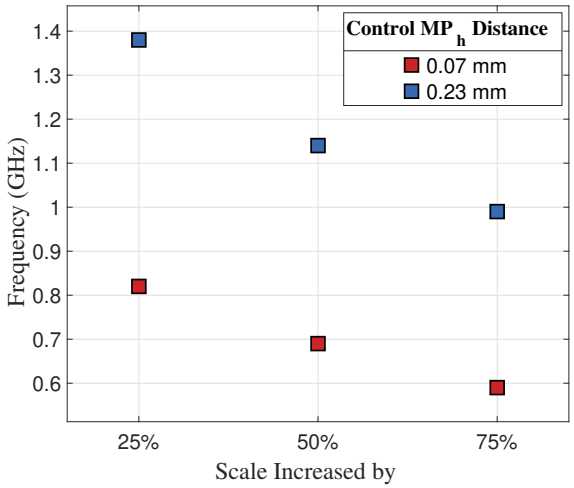
Table 4-17: Dimensions of scaled-up variant models

4-7-2 Results

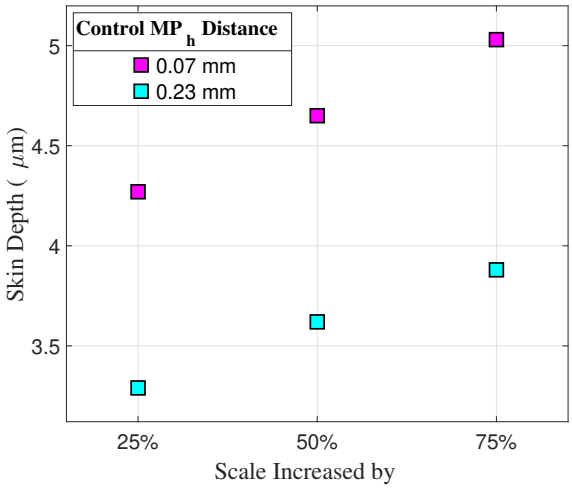
Scale When Increased by	Frequency		Total Q		Skin Depth (μm)
	Device Frequency (GHz)	Difference compared to Control Device	Device Total Q (-)	Difference compared to Control Device	
Control Device	1.05		638		3.77
25%	0.82	-24%	682	6%	4.27
50%	0.69	-41%	730	13%	4.65
75%	0.59	-56%	782	20%	5.03

Table 4-18: Comparison of results for Control MP_h Distance - 0.07mm

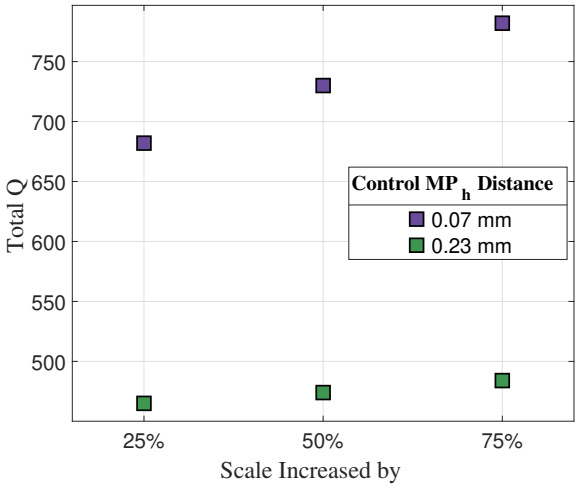
Scaling the device significantly impacts its operating characteristics. As the size increases, the resonance frequency decreases, as predicted by Equation: 3-26. This decrease is due to the increased capacitance resulting from the larger area of the scaled device. Additionally, the larger volume-to-surface area ratio leads to a slight improvement in the inductance (Equations 3-20 and 3-21). Tables 4-18 and 4-19 compare the results for two sets of simulations, each with a different control value for the gap distance (MP_h) between the tuning post and the membrane (0.07 mm and 0.23 mm).



(a) Impact on Frequency



(b) Impact on Skin Depth



(c) Impact on Total Q

Figure 4-23: Impact of scaling up device on Frequency, Skin Depth and Total Q

Scale When Increased by	Frequency		Total Q		Skin Depth (μm)
	Device Frequency (GHz)	Difference compared to Control Device	Device Total Q (-)	Difference compared to Control Device	
Control Device	1.73		464		2.94
25%	1.38	-22%	465	0.2%	3.29
50%	1.14	-41%	474	2%	3.62
75%	0.99	-54%	484	4%	3.88

Table 4-19: Comparison of results for Control MP_h Distance - 0.23mm

These observations are further illustrated in Figure 4-23.

The results in Tables 4-18 and 4-19 highlight a trade-off between device size and performance. As the device is scaled up, a gradual decrease in frequency is observed for both control gap distances. This is because the resonance frequency depends primarily on the device's inductance and capacitance, which are both influenced by its dimensions.

The skin depth increases as the frequency decreases as seen in Equation: 3-29, potentially leading to higher ohmic losses in the scaled devices. However, the total Q-factor exhibits a slight improvement due to the better volume-to-surface area ratio.

In conclusion, scaling up the device size lowers the operating frequency and slightly improves the Q-factor. This has the potential for long-range applications due to the lower operating frequencies.

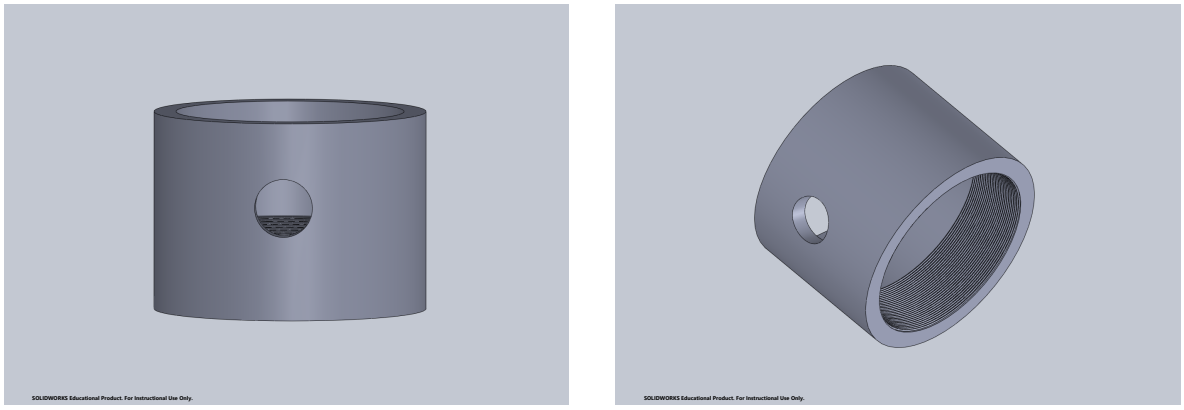
Biodegradable Microphone Fabrication

5-1 Microwave Resonator Fabrication

The detailed dimensions of all the parts are described in Table 5-1.

5-1-1 Resonant Cavity

Figure 5-1 shows the resonator cavity by itself. It is 17mm in height and has an outer diameter of 23.5mm and an inner diameter of 21.5mm. One end of the resonator has a threading as seen in Figure 5-1b until the insulator hole. The tuning post screws into a threaded end of the resonator. The other end is meant for affixing the membrane.



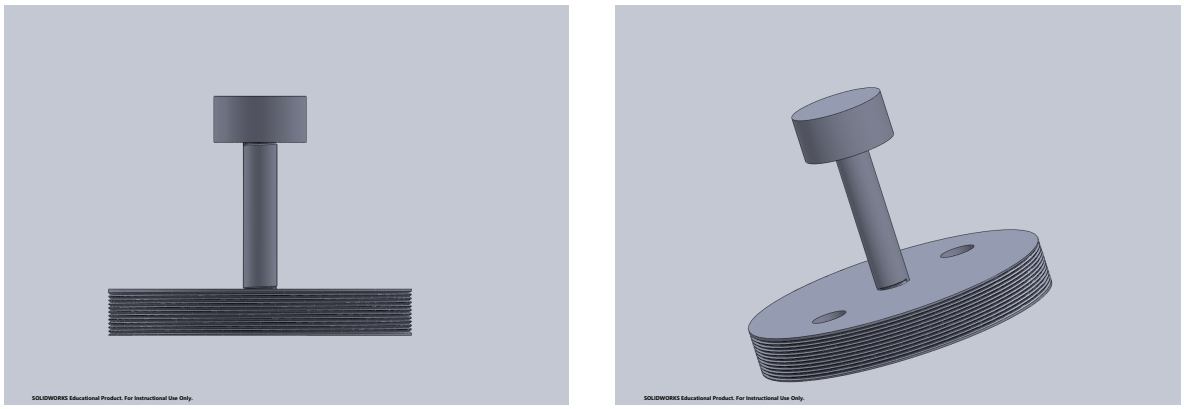
(a) **(b)**

Figure 5-1: CAD Model of resonant cavity

Figure 5-2 shows the tuning post component which consists of the threaded base which screws into the threaded end of the cavity, and the tuning post. The threading is present in order to facilitate adjustment of the distance between the membrane and the tuning post.

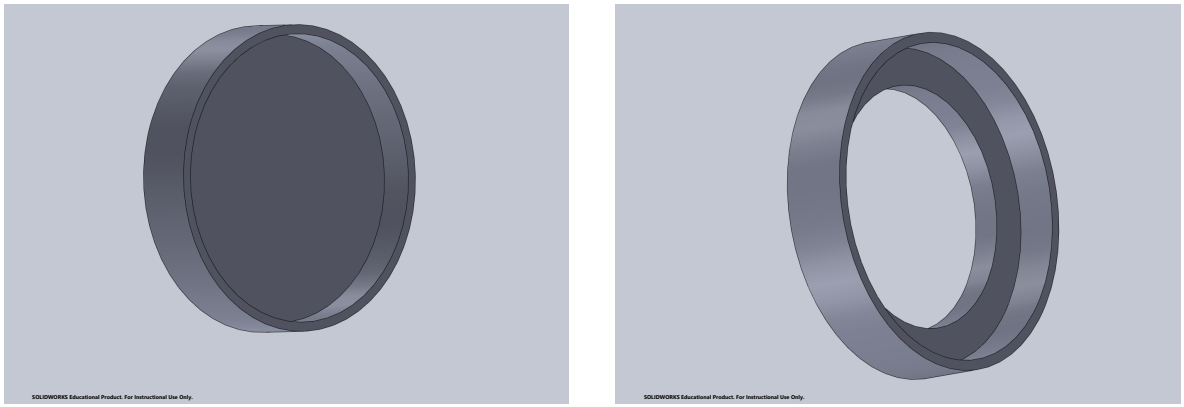
The main distinction between the Great Seal Bug and the proposed design of The BioThing is the cap that fits over the resonator covering the membrane. Unlike the original design, which employed a brass grill, this design adapts a simpler approach to a cap that still incorporates an opening for the membrane as seen in Figure 5-3b. In addition, threading on the caps has been eliminated to ease fabrication.

This does not impact the overall design since the function remains identical to the grill and both sides of the cavity are covered, with one side having an opening for the membrane.



(a) **(b)**

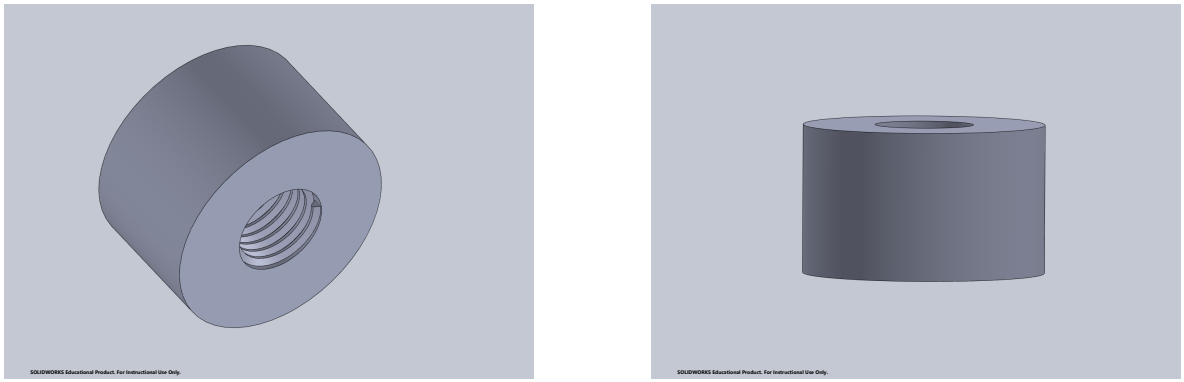
Figure 5-2: CAD Model of tuning post and thread



(a) Model of part D1 **(b)** Model of part D2

Figure 5-3: CAD Model of resonant cavity caps

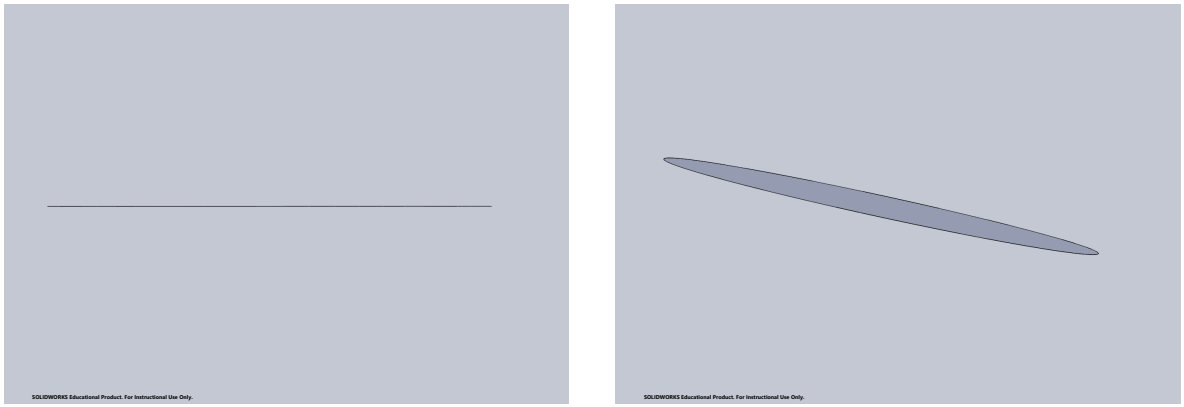
5-1-2 Insulator



(a) **(b)**

Figure 5-4: CAD Model of insulator

5-1-3 Membrane



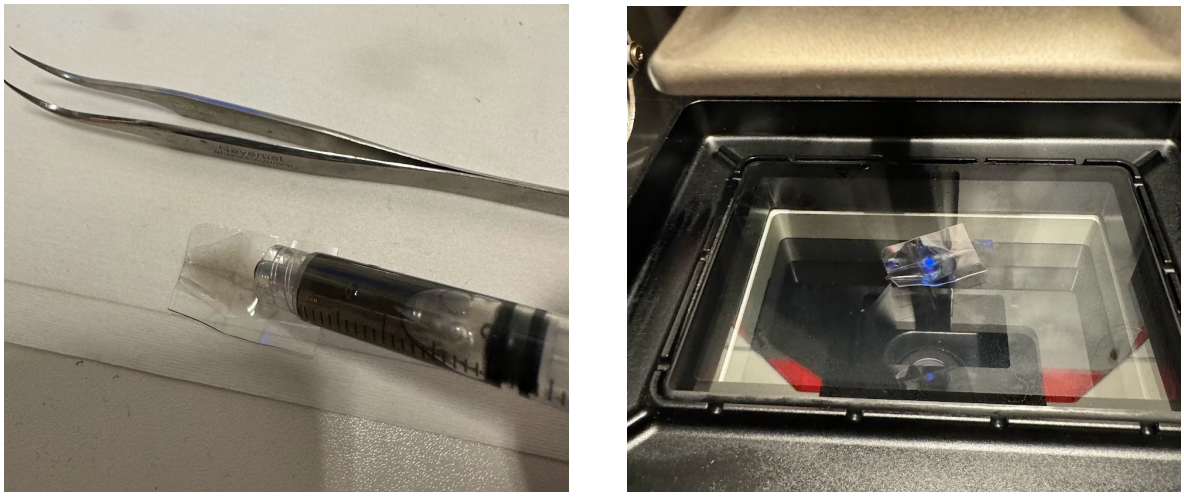
(a) **(b)**

Figure 5-5: CAD Model of membrane (diaphragm)

5-2 Fabricated Device, Results and Challenges

The device was fabricated in two stages. The metal components were fabricated using commercially available resin at the IWM workshop in 3Me, TU Delft. The insulator was 3D printed with a commercially available, plant-based resin.

In order to print using the plant-based resin, the material had to first be characterised, as seen in Figure 5-6. A number of tests were performed and the established protocol is detailed in Appendix B.



(a) **(b)**

Figure 5-6: Resin Characterization Tests

The fabricated device exhibited deviations from the original design, potentially due to manufacturing tolerances. These discrepancies are evident when comparing the cross-sections in

Figures 5-10a and 5-10b. Notably, Parts C (Cavity) and D (Cavity Caps) of the fabricated device show significant dimensional changes compared to the originals.

The modifications are compared in detail against the original dimensions in the table 5-1.

Part Name	**Part Description**	**Original Device Dimensions (mm)**	**Fabricated Device Dimensions (mm)**
Part A1 (Antenna rod)	Diameter	1.2	2
	Length	230	230
Part A2 (Antenna disc)	Diameter	6	3.8
	Height	3	3
Part A3 (Insulator)	Outer Diameter	5	4.9
	Inner Diameter	1.2	2
	Height	3	4.7
Part B1 (Tuning Post threaded base)	Height	3	3.5
	Diameter	21.50	19.4
	Hole for B2	2	2
	Pneumatic Holes	2.25	2.3
Part B2 (Tuning Post rod)	Height	15.5	18.5
	Diameter	2	1.9
Part B3 (Mushroom disc)	Height	3	3
	Diameter	6	6
Part C (Cavity)	Length	17	22.8
	Inner Diameter	21.5	19.5
	Outer Diameter	23.5	23.5
	Height from edge to insulating hole	6.3	10.6
Part D1 (Cavity Cap - Bottom End)	Outer Diameter	25.5	25
	Inner Diameter	23.5	23.6
	Height	5	5.4
Part D2 (Cavity Cap - Top End)	Outer Diameter	25.5	25
	Inner Diameter	23.5	23.5
	Height	3	5.4
	Membrane Hole Diameter Opening	17.5	17.8
Part E (Membrane)	Diameter	23.5	23
	Thickness	0.00635	-

Table 5-1: Dimensions of original device and fabricated device

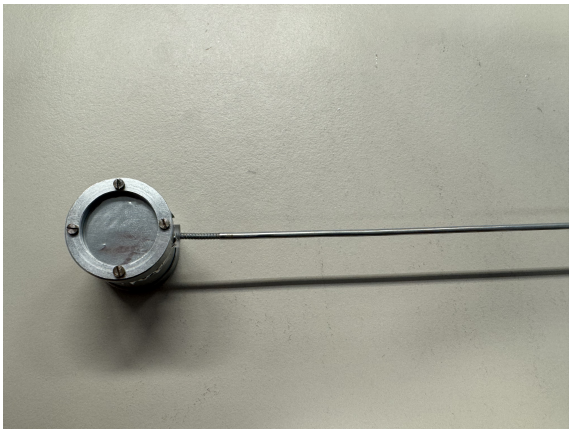
The crucial change was the fabricated Cavity (Part C) is longer than its original counterpart, potentially impacting internal component placement. The fabricated Cavity (Part C) and Top Cap (Part D2) have smaller inner diameters compared to the originals. This could affect the fit of other components within the cavity. The difference in these dimensions can be observed in Table 5-1.

Additionally, other changes in components include A2, A1, B1, and B2. However, the changes

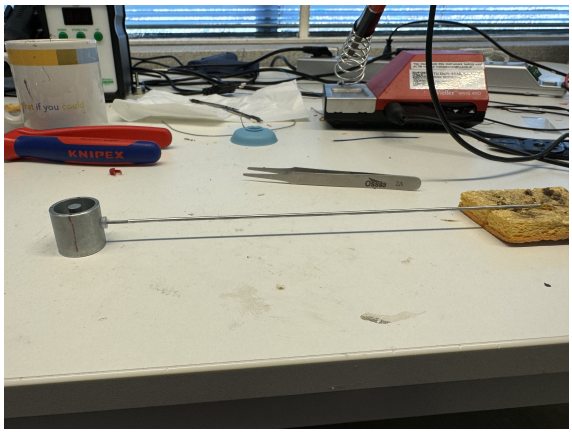
were foreseen as they were either a result of the changes in the aforementioned Part C or material unavailability, such as Part A1 and Part E.



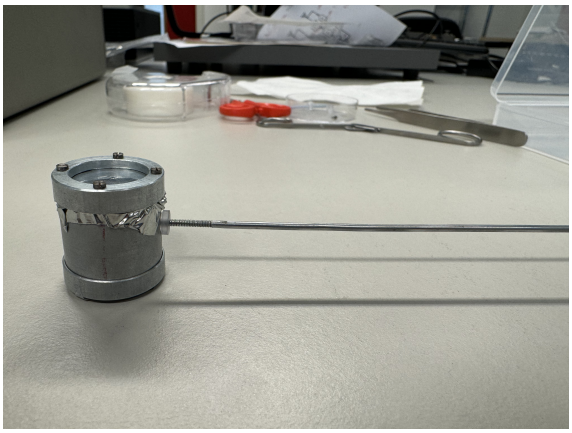
(a) Top View (Without Membrane)



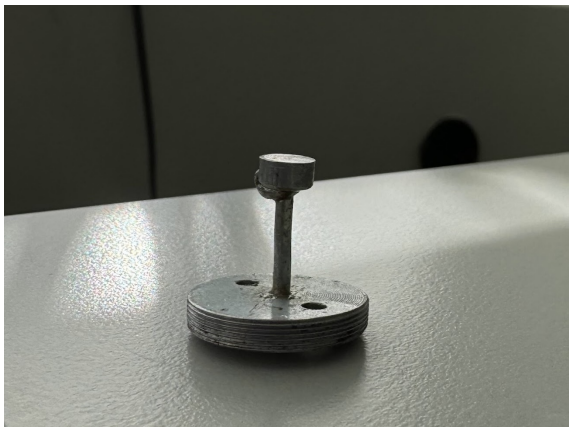
(b) Top View (With membrane)



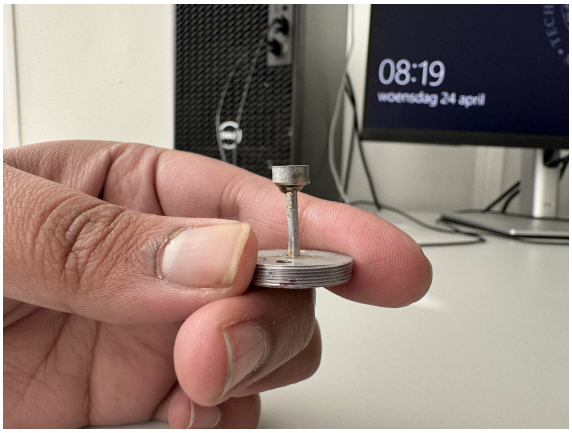
(c) View (Without Membrane)



(d) View (With Membrane)

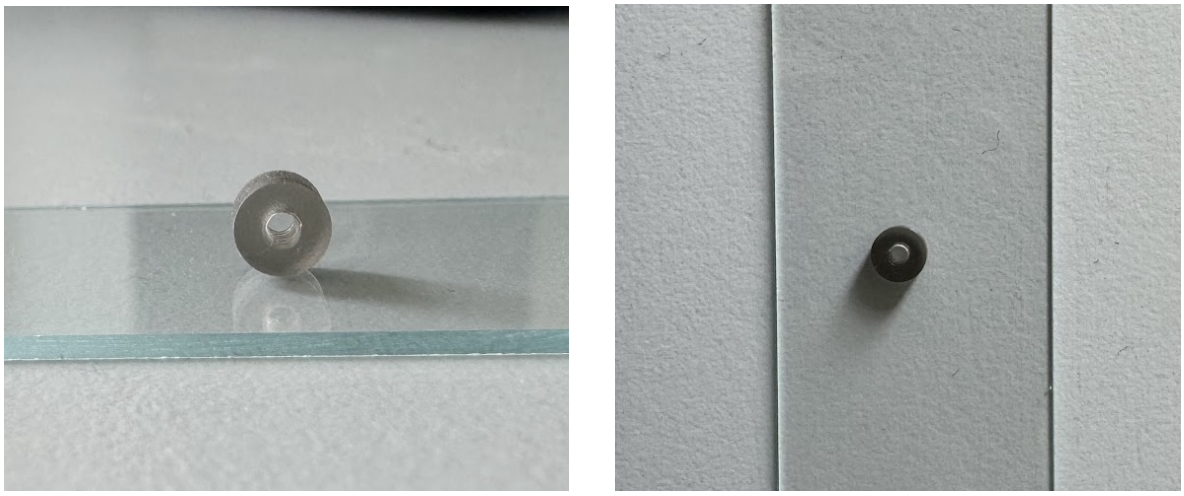


(e) Tuning Post Without Cavity



(f) Tuning Post Without Cavity

Figure 5-7: Images of device fabricated at IWM



(a) (b)

Figure 5-8: Images of 3D printed insulator with commercially available plant-based resin

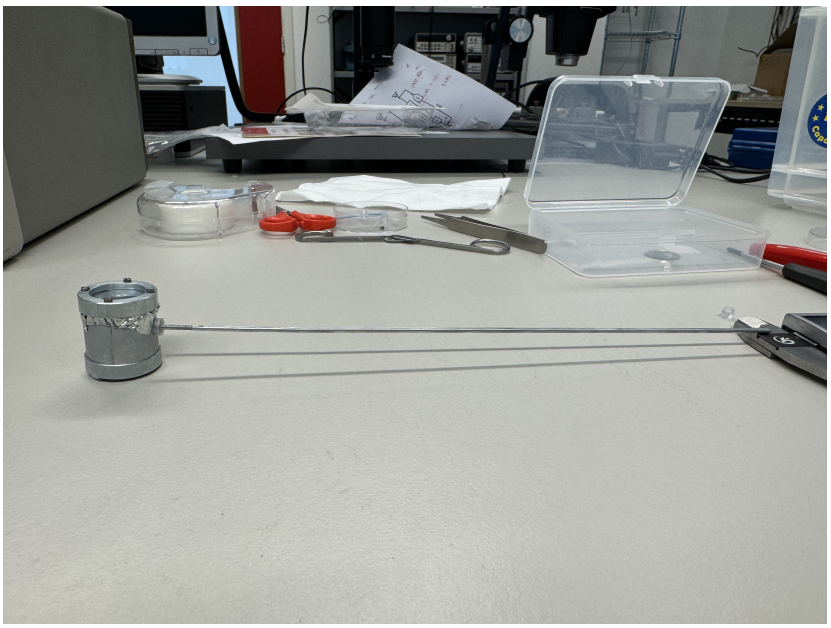
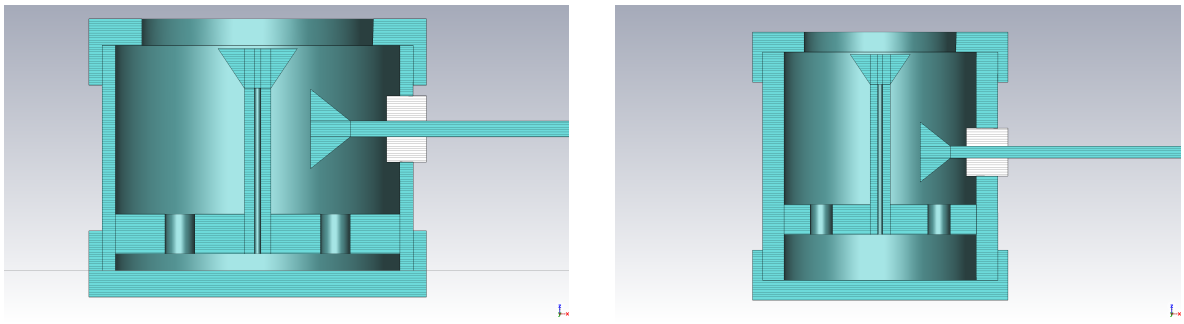


Figure 5-9: Full view of fabricated device

5-3 Anticipated performances of fabricated device vs original design

Due to deviations from the simulated models described in Chapter 4, the fabricated device was simulated to predict its performance before characterization. This pre-characterization simulation provides valuable insights into the anticipated performance changes compared to the original design, allowing for a more focused and efficient characterization process.

Figure 5-10 compares the cross-section of the originally proposed zinc variant and the fabri-



(a) Zinc variant model cross-section **(b)** Fabricated device model cross section

Figure 5-10: Comparison of cross-sections of devices

cated model. The differences in the dimensions are detailed in Table 5-1.



Figure 5-11: 3D Model of Fabricated Device

As indicated in Table 5-1, variations in critical dimensions occurred due to several factors including fabrication faults. As explained previously, modifications such as adjusting the antenna diameter and membrane thickness were implemented as a result of the unavailability of the necessary materials.

The height from the top edge of the cavity to the insulating hole has increased from 6.3mm to 10.6mm. The effect of variation in this parameter on device performance has not been studied in this project. This deviation can have an impact on device performance which needs further investigation to have a clear insight.

Model	Frequency (GHz)	Total Q	Skin Depth (μm)
Control Copper	1.73	580	1.567
Control Zinc	1.73	465	2.939
Fabricated Device	1.59	679	3.076

Table 5-2: Simulation Results Compared to Control Device

Table 5-2 provides the simulation results of the fabricated device which shows the frequency experiences a drop of 6% and Q factor increases by 27%.

The drop in frequency is due to the increased height of the tuning post which causes increased inductance as discussed in Section 4-6-4. Although there are now other parameters like the

insulator hole height and antenna radius that warrant further investigation for their impact on Q-factor increase, the volume-to-surface area is a contributing factor.

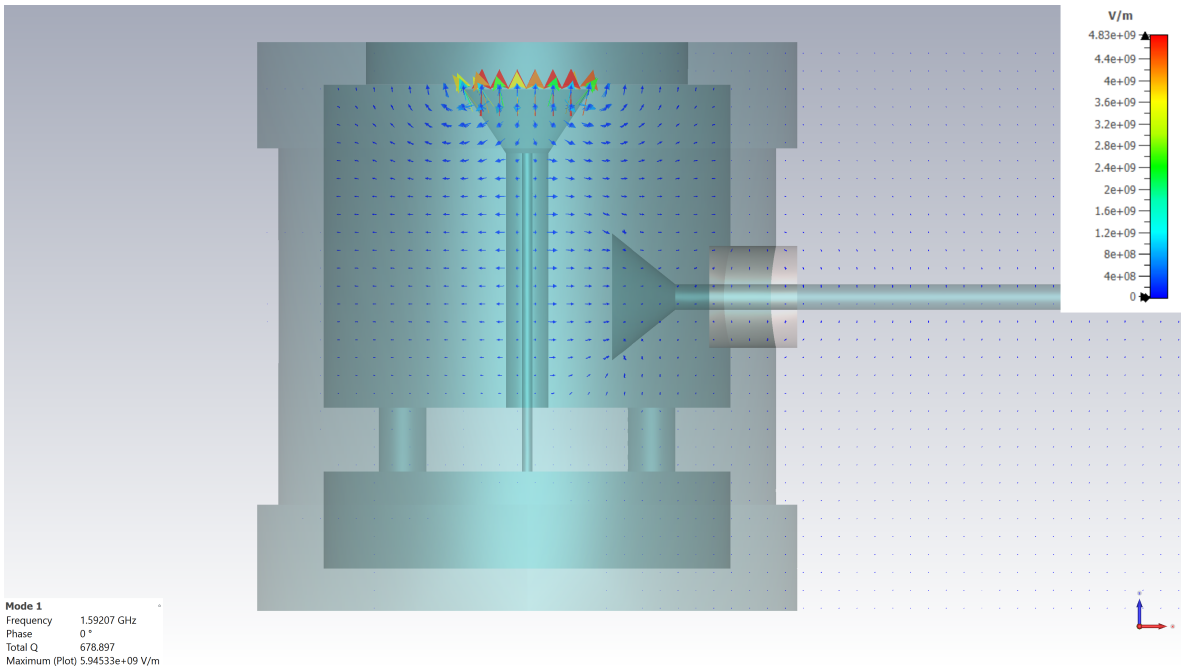


Figure 5-12: E-Field of fabricated device's dominant eigenmode

The pre-characterization simulations provided valuable insights, particularly regarding the resonant frequency of the device. This information is crucial for developing a focused characterization plan, as discussed in the upcoming section.

5-4 Characterization Plan

The characterization plan is divided into two sections as follows

5-4-1 Proof of Concept

The Proof of Concept aims to verify the concept of the characterisation plan.

The configuration illustrated in figure 5-13 is specifically tailored to the primary setup, but instead of using the prototype, a waveform generator is employed to transmit a low-frequency signal in order to replicate the behaviour of the device. This allows us to verify the effectiveness of the concept behind illuminating the device.

The AD8361 is a mean-responding power detector for use in high-frequency receiver and transmitter signal chains, up to 2.5 GHz. It requires a single supply only between 2.7 V and 5.5 V. The AD8361 is intended for true power measurement of simple and complex waveforms.

As depicted in Figure 5-13 A setup is established to transmit a high-frequency wave using an RF Signal Generator. This high-frequency wave is then superimposed on a low-frequency

wave generated by the waveform generator. The AD8361 Moduleboard is used to separate the low-frequency signal from the high-frequency signal and transmit it to the oscilloscope for visualisation.

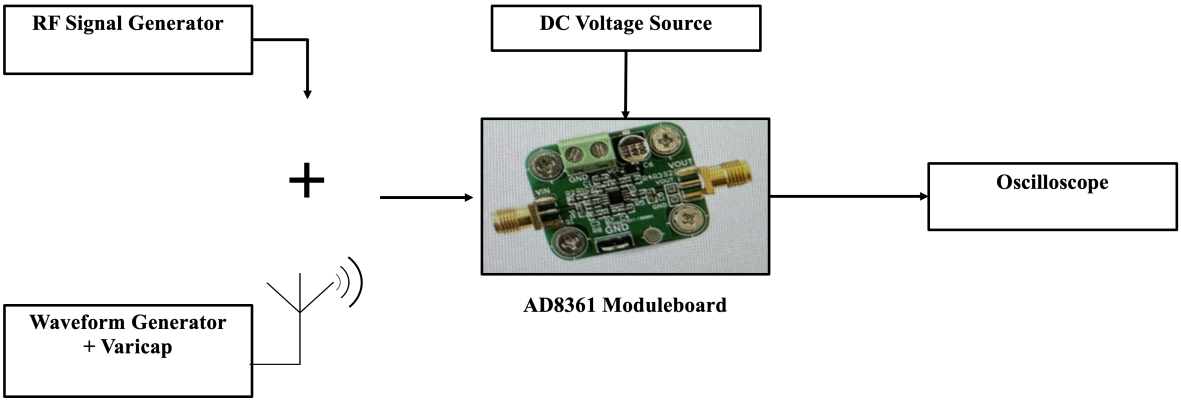


Figure 5-13: Proposed Proof of Concept Setup Illustration

A laboratory experiment as shown in Figure 5-14 was established to test this and is now prepared for testing.

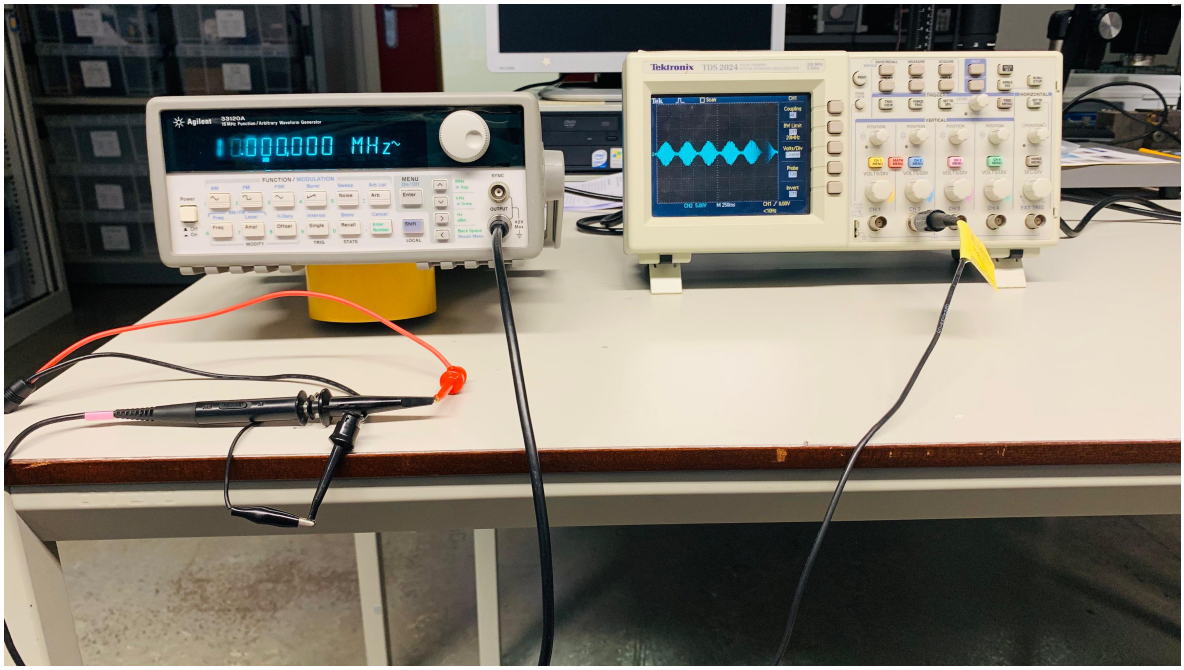


Figure 5-14: Proposed Proof of Concept Lab Setup

5-4-2 Proposed Readout Setup

The following setup as illustrated in Figure 5-15 was designed to characterize the device. As visualised, a modulating signal and carrier signal are superimposed, where the carrier signal generated by the RF Signal generator illuminates the device. The Spectrum Analyzer FSH8,

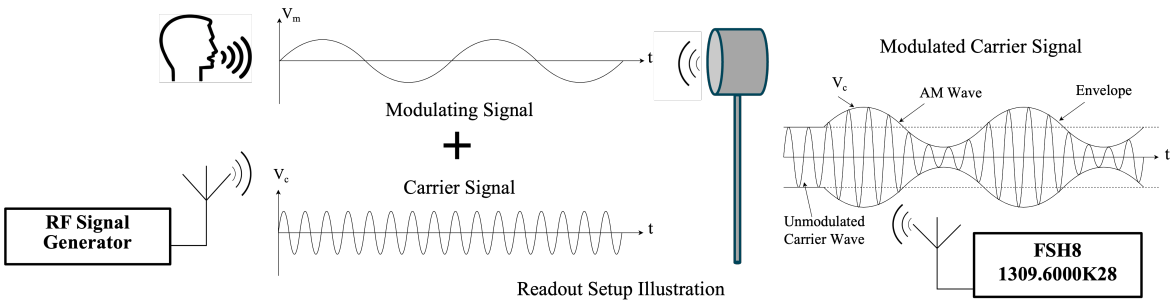


Figure 5-15: Schematic illustrating a readout setup designed to characterize a device's response to a modulated carrier signal: A radio frequency (RF) signal generator produces a carrier signal, which is subsequently modulated by an external signal. The modulated carrier signal generated is used to illuminate the device (The BioThing). The FSH-8 spectrum analyzer is capable of measuring the modulated carrier signal after interaction with the Device (The BioThing), enabling analysis of the device's functionality

which also functions as a vector analyzer, detects the modulated carrier signal waves. The AD 8361 board and the oscilloscope have been substituted with the spectrum analyzer, which, in theory, has the capability to isolate the signal and graphically depict it.

The same experimental set-up was arranged in the lab as depicted in Figure 5-16. The device and setup are ready for characterization.

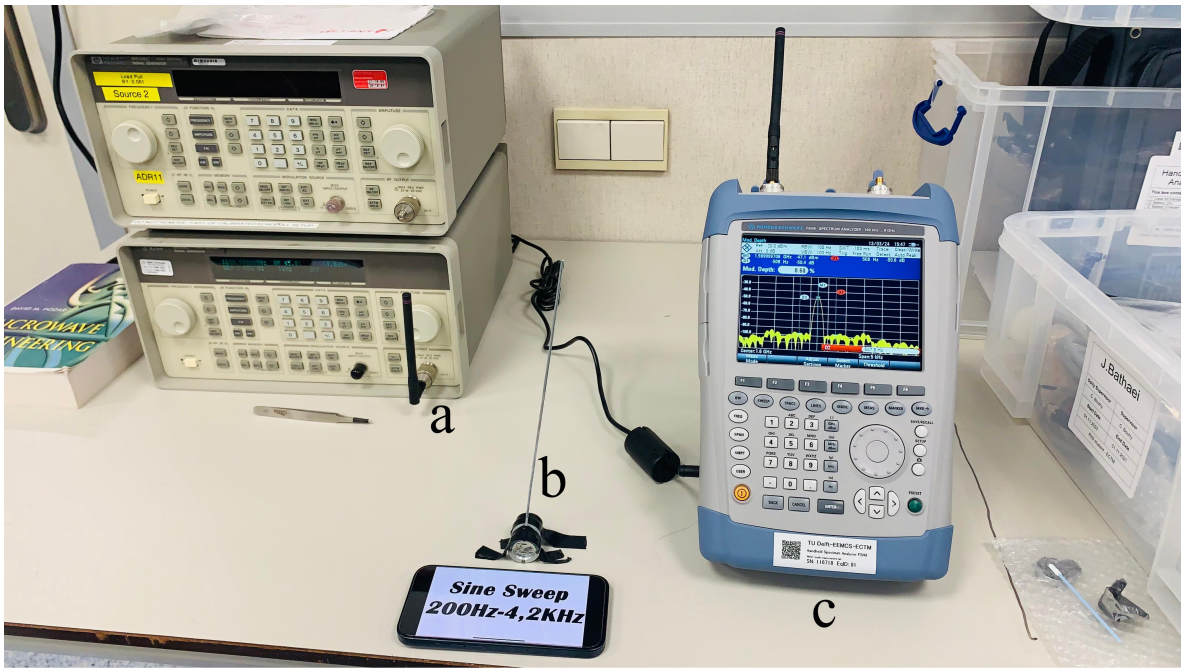


Figure 5-16: Characterization setup for the BioThing: Components (from left) (a). HP Agilent Keysight, 8648C (RF Signal Generator) (b). The BioThing (c). Rohde and Schwarz FSH-8 Spectrum Analyzer

Conclusion

6-1 Concluding Remarks

The research study focused on the primary obstacles to implementing passive acoustic monitoring for biodiversity: Working towards a biodegradable and battery-free audio recording device, a microphone design that is suitable for wireless operation without the need for batteries or a power source was identified. This design enables a more sustainable method of monitoring biodiversity and helps work towards alleviating some of the challenges encountered by the present state-of-the-art designs.

The simulations conducted in this study have identified several essential parameters that impact the microphone's functionality and efficiency, including the Membrane-Tuning Post gap and Antenna-Tuning Post distance, in addition to factors such as working frequency and material. Furthermore, the simulations have yielded valuable insights that can inform future design iterations. This data can be leveraged to reduce the device's footprint in order to facilitate faster degradation and also holds promise for scaling it up for long-range applications, catering to specific monitoring scenarios requiring broader coverage.

A prototype was successfully fabricated and assembled. A characterization setup has been developed and is ready for implementation. Furthermore, a protocol for characterizing external resin and potentially other materials for 3D printing was established.

6-2 Outlook

The first step would be to test the microphone operation and verification of the device functionality. Further, it is essential to develop a thinner membrane in order to effectively utilise the laboratory-ready readout setup and facilitate a more thorough assessment of the device's performance. In the next steps, the main emphasis will be to improve the device functionality and control the degradation process. Investigating the capabilities of a slightly bigger and more flat design, as well as the potential for an enlarged version, shows potential for optimizing device performance for various applications that require a biodegradable microphone, including monitoring biodiversity. Fabrication with biodegradable alloys (For example, Zn and Mg alloy) can be considered to accelerate degradation.

Further research along these lines will work towards the end goal of the project for a completely operational, biodegradable, passive and wireless microphone for passive acoustic monitoring, furthering the project's objective and promoting a more sustainable and ecosystem-friendly approach to environmental monitoring.

Bibliography

[1] W. (W. F. for Nature), "Living Planet Report 2022 - Building a nature-positive society," 2022. [Online]. Available: https://wwfeu.awsassets.panda.org/downloads/lpr_2022_full_report.pdf.

[2] G. Ceballos, P. R. Ehrlich, and R. Dirzo, "Biological annihilation via the ongoing sixth mass extinction signaled by vertebrate population losses and declines," *Proceedings of the National Academy of Sciences*, vol. 114, no. 30, 2017, ISSN: 1091-6490. DOI: 10.1073/pnas.1704949114. [Online]. Available: http://dx.doi.org/10.1073/pnas.1704949114.

[3] G. Ceballos, P. R. Ehrlich, and P. H. Raven, "Vertebrates on the brink as indicators of biological annihilation and the sixth mass extinction," *Proceedings of the National Academy of Sciences*, vol. 117, no. 24, pp. 13 596–13 602, 2020. DOI: 10.1073/pnas.1922686117. eprint: https://www.pnas.org/doi/pdf/10.1073/pnas.1922686117. [Online]. Available: https://www.pnas.org/doi/abs/10.1073/pnas.1922686117.

[4] [Online]. Available: https://www.worldwildlife.org/stories/what-is-the-sixth-mass-extinction-and-what-can-we-do-about-it.

[5] J. W. Bradbury and S. L. Vehrencamp, "Economic models of animal communication," *Animal Behaviour*, vol. 59, no. 2, pp. 259–268, Feb. 2000, ISSN: 0003-3472. DOI: 10.1006/anbe.1999.1330. [Online]. Available: http://dx.doi.org/10.1006/anbe.1999.1330.

[6] E. Browning, R. Gibb, P. Glover-Kapfer, and K. E. Jones, "Passive acoustic monitoring in ecology and conservation.," en, Tech. Rep., 2017. DOI: 10.25607/OBP-876. [Online]. Available: https://repository.oceanbestpractices.org/handle/11329/1370.

[7] A. S. Digby, R. P. Clay, and P. N. Manley, "Counting birds by sound: Methods and applications in a changing world," *Journal of Field Ornithology*, vol. 84, no. 1, pp. 15–24, 2013. DOI: 10.1111/jofo.12006.

[8] D. Sanders and D. J. Mennill, "Vocal diversity in social contexts: Characteristics of chick calls and adult alarm calls in colonial tufted puffins," *Behavioral Ecology*, vol. 25, no. 1, pp. 125–135, 2014. DOI: 10.1093/beheco/art082.

[9] M. Towsey, J. Roebuck, G. E. Austin, and A. P. Kirbyman, "The use of acoustic monitoring for long-term and large-scale surveys of owls," *Bird Study*, vol. 61, no. 2, pp. 140–149, 2014. DOI: 10.1080/00063657.2014.902042.

[10] P. Klingbeil and M. R. Willig, "Forest structure and vertical stratification affect the spatial distribution of bird communities in neotropical rainforests," *Avian Conservation and Ecology*, vol. 10, no. 2, p. 4, 2015. DOI: 10.5772/5424-1002-10-2-4.

[11] E. Bader, K. Jung, E. K. Kalko, R. A. Page, R. Rodriguez, and T. Sattler, "Mobility explains the response of aerial insectivorous bats to anthropogenic habitat change in the neotropics," *Biological Conservation*, vol. 186, pp. 97–106, 2015, ISSN: 0006-3207. DOI: https://doi.org/10.1016/j.biocon.2015.02.028. [Online]. Available: https://www.sciencedirect.com/science/article/pii/S0006320715000981.

[12] G. Jones, H. Rebelo, and R. Ransome, "Improving the accuracy of acoustic identification of cryptic bat species in south-east asia," *Mammalian Biology*, vol. 78, no. 2, pp. 123–132, 2013. DOI: 10.1016/j.mambio.2012.08.002.

[13] H. Klinck, D. K. Mellinger, K. Klinck, *et al.*, "Correction: Near-real-time acoustic monitoring of beaked whales and other cetaceans using a seaglider™," *PLoS ONE*, vol. 7, no. 8, A. Fahlman, Ed., Aug. 2012, ISSN: 1932-6203. DOI: 10.1371/annotation/57ad0b82-87c4-472d-b90b-b9c6f84947f8. [Online]. Available: http://dx.doi.org/10.1371/annotation/57ad0b82-87c4-472d-b90b-b9c6f84947f8.

[14] P. H. Wrege, E. D. Rowland, S. Keen, and Y. Shiu, "Acoustic monitoring for conservation in tropical forests: Examples from forest elephants," *Methods in Ecology and Evolution*, vol. 8, no. 10, pp. 1292–1301, 2017. DOI: https://doi.org/10.1111/2041-210X.12730. eprint: https://besjournals.onlinelibrary.wiley.com/doi/pdf/10.1111/2041-210X.12730. [Online]. Available: https://besjournals.onlinelibrary.wiley.com/doi/abs/10.1111/2041-210X.12730.

[15] G. J. Measey, B. C. Stevenson, T. Scott, R. Altwegg, and D. L. Borchers, "Counting chirps: Acoustic monitoring of cryptic frogs," *Journal of Applied Ecology*, vol. 54, no. 3, C. Bellard, Ed., 2016, ISSN: 1365-2664. DOI: 10.1111/1365-2664.12810. [Online]. Available: http://dx.doi.org/10.1111/1365-2664.12810.

[16] Wikipedia, *Transect — Wikipedia, the free encyclopedia*, http://en.wikipedia.org/w/index.php?title=Transect&oldid=1193295637, [Online; accessed 02-May-2024], 2024.

[17] Wikipedia, *Surveying — Wikipedia, the free encyclopedia*, http://en.wikipedia.org/w/index.php?title=Surveying&oldid=1217195369, [Online; accessed 02-May-2024], 2024.

[18] S. S. Sethi, M. Kovac, F. Wiesemüller, A. Miriyev, and C. M. Boutry, "Biodegradable sensors are ready to transform autonomous ecological monitoring," *Nature Ecology & Evolution*, vol. 6, pp. 1245–1247, 2022. DOI: 10.1038/s41559-022-01824-w.

[19] Wikipedia, *Earth observation satellite — Wikipedia, the free encyclopedia*, http://en.wikipedia.org/w/index.php?title=Earth%20observation%20satellite&oldid=1216683381, [Online; accessed 02-May-2024], 2024.

[20] N. Sullivan, *Drone-enabled remote sensing and environmental monitoring*, 2022. [Online]. Available: https://mapware.com/blog/drone-enabled-remote-sensing-and-environmental-monitoring/.

[21] C. Desjonquères, T. Gifford, and S. Linke, "Passive acoustic monitoring as a potential tool to survey animal and ecosystem processes in freshwater environments," *Freshwater Biology*, vol. 65, no. 1, pp. 7–19, 2020.

[22] R. Gibb, E. Browning, P. Glover-Kapfer, and K. E. Jones, "Emerging opportunities and challenges for passive acoustics in ecological assessment and monitoring," *Methods in Ecology and Evolution*, vol. 10, no. 2, L. Börger, Ed., pp. 169–185, Nov. 2018. DOI: 10.1111/2041-210x.13101. [Online]. Available: https://doi.org/10.1111/2041-210x.13101.

[23] M. Ritts, *SAFE (Stability of Altered Forest Ecosystem) Project — Smart Forests Atlas — atlas.smartforests.net*, https://atlas.smartforests.net/en/logbooks/safe-project/.

[24] S. S. Sethi, R. M. Ewers, N. S. Jones, A. Signorelli, L. Picinali, and C. D. L. Orme, "Safe acoustics: An open-source, real-time eco-acoustic monitoring network in the tropical rainforests of borneo," *Methods in Ecology and Evolution*, vol. 11, no. 10, pp. 1182–1185, 2020. DOI: https://doi.org/10.1111/2041-210X.13438. eprint: https://besjournals.onlinelibrary.wiley.com/doi/pdf/10.1111/2041-210X.13438. [Online]. Available: https://besjournals.onlinelibrary.wiley.com/doi/abs/10.1111/2041-210X.13438.

[25] R. B. Lindsay, "The story of acoustics," *The Journal of the Acoustical Society of America*, vol. 39, no. 4, pp. 629–644, Apr. 1966, ISSN: 1520-8524. DOI: 10.1121/1.1909936. [Online]. Available: http://dx.doi.org/10.1121/1.1909936.

[26] *Phonoautograph*, 2024. [Online]. Available: en.wikipedia.org/wiki/Phonautograph.

[27] R. E. Conot and M. Josephson, "Thomas edison," in *Encyclopedia Britannica*. Dec. 2023.

[28] T. A. Edison, "The phonograph and its future," *The North American Review*, vol. 126, no. 262, pp. 527–536, 1878, ISSN: 00292397. [Online]. Available: http://www.jstor.org/stable/25110210 (visited on 01/08/2024).

[29] J. Eargle, *The Microphone Book* (Audio Engineering Society Presents Series). Focal Press, 2004, ISBN: 9780240519616. [Online]. Available: https://books.google.nl/books?id=w8kXMVKOsY0C.

[30] H. Robjohns, *A brief history of microphones*, 2022. [Online]. Available: https://micpedia.com/brief-history-of-microphones/.

[31] D. M. Huber and R. E. Runstein, *Modern Recording Techniques* (Audio Engineering Society Presents), en, 7th ed. Oxford, England: Focal Press, Sep. 2009.

[32] M. Duquesnoy, "Tuning forks in photoacoustic spectroscopy : Comparative study and new developments," Ph.D. dissertation, Mar. 2021. DOI: 10.13140/RG.2.2.10772.63361.

[33] A. Van Rhijn.

[34] D. Friedman, *Sound advice*. Bloomington, MN: AuthorHouse, Aug. 2010.

[35] J. Benesty and C. Jingdong, *Study and Design of Differential Microphone Arrays* (Springer Topics in Signal Processing). Springer Berlin Heidelberg, 2012, ISBN: 9783642337529. [Online]. Available: https://books.google.nl/books?id=tym4kKVPfaAC.

[36] *10.2: Microphones - human.libretexts.org*. [Online]. Available: https://www.mediacollege.com/audio/microphones/dynamic.html.

[37] W. S. Lee and S. S. Lee, "Piezoelectric microphone built on circular diaphragm," *Sensors and Actuators A: Physical*, vol. 144, no. 2, pp. 367–373, Jun. 2008, ISSN: 0924-4247. DOI: 10.1016/j.sna.2008.02.001. [Online]. Available: http://dx.doi.org/10.1016/j.sna.2008.02.001.

[38] *10.2: Microphones human.libretexts.org*. [Online]. Available: https://human.libretexts.org/Bookshelves/Theater_and_Film/Video_Production_Handbook/10%3A_Sound/10.02%3A_Microphones.

[39] D. M. Pozar, *Microwave Engineering*, en, 4th ed. Chichester, England: John Wiley & Sons, Nov. 2011.

[40] M. Simmons and P. Reuvers, *The great seal bug*. [Online]. Available: https://www.cryptomuseum.com/covert/bugs/thing/.

[41] *Schoolphysics:: Schoolphysics.co.uk*. [Online]. Available: https://www.schoolphysics.co.uk/age11-14/Electricity%20and%20magnetism/Electromagnetism/text/Carbon_microphone/index.html.

[42] D. Garthe, "A fiber-optic microphone," *Sensors and Actuators A: Physical*, vol. 26, no. 1, pp. 341–345, 1991, Proceedings of Eurosensors IV held in jointly with Sensoren Technologies und Anwendung, ISSN: 0924-4247. DOI: https://doi.org/10.1016/0924-4247(91)87014-T. [Online]. Available: https://www.sciencedirect.com/science/article/pii/092442479187014T.

[43] *Us4479265a - patent laser microphone*. [Online]. Available: https://patents.google.com/patent/US4479265?oq=laser+microphone#citedBy.

[44] M. A. Shah, I. A. Shah, D.-G. Lee, and S. Hur, "Design approaches of mems microphones for enhanced performance," *Journal of Sensors*, vol. 2019, p. 9 294 528, 2019, ISSN: 1687-725X. DOI: 10.1155/2019/9294528. [Online]. Available: https://doi.org/10.1155/2019/9294528.

[45] H. Akino and et al, "On the study of the ionic microphone," *Journal of the Audio Engineering Society*, vol. 62, no. 4, pp. 254–264, Apr. 2014, ISSN: 1549-4950. DOI: 10.17743/jaes.2014.0013. [Online]. Available: http://dx.doi.org/10.17743/jaes.2014.0013.

[46] F. E. Terman, *Radio Engineer's Handbook*. New York, NY: McGraw-Hill, Dec. 1943.

[47] A. Akkoç, "Design and implementation of a microwave cavity resonator for modulated backscattered wave," M.S. thesis, Middle East Technical University, 2015.

[48] A. Glinsky, *Theremin* (Music in American Life). Baltimore, MD: University of Illinois Press, Sep. 2000.

[49] *The thing, listening device*, 2023. [Online]. Available: https://en.wikipedia.org/wiki/The_Thing_(listening_device).

[50] FBI, *Final technical report of the fbi laboratory's analysis and experiments*. 1952. [Online]. Available: https://www.cryptomuseum.com/covert/bugs/thing/files/GREAT_SEAL_BUG.pdf.

[51] CIA, *Results of laboratory examination, appendix*.

[52] I. Conrad, "Results of laboratory examination," in Released under the FIOA (FOI/PA 1173422-1) on 11 May 2014, 1952. [Online]. Available: https://cryptome.org/2014/12/ru-cavity-microphone.pdf.

[53] H. Li, Y. Zheng, and L. Qin, "Progress of biodegradable metals," *Progress in Natural Science: Materials International*, vol. 24, no. 5, pp. 414–422, 2014, ISSN: 1002-0071. DOI: https://doi.org/10.1016/j.pnsc.2014.08.014. [Online]. Available: https://www.sciencedirect.com/science/article/pii/S1002007114001178.

[54] Y. Zheng, X. Gu, and F. Witte, "Biodegradable metals," *Materials Science and Engineering: R: Reports*, vol. 77, pp. 1–34, 2014, ISSN: 0927-796X. DOI: https://doi.org/10.1016/j.mser.2014.01.001. [Online]. Available: https://www.sciencedirect.com/science/article/pii/S0927796X14000023.

[55] Y. Liu, Y. Zheng, X.-H. Chen, *et al.*, "Fundamental theory of biodegradable metals—definition, criteria, and design," *Advanced Functional Materials*, vol. 29, no. 18, p. 1 805 402, DOI: https://doi.org/10.1002/adfm.201805402. eprint: https://onlinelibrary.wiley.com/doi/pdf/10.1002/adfm.201805402. [Online]. Available: https://onlinelibrary.wiley.com/doi/abs/10.1002/adfm.201805402.

[56] H. Hermawan, *Biodegradable Metals: From Concept to Applications*. Springer Berlin Heidelberg, 2012, ISBN: 9783642311703. DOI: 10.1007/978-3-642-31170-3. [Online]. Available: http://dx.doi.org/10.1007/978-3-642-31170-3.

[57] K. Sangeetha, A. Jisha Kumari, J. Venkatesan, A. Sukumaran, S. Aisverya, and P. Sudha, "13 - degradable metallic biomaterials for cardiovascular applications," in *Fundamental Biomaterials: Metals*, ser. Woodhead Publishing Series in Biomaterials, P. Balakrishnan, S. M S, and S. Thomas, Eds., Woodhead Publishing, 2018, pp. 285–298, ISBN: 978-0-08-102205-4. DOI: https://doi.org/10.1016/B978-0-08-102205-4.00013-1. [Online]. Available: https://www.sciencedirect.com/science/article/pii/B9780081022054000131.

[58] H. Dong, F. Lin, A. R. Boccaccini, and S. Virtanen, "Corrosion behavior of biodegradable metals in two different simulated physiological solutions: Comparison of mg, zn and fe," *Corrosion Science*, vol. 182, p. 109 278, 2021, ISSN: 0010-938X. DOI: https://doi.org/10.1016/j.corsci.2021.109278. [Online]. Available: https://www.sciencedirect.com/science/article/pii/S0010938X21000445.

[59] D. Vojtěch, J. Kubásek, J. Šerák, and P. Novák, "Mechanical and corrosion properties of newly developed biodegradable zn-based alloys for bone fixation," *Acta Biomaterialia*, vol. 7, no. 9, pp. 3515–3522, 2011, ISSN: 1742-7061. DOI: https://doi.org/10.1016/j.actbio.2011.05.008. [Online]. Available: https://www.sciencedirect.com/science/article/pii/S1742706111002017.

[60] R. P. Buck, S. Rondinini, A. K. Covington, *et al.*, "Measurement of ph. definition, standards, and procedures (iupac recommendations 2002)," *Pure and Applied Chemistry*, vol. 74, no. 11, pp. 2169–2200, Jan. 2002, ISSN: 0033-4545. DOI: 10.1351/pac200274112169. [Online]. Available: http://dx.doi.org/10.1351/pac200274112169.

[61] R. Boardman and D. McGuire, "The role of zinc in forestry. i. zinc in forest environments, ecosystems and tree nutrition," *Forest Ecology and Management*, vol. 37, no. 1, pp. 167–205, 1990, Boron, Copper and Zinc in Plantation Forestry, ISSN: 0378-1127. DOI: https://doi.org/10.1016/0378-1127(90)90054-F. [Online]. Available: https://www.sciencedirect.com/science/article/pii/037811279090054F.

[62] F. Ulaby and U. Ravaioli, *Fundamentals of Applied Electromagnetics*. Pearson, 2019, ISBN: 9780135199008. [Online]. Available: https://books.google.nl/books?id=nWQwuQEACAAJ.

[63] N. Paliwal, N. Mukhija, and D. Bhatia, "Design and optimization of high quality factor mems piezoelectric resonator with pseudo electrodes," in *2015 4th International Conference on Reliability, Infocom Technologies and Optimization (ICRITO) (Trends and Future Directions)*, IEEE, Sep. 2015. DOI: 10.1109/icrito.2015.7359360. [Online]. Available: http://dx.doi.org/10.1109/ICRITO.2015.7359360.

[64] D. Kajfez, "Q factor measurements, analog and digital 1," 1999. [Online]. Available: https://api.semanticscholar.org/CorpusID:107913347.

[65] C. A. Balanis, *Antenna theory*, en, 4th ed. Hoboken, NJ: Wiley-Blackwell, Jan. 2016.

[66] C. A. Balanis, *Advanced Engineering Electromagnetics*. John Wiley & Sons, 2012.

[67] X. Li and Y. Jiang, "Design of a cylindrical cavity resonator for measurements of electrical properties of dielectric materials," M.S. thesis, 2010.

[68] M. Ur-Rehman, Y. Alfadhl, X. Chen, *et al.*, "A resonant cavity system for exposing cell cultures to intense pulsed rf fields," *Scientific Reports*, vol. 12, no. 1, Mar. 2022, ISSN: 2045-2322. DOI: 10.1038/s41598-022-08662-7. [Online]. Available: http://dx.doi.org/10.1038/s41598-022-08662-7.

[69] H. S. Kim, "Electromagnetic wave in cavity design," in Jun. 2011.

[70] H. Hamzah, A. Abduljabar, J. Lees, and A. Porch, "A compact microwave microfluidic sensor using a re-entrant cavity," *Sensors*, vol. 18, no. 3, p. 910, Mar. 2018, ISSN: 1424-8220. DOI: 10.3390/s18030910. [Online]. Available: http://dx.doi.org/10.3390/s18030910.

[71] A. Aykan, "Calibration of circular loop antennas," *Instrumentation and Measurement, IEEE Transactions on*, vol. 47, pp. 446–452, May 1998. DOI: 10.1109/19.744189.

[72] D. Peroulis, E. Naglich, M. Sinanis, and M. Hickle, "Tuned to resonance: Transfer-function-adaptive filters in evanescent-mode cavity-resonator technology," *Microwave Magazine, IEEE*, vol. 15, pp. 55–69, Jul. 2014. DOI: 10.1109/MMM.2014.2321103.

[73] W. Barrow and W. Mieher, "Natural oscillations of electrical cavity resonators," *Proceedings of the IRE*, vol. 28, no. 4, pp. 184–191, 1940. DOI: 10.1109/JRPROC.1940.228082.

[74] W. Barrow and W. Mieher, "Natural oscillations of electrical cavity resonators," *Proceedings of the IRE*, vol. 28, no. 4, pp. 184–191, 1940. DOI: 10.1109/JRPROC.1940.228082.

[75] F. Ulaby, *Fundamentals of applied electromagnetics, 1999 edition*. Upper Saddle River, NJ: Pearson, Dec. 1998.

[76] R. Y, *What is Horn Antenna? Need, Working, Design Equation and Applications of Horn Antenna - Electronics Desk electronicsdesk.com*, https://electronicsdesk.com/horn-antenna.html, [Accessed 13-05-2024].

[77] L. E. Frenzel, *Principles of electronic communication systems*, en. 2021.

[78] F. P. Kapron, R. D. Maurer, and M. P. Teter, "Theory of backscattering effects in waveguides," *Appl. Opt.*, vol. 11, no. 6, pp. 1352–1356, 1972. DOI: 10.1364/AO.11.001352. [Online]. Available: https://opg.optica.org/ao/abstract.cfm?URI=ao-11-6-1352.

[79] V. R. K. S. H. D. w. W. Koepsel, *BACKSCATTER OF ELECTROMAGNETIC WAVES FROM A ROUGH LAYER*, https://ntrs.nasa.gov/api/citations/19670008757/downloads/19670008757.pdf, [Accessed 14-05-2024], 1996.

[80] D. Dobrykh, D. Shakirova, S. Krasikov, *et al.*, "Multipole engineering for enhanced backscattering modulation," *Physical Review B*, vol. 102, no. 19, 2020, ISSN: 2469-9969. DOI: 10.1103/physrevb.102.195129. [Online]. Available: http://dx.doi.org/10.1103/PhysRevB.102.195129.

[81] R. Torres, R. Correia, N. Carvalho, *et al.*, "Backscatter communications," *IEEE Journal of Microwaves*, vol. 1, no. 4, pp. 864–878, Oct. 2021, ISSN: 2692-8388. DOI: 10.1109/jmw.2021.3110058. [Online]. Available: http://dx.doi.org/10.1109/JMW.2021.3110058.

[82] [Online]. Available: https://space.mit.edu/RADIO/CST_online/.

[83] G. Brooker and J. Gomez, "Lev termen's great seal bug analyzed," *IEEE Aerospace and Electronic Systems Magazine*, vol. 28, no. 11, pp. 4–11, 2013. DOI: 10.1109/MAES.2013.6678486.

[84] *Immediate electronics support — chrisangove.com*, https://chrisangove.com/Q_SRF_TD_1.html, [Accessed 14-05-2024].

[85] H. Klehr and R. Radosh, *The Amerasia Spy Case: Prelude to McCarthyism*. University of North Carolina Press, 1996, ISBN: 9780807822456. [Online]. Available: https://books.google.nl/books?id=tfrTpBLdl50C.

[86] F. R. Barkley, *Fbi seizes 6 as spies, two in state dept.; arrested by the f.b.i.. in espionage investigation*, 1945. [Online]. Available: https://www.nytimes.com/1945/06/07/archives/fbi-seizes-6-as-spies-two-in-state-dept-arrested-by-the-fbi-in.html.

[87] *Report of the united states senate subcommittee on the investigation of loyalty of state department employees*, 1950. [Online]. Available: https://library.cqpress.com/cqalmanac/document.php?id=cqal50-1378434.

[88] *Fbi vault file on mccarthy*, 2010. [Online]. Available: https://vault.fbi.gov/Sen.%20Joseph%20%28Joe%29%20McCarthy.

[89] P. Siegel, "Microwaves are everywhere: Rfid-do you know where your pet is?" *IEEE Journal of Microwaves*, vol. PP, pp. 1–10, Jun. 2021. DOI: 10.1109/JMW.2021.3081022.

Appendix - The Thing: History and Background

In 1945, Kenneth Wells, an analyst for the Office of Strategic Services (OSS), the intelligence agency of the United States of America during the period of World War II, observed that an article published in the Amerasia Journal, on January 26, 1945 was almost exactly comparable to a report that he had written on Thailand[85] in 1944. On March 11, 1945, OSS agents broke into the Amerasia headquarters in New York and discovered hundreds of classified papers from the Department of State, the Navy, and the OSS. The FBI arrested Philip Jaffe, a naturalized American citizen who was born in Russia, and six others on June 6, 1945, on suspicion of leaking classified information to foreign governments[86].
In parallel, the Amerasia offices were raided, resulting in the seizure of about 1,700 classified State Department, Navy, OSS, and Office of War Information papers[87]. The Justice Department in the end, however, decided not to seek an indictment under the Espionage Act because no evidence was uncovered suggesting that any materials had been passed directly to a foreign power[88].
Post this incident, the United States harboured suspicions of potential listening devices being planted in its embassies abroad, particularly in Moscow. These concerns heightened in the autumn of 1951, when a British military officer, monitoring Russian military aircraft traffic, unexpectedly intercepted the voice of the British Air Attaché on his radio. In response to this, an engineer, Don Bailey from the Diplomatic Wireless Service (DWS) was dispatched to Moscow for an investigation. Despite no bugs being discovered, it was evident that the Russians had been forewarned and had deactivated the device. Bailey, however, reported the existence of robust radio signals during the device's operation.

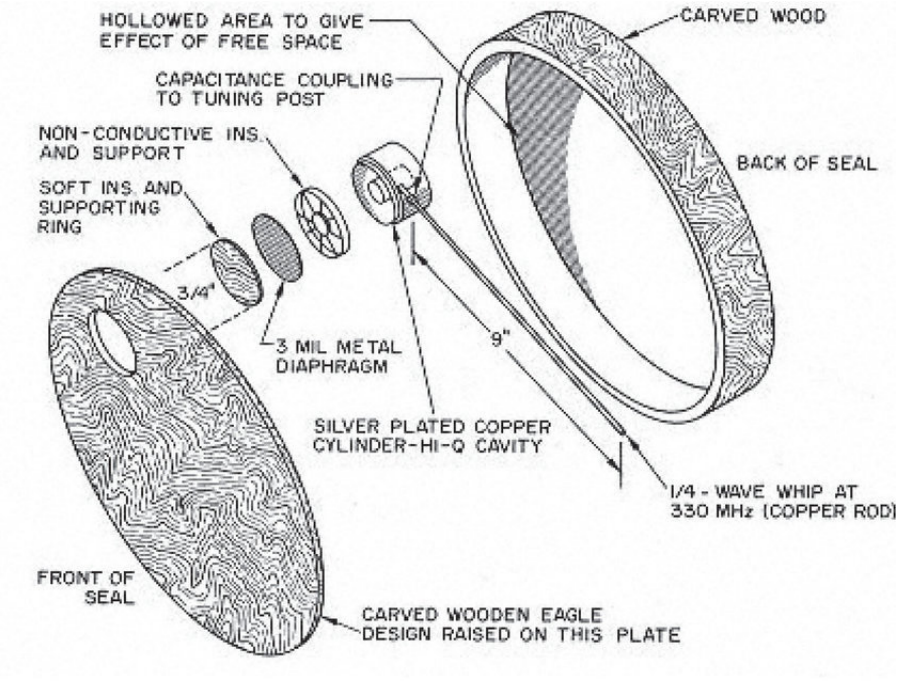


Figure A-1: Structure of the Theremin's Great Seal Bug [89]

This led the British to speculate that the Russians, much like themselves, were experimenting with a resonance device. Not too long after this incident, a U.S. military officer experienced a similar encounter, when he overheard a conversation from Spaso House, the residence of the U.S. Ambassador to the Soviet Union, and since 1991, to the Russian Federation. Georgen Kennan, the then newly appointed ambassador along with Joseph Bezjian conducted a covert operation using his crystal video receiver in an attempt to locate the bug. He managed to locate the bug in the Ambassador's library hidden in a wooden model, as depicted in Figure A-2 of the Great American Seal which was gifted to the then United States Ambassador, W. Averell Harriman by Russian schoolchildren.



Figure A-2: The Great Seal Bug Housing[83]

The initial report included the following preliminary statement [52],

"It was found that the 'ultramodern radio transmitter' consisted of a cavity resonator with a condenser microphone built into the high impedance end of the cavity and with a 1½ wave length antenna extending out the side of the cavity. It was immediately apparent that the device was designed for use as a microphone unit without any external wire connections by beaming a UHF radio signal of suitable strength and frequency toward the antenna of the unit and by using suitable UHF radio receiving equipment which would pick up and demodulate the re-radiated and modulated signal emitted by the antenna of the device."